

**OPTIMIZATION OF DYE-SENSITIZED SOLAR CELLS WITH
POLYACRYLONITRILE GEL POLYMER ELECTROLYTES
BLENDED WITH ALKYL AMMONIUM SALTS
AND IONIC LIQUIDS**

FAISAL ISLAM CHOWDHURY

**FACULTY OF SCIENCE
UNIVERSITY OF MALAYA
KUALA LUMPUR**

2018

**OPTIMIZATION OF DYE-SENSITIZED SOLAR CELLS
WITH POLYACRYLONITRILE GEL POLYMER
ELECTROLYTES BLENDED WITH ALKYL
AMMONIUM SALTS AND IONIC LIQUIDS**

FAISAL ISLAM CHOWDHURY

**THESIS SUBMITTED IN FULFILMENT OF THE
REQUIREMENTS FOR THE DEGREE OF DOCTOR OF
PHILOSOPHY**

**DEPARTMENT OF PHYSICS
FACULTY OF SCIENCE
UNIVERSITY OF MALAYA
KUALA LUMPUR**

2018

**UNIVERSITY OF MALAYA
ORIGINAL LITERARY WORK DECLARATION**

Name of Candidate: **FAISAL ISLAM CHOWDHURY**

Name of Degree: **DOCTOR OF PHILOSOPHY**

Title of Thesis:

OPTIMIZATION OF DYE-SENSITIZED SOLAR CELLS WITH POLYACRYLONITRILE GEL POLYMER ELECTROLYTES BLENDED WITH ALKYL AMMONIUM SALTS AND IONIC LIQUIDS

Field of Study: **EXPERIMENTAL PHYSICS**

I do solemnly and sincerely declare that:

- (1) I am the sole author/writer of this Work;
- (2) This Work is original;
- (3) Any use of any work in which copyright exists was done by way of fair dealing and for permitted purposes and any excerpt or extract from, or reference to or reproduction of any copyright work has been disclosed expressly and sufficiently and the title of the Work and its authorship have been acknowledged in this Work;
- (4) I do not have any actual knowledge nor do I ought reasonably to know that the making of this work constitutes an infringement of any copyright work;
- (5) I hereby assign all and every rights in the copyright to this Work to the University of Malaya ("UM"), who henceforth shall be owner of the copyright in this Work and that any reproduction or use in any form or by any means whatsoever is prohibited without the written consent of UM having been first had and obtained;
- (6) I am fully aware that if in the course of making this Work I have infringed any copyright whether intentionally or otherwise, I may be subject to legal action or any other action as may be determined by UM.

Candidate's Signature

Date:

Subscribed and solemnly declared before,

Witness's Signature

Date:

Name:

Designation:

OPTIMIZATION OF DYE-SENSITIZED SOLAR CELLS WITH POLYACRYLONITRILE GEL POLYMER ELECTROLYTES BLENDED WITH ALKYL AMMONIUM SALTS AND IONIC LIQUIDS

ABSTRACT

Gel polymer electrolytes (GPEs) consisting of polyacrylonitrile (PAN) polymer, ethylene carbonate (EC) and propylene carbonate (PC) plasticizers and different compositions of quaternary ammonium iodide salt (tetrapropylammonium iodide, TPAI or tetrabutylammonium iodide, TBAI) have been prepared and investigated. To understand the nature of GPEs containing different quaternary ammonium iodide salts (TPAI or TBAI) and/or room temperature ionic liquids (1-propyl-3-methyl imidazolium iodide, PMII or 1-butyl-3-methyl imidazolium iodide, BMII), four sets of GPEs: (i) PAN:EC:PC:TPAI:I₂, (ii) PAN:EC:PC:TBAI:I₂, (iii) PAN:EC:PC:TPAI:PMII:I₂ and (iv) PAN:EC:PC:TPAI:BMII:I₂ have been prepared and investigated. To characterize the GPEs, electrochemical impedance spectroscopy (EIS), linear sweep voltammetry (LSV) and X-ray diffraction (XRD) techniques have been utilized. The DSSCs fabricated with these electrolytes have been characterized using J-V, IPCE, IMPS and IMVS techniques. The GPE with TPAI shows higher conductivity ($3.62 \times 10^{-3} \text{ S.cm}^{-1}$) than that of TBAI ($3.46 \times 10^{-3} \text{ S.cm}^{-1}$). For further improvement of electrolyte performance TPAI based GPE has been chosen to be added with PMII and BMII ionic liquids. The conductivity of PMII ($5.90 \times 10^{-3} \text{ S.cm}^{-1}$) > BMII ($3.54 \times 10^{-3} \text{ S.cm}^{-1}$). The activation energy for ion conduction, E_a decreases accordingly as: TBAI (12.59 kJ/mol) > TPAI (10.09 kJ/mol) > TPAI+BMII (6.20 kJ/mol) > TPAI+PMII (6.14 kJ/mol). The values of J_{lim} , $D_{I_3}^*$ and J_0 are higher (12.76 mAcm⁻², $16.83 \times 10^{-7} \text{ cm}^2\text{s}^{-1}$ and 11.22 mAcm⁻², respectively) for TPAI containing GPE when compared to all other systems. The J_{sc} , V_{oc} and η of the DSSC with 30 % TPAI GPE exhibit the higher values compared to the values of TBAI based DSSCs. Also, 10 % PMII containing GPE based DSSC shows the higher values of J-V parameters than those of BMII based DSSCs. The IPCE values for the DSSCs are found to follow the order

TPAI+PMII (69.00 %) > TPAI+BMII (62.5 %) > TPAI (58.50 %) > TBAI (54.00 %). IMPS and IMVS data show that the electron transfer time, τ_{tr} decreases and electron recombination time, τ_{rec} increases from TBAI to TPAI salt and PMII to BMII IL. The current collector (η_{cc}), electron diffusion (D) and diffusion length (L_D) increase from TBAI to TPAI and BMII to PMII IL in their respective DSSCs. We also observe that the propyl group (CH₃-CH₂-CH₂-) side chain containing quaternary ammonium iodide salts and ILs show better DSSC performance compared to butyl group (CH₃-CH₂-CH₂-CH₂-) side chain containing salts and ILs.

Keywords: gel polymer electrolytes, polyacrylonitrile, dye-Sensitized Solar Cells

University of Malaya

**PENGOPTIMUMAN SOLAR SEL BERASASKAN PENCELUP PEKA
DENGAN GEL POLIAKRILNITRIL POLIMER ELEKTROLIT DIADUN
DENGAN GARAM AMMONIUM DAN CECAIR ION**

ABSTRAK

Elektrolit gel polimer (GPEs) mengandungi polimer poliakronitril (PAN), pemangkin etilena karbonat (EC) dan propilena karbonat (PC) dengan berlainan komposisi garam kuarterner amonium iodida (tetrapropilamonium iodida, TPAI atau tetrabutylamonium iodide, TBAI) telah disediakan dan dianalisa. Untuk memahami sifat GPE terkandung garam kuarterner ammonium iodida (TPAI or TBAI) yang berbeza dengan/atau cecair ionik (1-propil-3-methyl imidazolium iodida, PMII atau 1-butyl-3-methyl imidazolium iodide BMII), empat set GPE: (i) PAN:EC:PC:TPAI:I₂, (ii) PAN:EC:PC:TBAI:I₂, (iii) PAN:EC:PC:TPAI:PMII:I₂ dan (iv) PAN:EC:PC:TPAI:BMII:I₂ disediakan dan dikaji. Dalam mengenalpasti ciri-ciri GPE, spektroskopi impedan elektrokimia (EIS), voltan sapuan linear (LSV) dan difraksi sinar-X (XRD) telah digunakan. DSSCs dipasang dengan elektrolit-elektrolit ini telah dicirikan dengan teknik J-V, IPCE, IMPS dan IMVS. GPE dengan TPAI menunjukkan kekondusian tertinggi ($3.62 \times 10^{-3} \text{ S.cm}^{-1}$) berbanding dengan TBAI ($3.46 \times 10^{-3} \text{ S.cm}^{-1}$). Untuk penambahbaikan prestasi elektrolit, GPE dengan TPAI dipilih untuk ditambah cecair ionik PMII dan BMII. Kekondusian PMII ($5.90 \times 10^{-3} \text{ S.cm}^{-1}$) > BMII ($3.54 \times 10^{-3} \text{ S.cm}^{-1}$). Tenaga pengaktifan, E_a untuk konduksi ion berkurangan menurut TBAI (12.59 kJ/mol) > TPAI (10.09 kJ/mol) > TPAI+BMII (6.20 kJ/mol) > TPAI+PMII (6.14 kJ/mol). Nilai J_{lim} , $D_{I_3}^*$ dan J_0 adalah tinggi (masing-masing 12.76 mAcm^{-2} , $16.83 \times 10^{-7} \text{ cm}^2\text{s}^{-1}$ dan 11.22 mAcm^{-2}) untuk GPE mengandungi TPAI apabila dibandingkan dengan lain-lain sistem. Nilai J_{sc} , V_{oc} dan η untuk DSSC dengan 30 % TPAI GPE mencatat nilai tertinggi berbanding nilai dicatatkan oleh DSSC dengan TBAI GPE. Selain itu, DSSC dengan 10% PMII GPE menunjukkan nilai-nilai parameter J-V tertinggi berbanding DSSC dengan BMII. Nilai IPCE untuk DSSC didapati mengikut turutan TPAI+PMII (69.00 %) > TPAI+BMII (62.5 %) > TPAI (58.50

$\%$) > TBAI (54.00 %). Data IMPS dan IMVS menunjukkan masa pemindahan elektron, τ_{tr} berkurangan dan masa penggabungan elektron, τ_{rec} meningkat dari TBAI ke TPAI dan BMII ke PMII. Pengumpul arus (η_{cc}), penyebaran elektron (D) and jarak penyebaran (L_D) meningkat dari TBAI ke TPAI dan PMII ke BMII IL dalam DSSC masing-masing. Turut diperhatikan rantaian sampingan kumpulan propil ($\text{CH}_3\text{-CH}_2\text{-CH}_2\text{-}$) mengandungi garam kuarterner amonium iodida dan cecair ionik menunjukkan prestasi DSSC lebih baik berbanding rantaian sampingan kumpulan butyl ($\text{CH}_3\text{-CH}_2\text{-CH}_2\text{-CH}_2\text{-}$) yang mengandungi garam dan IL.

Katakunci: elektrolit gel polimer, poliakronitril, pengoptimuman solar sel

University of Malaya

ACKNOWLEDGEMENTS

Alhamdulillah, all admirations go to Allah (SWT) for giving me strength, patience and fitness in completing the PhD thesis. I am humbled to express my endless gratitude and gratefulness to my supervisor, Professor Dr. Abdul Karim bin Haji Mohd Arof for his continuous guidance and inspiration in completing this research work. He was not only my academic mentor but also a pathfinder in almost every step through the uneven road to finish this thesis. Also, I would like to extend my thanks to my co-supervisor, Professor Dr. Mayeen Uddin Khandaker for his continuous support and inspiration in this work.

I would like to thank all of my lab mates and officers in Centre for Ionics University of Malaya (CIUM) for their support in completing this research work. Moreover, my gratitude also goes to Department of Physics, University of Malaya for providing me all facilities to complete my research work. Also, I would like to acknowledge the financial support by the grants RG375-15AFR and RU022G-2014 and PG082-2015A from the Institute of Research Management & Monitoring (IPPP) of University of Malaya. Furthermore, I would like to extend my thankfulness to the University of Chittagong for granting me study leave and financial support.

Last but not least, I would like to gratify my parents (Rafiqul Islam Chowdhury and Mazed Begum) for their unceasing prayers, support and encouragement in this journey. I owe thanks to a very distinct person, my beloved wife, Dr. Rumi Afroze for her continuous and trustworthy love, sacrifice, support and understanding throughout the Ph.D. study period. Without her such cooperation, I could not be able to finish this massive work within the stipulated time. I appreciate my adored little son, Farzad Chowdhury for accepting my ignorance and the patience he showed during my experimental work and thesis writing.

TABLE OF CONTENTS

ABSTRACT	iii
ABSTRAK	v
ACKNOWLEDGEMENTS	vii
TABLE OF CONTENTS	viii
LIST OF FIGURES	xiii
LIST OF TABLES	xvii
LIST OF SYMBOLS AND ABBREVIATIONS	xx
CHAPTER 1: INTRODUCTION	1
1.1 Introduction	1
1.2 Problem statement	4
1.3 Objectives of the Thesis	5
1.4 Scope of the Thesis.....	5
CHAPTER 2: LITERATURE REVIEWS	7
2.1 Introduction of the chapter	7
2.2 Solar cells	7
2.3 Dye-Sensitized Solar Cells	10
2.3.1 Benefits of using DSSCs	10
2.3.2 Basic Principles of DSSCs	12
2.3.3 The components of the DSSCs.....	15
2.3.3.1 Transparent conducting films (TCFs).....	15
2.3.3.2 The working electrodes.....	16
2.3.3.3 The sensitizing dyes.....	17
2.3.3.4 The counter electrodes	19
2.3.3.5 The electrolytes.....	21

2.4	Gel Polymer Electrolytes.....	21
2.4.1	Factors affecting the ionic conductivity of GPE and DSSC performance	26
2.4.1.1	Polymer concentration	26
2.4.1.2	The iodide salts	27
2.4.1.3	The concentration of the iodide salts.....	27
2.4.1.4	Size of the inorganic cation of iodide salts	29
2.4.1.5	Length of side chains of the organic iodide salts.....	29
2.4.1.6	Organic solvent	31
2.4.1.7	Temperature	31
2.4.1.8	Addition of room temperature ionic liquid (RTIL)	32
2.5	Summary of the chapter.....	35
CHAPTER 3: METHODOLOGY.....		36
3.1	Introduction to the chapter.....	36
3.2	Materials	36
3.3	Research layouts	38
3.4	Preparation of Gel Polymer Electrolytes	38
3.5	Characterization of the Gel Polymer Electrolytes	41
3.5.1	Electrochemical Impedance Spectroscopy (EIS)	41
3.5.1.1	Ionic Conductivity measurement	42
3.5.1.2	Calculation of activation energy (E_a) for ion conduction	42
3.5.2	Linear sweep voltammetry (LSV).....	42
3.5.2.1	Limiting current density, J_{lim}	43
3.5.2.2	Exchange current density, J_0	44
3.5.3	X-ray Diffraction (XRD) study	45
3.6	Fabrication of DSSC.....	45
3.6.1	Preparation of the working electrodes.....	45

3.6.2	Preparation of the counter electrodes	47
3.6.3	Fabrications of the DSSCs	47
3.7	DSSC characterization.....	48
3.7.1	Photovoltaic (J-V) characteristics	49
3.7.1.1	Open Circuit Voltage (V_{OC})	49
3.7.1.2	Short Circuit Current (J_{SC}).....	50
3.7.1.3	Fill factor (FF).....	50
3.7.1.4	Efficiency.....	51
3.7.2	Incident Photon to Charge Carrier Efficiency (IPCE)	52
3.7.3	Study of electron transfer mechanism in DSSCs	52
3.7.3.1	Intensity-modulated photocurrent spectroscopy (IMPS).....	54
3.7.3.2	Intensity-modulated photovoltage spectroscopy (IMVS).....	55
3.7.3.3	Charge-collection efficiency (η_{cc}).....	55
3.7.3.4	Electron diffusion coefficient (D).....	56
3.8	Summary of the chapter.....	56
CHAPTER 4: RESULTS ON THE PAN:EC:PC:TPAI:I₂ GPE SYSTEM.....		57
4.1	Electrochemical impedance spectroscopy (EIS) measurement	57
4.1.1	Ionic conductivity study	57
4.1.2	Activation energy for ionic conduction.....	57
4.2	Linear sweep voltammetry (LSV) measurement.....	59
4.2.1	Limiting current and I_3^- Diffusion coefficient study	59
4.2.2	Tafel polarization curve and Exchange current density, J_0	61
4.3	X-ray diffraction (XRD) studies	62
4.4	DSSC performance analysis	64
4.4.1	Photovoltaic (J-V) characteristics	64
4.4.2	Incident-photon-to-current efficiency (IPCE).....	65

4.4.3	IMPS and IMVS study of DSSCs	66
4.5	Summary of the chapter	68
CHAPTER 5: RESULTS ON THE PAN:EC:PC:TBAI:L₂ GPE SYSTEM		71
5.1	Electrochemical impedance spectroscopy (EIS) measurement	71
5.1.1	Ionic conductivity study	71
5.1.2	Activation energy for ionic conduction.....	71
5.2	Linear sweep voltammetry (LSV) measurement.....	73
5.2.1	Limiting current and I_3^- Diffusion coefficient study	73
5.2.2	Tafel polarization curve and Exchange current density, J_0	74
5.3	X-ray diffraction (XRD) studies.....	75
5.4	DSSC performance analysis	77
5.4.1	Photovoltaic (J-V) characteristics	77
5.4.2	Incident-photon-to-current efficiency (IPCE).....	78
5.4.3	IMPS and IMVS study of DSSCs	79
5.5	Summary of the chapter.....	81
CHAPTER 6: RESULTS ON THE PAN:EC:PC:TPAI:PMII:L₂ GPE SYSTEM..		83
6.1	Electrochemical impedance spectroscopy (EIS) measurement	83
6.1.1	Ionic conductivity study	83
6.1.2	Activation energy for ionic conduction.....	83
6.2	Linear sweep voltammetry (LSV) measurement.....	85
6.2.1	Limiting current and I_3^- Diffusion coefficient study	85
6.2.2	Tafel polarization curve and Exchange current density, J_0	87
6.3	X-ray diffraction (XRD) studies.....	88
6.4	DSSC performance analysis	89
6.4.1	Photovoltaic (J-V) characteristics.....	89
6.4.2	Incident-photo-to-current efficiency (IPCE).....	90

6.4.3	IMPS and IMVS study of DSSCs	91
6.5	Summary of the chapter	94
CHAPTER 7: RESULTS ON THE PAN:EC:PC:TPAI:BMII:L₂ GPE SYSTEM..		96
7.1	Electrochemical impedance spectroscopy (EIS) measurement	96
7.1.1	Ionic conductivity study	96
7.1.2	Activation energy for ionic conduction.....	96
7.2	Linear sweep voltammetry (LSV) measurement	98
7.2.1	Limiting current and I_3^- Diffusion coefficient study	98
7.2.2	Tafel polarization curve and Exchange current density, J_0	99
7.3	X-ray diffraction (XRD) studies	100
7.4	DSSC performance analysis	102
7.4.1	Photovoltaic (J - V) characteristics.....	102
7.4.2	Incident-photon-to-current efficiency (IPCE)	103
7.4.3	IMPS and IMVS study of DSSCs	104
7.5	Summary of the chapter	106
CHAPTER 8: DISCUSSION		108
CHAPTER 9: CONCLUSIONS AND SUGGESTIONS FOR FUTURE WORK		117
9.1	Conclusions	117
9.2	Suggestions for future work	118
REFERENCES.....		120
LIST OF PUBLICATIONS AND PAPERS PRESENTED		134

LIST OF FIGURES

Figure 2.1:	Research-cells efficiencies (source: National Renewable Energy Laboratory, NREL).....	9
Figure 2.2:	National Renewable Energy Laboratory (NREL) Research Cell Efficiency Records (source: National Renewable Energy Laboratory, NREL).	11
Figure 2.3:	General configuration and operational principal of a DSSC.....	12
Figure 2.4:	Electron trapping/detrapping model.	13
Figure 2.5:	State of ions in solvent according to pair-ions model (Wang, 2009)...	28
Figure 3.1:	Schematic diagram of GPEs preparation.....	40
Figure 3.2:	Gel polymer electrolytes.....	41
Figure 3.3:	Schematic diagram of a linear sweep voltamogram.....	44
Figure 3.4:	Tafel polarization curve.....	44
Figure 3.5:	Preparation of working electrode (a) grinding of TiO ₂ powder, (b) checking conducting side of the FTO glass, (c) partial masking of FTO glass, (d) dried TiO ₂ coated FTO glass, (e) TiO ₂ coated FTO glass into the furnace for sintering and (f) soaking of TiO ₂ coated FTO glass into dye solution.....	47
Figure 3.6:	Flow chart of DSSC fabrication.....	48
Figure 3.7:	Dye-sensitized solar cell (DSSC) (a) a complete DSSC, (b) DSSC under solar simulator light and (c) DSSC characterization by AutoLab station.....	48
Figure 3.8:	Schematic illustration of <i>J-V</i> curve of dye-sensitised solar cell.....	51
Figure 3.9:	Sketch of the light signal focused on a DSSC during IMPS and IMVS.	52
Figure 3.10:	<i>J-V</i> curves of a DSC showing the regions covered by EIS, IMPS and IMVS.	53
Figure 3.11:	Estimation of characteristic frequency, f_{IMPS} from Nyquist type plot.	54
Figure 4.1:	Nyquist plots for PAN:EC:PC:TPAI:I ₂ GPEs: (i) 0 wt % TPAI, (ii) 10 wt % TPAI, (iii) 20 wt % TPAI, (iv) 30 wt % TPAI and (v) 40 wt % TPAI.	58
Figure 4.2:	$\ln\sigma$ versus $1000/T$ graphs for different TPAI containing GPEs.....	59

Figure 4.3:	Linear sweep voltammograms (LSV) of GPEs at varying concentration of TBAI with Pt-ultramicroelectrode. Scan rate: 10 mV/s.....	60
Figure 4.4:	Tafel polarization curves for the electrolytes with different TPAI containing GPEs.	61
Figure 4.5:	XRD pattern of (i) PAN and (ii) PAN:EC:PC GPE.....	63
Figure 4.6:	XRD pattern of (i) PAN:EC:PC:TPAI:10 wt % TPAI:I ₂ , (ii) PAN:EC:PC:TPAI:20 wt % TPAI-I ₂ , (iii) PAN:EC:PC:TPAI:30 wt % TPAI:I ₂ and (iv) PAN:EC:PC:TPAI:40 wt % TPAI:I ₂ GPEs.	64
Figure 4.7:	<i>J</i> – <i>V</i> curves of DSSCs for PAN:EC: PC:TPAI:I ₂ GPEs systems.....	65
Figure 4.8:	IPCE % vs. wavelength for the DSSCs with different TPAI containing GPEs.	66
Figure 4.9:	IMPS Nyquist type plots at different intensities for the DSSCs assembled with GPEs containing (i) 10 wt %, (ii) 20 wt %, (iii) 30 wt % and (iv) 40 wt % TPAI.	67
Figure 4.10:	IMVS Nyquist type plots at different intensities for the DSSCs assembled with GPEs containing (i) 10 wt %, (ii) 20 wt %, (iii) 30 wt % and 40 wt % TPAI.	68
Figure 5.1:	Nyquist plots for PAN:EC:PC:TBAI:I ₂ GPEs, (i) 0 wt % TBAI, (ii) 10 wt % TBAI, (iii) 20 wt % TBAI, (iv) 30 wt % TBAI and (v) 40 wt % TBAI.	72
Figure 5.2:	lnσ versus 1000/ <i>T</i> graphs for different TBAI containing GPEs.....	73
Figure 5.3:	Linear sweep voltammograms (LSV) of GPEs at varying concentration of TBAI with Pt ultramicroelectrode. Scan rate: 10 mV/s.	74
Figure 5.4:	Tafel polarization curves for the electrolytes with different TBAI containing GPEs.	75
Figure 5.5:	XRD pattern of PAN:EC:PC:xTBAI:I ₂ GPEs, x = (i) 10 wt %, (ii) 20 wt %, (iii) 30 wt % and (iv) 40 wt %.....	77
Figure 5.6:	<i>J</i> – <i>V</i> curves of DSSCs for PAN:EC:PC:TBAI:I ₂ GPEs systems.	78
Figure 5.7:	IPCE % vs. wavelength for the DSSCs with different TBAI containing GPEs.	79
Figure 5.8:	IMPS Nyquist type plots at different intensities for the DSSCs assembled with GPEs containing (i) 10 wt %, (ii) 20 wt %, (iii) 30 wt % and 40 wt % TBAI.	80

Figure 5.9:	IMVS Nyquist type plots at different intensities for the DSSCs assembled with GPEs containing (i) 10 wt %, (ii) 20 wt %, (iii) 30 wt % and 40 wt % TBAI.	81
Figure 6.1:	Nyquist plots for PAN:EC:PC:TPAI:PMII:I ₂ GPEs: (i) 4 wt % PMII, (ii) 6 wt % PMII, (iii) 8 wt % PMII, (iv) 10 wt % PMII and (v) 12 wt % PMII.	84
Figure 6.2:	ln σ versus 1000/T graphs for different PMII containing GPEs.....	85
Figure 6.3:	Linear sweep voltammograms (LSV) of GPEs at varying concentration of PMII with Pt ultramicroelectrode. Scan rate: 10 mV/s.	86
Figure 6.4:	Tafel polarization curves for the electrolytes with different PMII containing GPEs.	87
Figure 6.5:	XRD pattern of PAN:EC:PC:30 wt % TPAI:PMII-I ₂ : (i) 0 wt % PMII, (ii) 6 wt % PMII, (iii) 8 wt % PMII, (iv) 10 wt % PMII and (v) 12 wt % PMII.	89
Figure 6.6:	<i>J-V</i> curves of DSSCs for PAN:EC:PC:TPAI-I ₂ GPEs systems.....	90
Figure 6.7:	IPCE % vs. wavelength for the DSSCs with different TPAI containing GPEs.	91
Figure 6.8:	IMPS Nyquist type plots at different intensities for the DSSCs assembled with PAN:EC:PC:30 wt % TPAI:PMII:I ₂ GPEs.....	93
Figure 6.9:	IMVS Nyquist type plots at different intensities for the DSSCs assembled with PAN:EC:PC:30 wt % TPAI:PMII:I ₂ GPEs.....	94
Figure 7.1	Nyquist plots for PAN:EC:PC:TPAI:BMII:I ₂ GPEs: (i) 4 wt % BMII, (ii) 6 wt % BMII, (iii) 8 wt % BMII, (iv) 10 wt % BMII and (v) 12 wt % BMII.	97
Figure 7.2:	ln σ versus 1000/T graphs for different BMII containing GPEs.....	98
Figure 7.3:	Linear sweep voltammograms (LSV) of GPEs at varying concentration of BMII with Pt ultramicroelectrode. Scan rate: 10 mV/s.	99
Figure 7.4:	Tafel polarization curves for the electrolytes with different BMII containing GPEs.	100
Figure 7.5:	XRD pattern of PAN:EC:PC:30 wt % TPAI:I ₂ GPEs with different amount of BMII (i) 0 wt % (ii) 4 wt % (iii) 6 wt % , (iv) 8 wt % , (v) 10 wt % and (vi) wt 12 %.....	101
Figure 7.6:	<i>J-V</i> curves of DSSCs for PAN:EC:PC:TPAI:BMII:I ₂ GPEs systems.	102

Figure 7.7:	IPCE % vs. wavelength for the DSSCs with different TPAI containing GPEs.	103
Figure 7.8:	IMPS Nyquist type plots at different intensities for the DSSCs assembled with GPEs containing different percentages of BMII.....	105
Figure 7.9:	IMVS Nyquist type plots at different intensities for the DSSCs assembled with GPEs containing different percentage of BMII.....	106

University of Malaya

LIST OF TABLES

Table 2.1:	Ru-based synthetic dye and their chemical structure which are used in DSSCs.	18
Table 2.2:	The structures of triphenylamine (TPA), coumarin and indoline.....	19
Table 2.3:	List of GPEs based on PAN applied in DSSCs and corresponding parameters: conductivity (σ), open circuit voltage (V_{oc}), short circuit current (J_{sc}), fill factor (FF) and efficiency (η %).	24
Table 2.4:	some ILs with their chemical structures.....	30
Table 2.5:	Commonly used cations that comprise ionic liquids Common Cations Structures.	33
Table 2.6:	Commonly used anions that comprise ionic liquids Common Anions Structures.....	33
Table 3.1:	Chemical structures of materials used in the research.....	36
Table 3.2:	Composition of the PAN:EC: PC: TPAI:I ₂ gel polymer electrolytes.....	39
Table 3.3:	Composition of the PAN:EC: PC: TBAI:I ₂ gel polymer electrolytes.....	39
Table 3.4:	Composition of the PAN:EC:PC:TPAI:PMII:I ₂ gel polymer electrolytes.....	40
Table 3.5:	Composition of the PAN:EC:PC:TPAI:BMII:I ₂ gel polymer electrolytes.....	40
Table 4.1:	Bulk impedance, R_b (ohm), ionic conductivity, $\sigma \times 10^{-3}$ (S/cm) and activation energy, E_a (eV) for ion conduction for the TPAI containing GPEs.....	59
Table 4.2:	Limiting current or steady state current (J_{lim}), diffusion coefficients of I ₃ ⁻ ion ($D_{I_3^-}$), exchange current density (J_0) of GPEs containing different composition of iodine.	62
Table 4.3:	Photovoltaic performance of PAN:EC:PC:TPAI:I ₂ with different weight contents of TPAI-added polymer electrolytes.....	65
Table 4.4:	Summary of parameters obtained from IMPS and IMVS experiments for different DSSCs fabricated with GPEs containing various percentages of TPAI.	68
Table 5.1:	Bulk impedance, R_b (ohm), ionic conductivity, $\sigma \times 10^{-3}$ (S/cm) and Activation energy, E_a (kJ/mol) for ion conduction for the TBAI containing GPEs.	73

Table 5.2:	Limiting current or steady state current (J_{lim}), diffusion coefficients of I_3^- ion ($D_{I_3^-}$), exchange current density (J_0) of GPEs containing different composition of iodine.	75
Table 5.3:	Photovoltaic performance of PAN:EC:PC:TBAI:I ₂ with different weight contents of TBAI-added polymer electrolytes.....	78
Table 5.4:	Summary of parameters obtained from IMPS and IMVS experiments for different DSSCs fabricated with GPEs containing various percentages of TBAI.	80
Table 6.1:	Bulk impedance, R_b (ohm), ionic conductivity, $\sigma \times 10^{-3}$ (S/cm) and Activation energy, E_a (kJ/mol) for ion conduction for the PMII containing GPEs.	85
Table 6.2:	Limiting current or steady state current (J_{lim}), diffusion coefficients of I_3^- ion ($D_{I_3^-}$), exchange current density (J_0) of GPEs containing different composition of iodine.	88
Table 6.3:	Photovoltaic performance of PAN:EC:PC:TPAI:I ₂ with different weight contents of PMII-added polymer electrolytes.....	89
Table 6.4:	Summary of parameters obtained from IMPS and IMVS experiments for different DSSCs fabricated with GPEs containing various percentages of PMII.	92
Table 7.1:	Bulk impedance, R_b (ohm), ionic conductivity, $\sigma \times 10^{-3}$ (S/cm) and Activation energy, E_a (eV) for ion conduction for the BMII containing GPEs.....	98
Table 7.2:	Limiting current or steady state current (J_{lim}), diffusion coefficients of I_3^- ion ($D_{I_3^-}$), exchange current density (J_0) of GPEs containing different composition of iodine.	100
Table 7.3:	Photovoltaic performance of PAN:EC:PC:TPAI:BMII:I ₂ with different weight contents of TPAI-added polymer electrolytes.....	102
Table 7.4:	Summary of parameters obtained from IMPS and IMVS experiments for different DSSCs fabricated with GPEs containing various percentages of BMII.	105
Table 8.1:	Conductivity (σ) and activation energy (E_a) of GPEs with different percentage of TPAI and TBAI, respectively.	108
Table 8.2:	Maximum values of limiting current density (J_{lim}), triiodide ion diffusion coefficient ($D_{I_3^-}$), and exchange current density (J_0).....	110
Table 8.3:	Maximum values of short circuit current (J_{sc}), open circuit voltage (V_{oc}) and fill factor (FF) for DSSCs fabricated with different salt and or ILS containing GPEs.	111

Table 8.4: The electron transfer time (τ_{tr}), electron recombination time (τ_{rec}), charge collection efficiency (η_{cc}), electron diffusion coefficient (D) and diffusion length (L_D) for DSSCs fabricated with different salts and or ILs containing GPEs. 115

University of Malaya

LIST OF SYMBOLS AND ABBREVIATIONS

BMII	:	1-butyl-3-methyl imidazolium iodide
CB	:	Conduction band
CE	:	Counter electrode (CE)
D	:	Electron diffusion coefficient
D_n	:	Diffusion coefficient
DSSCs	:	Dye-sensitized solar cells
E_a	:	Activation energy
EC	:	Ethylene carbonate
EIS	:	Impedance spectroscopy
F	:	Faraday's constant
FF	:	Fill Factor
FTO	:	Fluorine-doped tin dioxide
GPEs	:	Gel polymer electrolytes
HOMO	:	Highest occupied molecular orbital
ILs	:	Ionic liquids
IMPS	:	Intensity-modulated photocurrent spectroscopy
IMVS	:	Intensity-modulated photovoltage spectroscopy
IPCE	:	Incident photon-to-current efficiency
ITO	:	Indium-doped tin oxide
J_0	:	Exchange current density
J_{lim}	:	Limiting current densities
J_{sc}	:	Short-circuit current density
LE	:	Liquid electrolyte
L_n	:	Electron diffusion length

LSV	: Linear sweep voltammetry
LUMO	: Lowest unoccupied molecular orbital
MOFs	: Metal–organic frameworks
NREL	: National Renewable Energy Laboratory
PAN	: Polyacrylonitrile
PANI	: Polyaniline
PC	: Propylene carbonate
PEDOT	: Poly(3,4-ethylenedioxythiophene)
PEO	: Poly (ethylene oxide)
PMII	: 1-propyl-3-methyl imidazolium iodide
PMMA	: Poly (methyl methacrylate)
PV	: Photovoltaic
PVA	: Polyvinyl alcohol
PVAc	: Poly(vinyl acetate)
PVC	: Poly(vinyl chloride)
PVdF	: Poly (vinylidene fluoride)
PVdF-HFP	: Poly(vinylidene fluoride-co-hexafluoropropylene)
QE	: Quantum efficiency
QSPEs	: Quasi-solid polymer electrolytes
R_b	: Bulk resistance
R_s	: Series resistance
RT	: Room temperature
RTILs	: Room temperature ionic liquids
SPEs	: Solid polymer electrolytes
TBAI	: Tetrabutylammonium iodide
TBP	: 4-Tert-butylpyridine

TCFs	:	Transparent conducting films
TCO	:	Transparent conducting oxide substrate
TEAI	:	Tetraethylammonium iodide
TPAI	:	Tetrapropylammonium iodide
V_{oc}	:	Open-circuit voltage
XRD	:	X-ray diffraction spectroscopy (XRD)
η_{cc}	:	Charge-collection efficiency
η	:	Efficiency
τ_n	:	Free electron lifetime

University of Malaya

CHAPTER 1: INTRODUCTION

1.1 Introduction

Attempts to replace liquid electrolytes with gel polymer electrolytes (GPEs) (Ileperuma et al., 2011; Jayathilaka et al., 2002) in many electrochemical devices such as dye-sensitized solar cells (DSSCs) are being undertaken. To ensure the good DSSC performance, the polymer electrolytes should have good ionic conductivity, electrocatalytic activity, thermal, mechanical and electrochemical stabilities. In the present work, emphasis is placed on ionic conductivity and electrocatalytic activity of the GPEs.

Introduction of ionic liquids (ILs) or nanoparticle fillers into the GPEs enhances ionic conductivity (Buzzeo et al., 2004; Kim et al., 2013; Lu et al., 2008) (Yang et al., 2011). Though DSSC with liquid electrolyte (LE) has high photovoltaic efficiency of 13% (Mathew et al., 2014), they suffer from problems that involve electrolyte evaporation, leakages and corrosion of the platinum secondary electrode (Hsu et al., 2013; Tiautit et al., 2014; Vittadello et al., 2011). To replace liquid electrolytes, researchers have observed the use of an all-solid, quasi-solid and ionic liquid types of electrolytes. The blend of coordinating polymers and an appropriate salt is advantageous in their conductive properties in the solid state. Nevertheless, the increased viscosity results in slow ionic transport and an inadequate diffusivity of ions in the electrolyte into the nanoporous titania photoelectrode (Freitas et al., 2009). DSSCs with solid polymer electrolytes (SPEs) show low current density, fill factor, and efficiency (Günes & Sariciftci, 2008; Nogueira et al., 2001) compared to DSSC with liquid electrolytes.

GPEs or quasi-solid polymer electrolytes (QSPEs) are potential candidates to replace LEs and SPEs in DSSCs because of their considerably good electrical conductivity and reasonably long term stability (Lan et al., 2010; Li et al., 2014). Among the polymers

used in GPEs are polyacrylonitrile (PAN), poly (ethylene oxide) (PEO), polyvinyl alcohol (PVA), poly (methyl methacrylate) (PMMA), poly (vinylidene fluoride (PVDF), poly(vinyl chloride) (PVC), poly(vinyl acetate) (PVAc), and poly(vinylidene fluoride-co-hexafluoropropylene) (PVdF-HFP). Salts used include LiI, NaI, KI etc. and organic quaternary ammonium iodide salts like tetraethylammonium iodide (TEAI), tetrapropylammonium iodide (TPAI), tetrabutylammonium iodide (TBAI) etc. (Ileperuma et al., 2004; Ileperuma et al., 2007; Shen et al., 2008; Wu et al., 2006). The organic salts have become important for DSSC electrolytes due to their low lattice energy and higher dissociative nature (Bandara et al., 2010). The size of the alkyl chain attached to the salt cation governs the electrolyte as well as cell performance. Photocurrent density and photovoltage decreased and increased, respectively with increase in cation radius (Bandara et al., 2013). This is because the conduction band energy (E_c) of the TiO_2 and the associated influence on the electron injection vary with the nature of cations (Liu et al., 1998). Unfortunately, there are very few reports that address this issue. Bandara et al. (Bandara et al., 2016) studied the PAN:EC:PC gel polymer system with Me_4NI , Et_4NI , Pr_4NI , Bu_4NI , Pen_4NI and Hex_4NI salts and reported that the DSSC with GPE containing Pr_4NI exhibited the highest efficiency of 4.3 %. However, the GPE containing Me_4NI exhibited the highest conductivity of $2.62 \times 10^{-3} \text{ S} \cdot \text{cm}^{-1}$. Bandara and co-workers (Bandara et al., 2016) reported a DSSC with PAN:EC:PC: Pr_4NI : I_2 GPE that exhibited 4.47 % efficiency. Ileperuma et al. (Ileperuma et al., 2004) studied PAN:EC:PC: Bu_4NI :TBP: I_2 GPEs and obtained a DSSC with 7 % efficiency. Bandara et al. (Bandara et al., 2013) observed that DSSC with TPAI containing GPE exhibited a higher efficiency compared to the DSSC employing a GPE containing TBAI. Lee and co-workers (Lee et al., 2009) reported otherwise for DSSC employing PVDF-HFP:PC and PVDF-HFP:AN QSPEs. To the author's knowledge, there are no data to verify this fact. Apart from the reports of Bandara et al. (Bandara et al., 2012; Bandara et al., 2013), there

is no study concerning the alkyl side chain length or ion size of the salts in the GPEs on the DSSC efficiency. Therefore, there is a great need of more study for the better choice of salt for the DSSCs application, in the author's opinion.

For further improvement of electrochemical performance as well as DSSC efficiency, researchers incorporated room temperature ionic liquids (RTILs) into the gel polymer matrix. ILs have high chemical, electrochemical and thermal stabilities. Apart from these, they have negligible vapor pressure, nonflammability, adjustable viscosity, solvent ability, high room temperature (RT) ionic conductivity and a wide electrochemical window. ILs used in electrolytes with iodide-based redox mediators for DSSCs have improved the cell performance (Kubo et al., 2002; Papageorgiou et al., 1996; Wang et al., 2002). Though, the ILs with various cations, such as sulfonium, guanidinium, ammonium, phosphonium, pyridinium, pyrrolidinium, and piperidinium, have been explored and used as electrolytes for DSSCs (Cho et al., 2011; Son et al., 2008), ILs with imidazolium cation exhibit good performance in DSSCs due to the higher conductivity and lower viscosity (Hagiwara & Ito, 2000; Nishida et al., 2003; Xi et al., 2008). The iodide anion serves as the source of I^- necessary for the reduction of the oxidized dye molecules (Wishart, 2009). Among all of the ILs, imidazolium salt 1-propyl-3-methyl imidazolium iodide (PMII) shows the lowest viscosity (1024 cP) and highest conductivity (0.54 mS cm^{-1}) at room temperature and that is why it has been widely used in DSSCs (Bai et al., 2008). As far as our knowledge, there are no detail study on electrochemical, electrocatalytic and DSSC performance of PAN-EC-PC-TPAI GPEs with the incorporation of PMII or BMII ionic liquids. Furthermore, it is also important to examine the size or length of alkyl moiety present in the ILs on these GPEs in terms of electrochemical, electrocatalytic as well as DSSC characteristics.

There is also no report concluding the best choice of RTILs (either PMII or BMII) with this GPE for electrochemical device applications. Therefore, in the present work, we will use polyacrylonitrile (PAN) as polymer framework material and EC/PC as plasticizers to formulate RTIL [1-propyl-3-methyl imidazolium iodide (PMII) and 1-butyl-3-methyl imidazolium iodide (BMII)]-based GPEs for better electrochemical performance as well as high DSSC efficiency. The organic cations may form coordination with PAN polymer chains in the gel electrolyte offering channels to transport the Γ^- anion freely (Longo & Paoli, 2003). In this study we will employ organic cationic iodide salt, tetra-propylammonium iodide (TPAI) room temperature ionic liquid PMII and BMII in separate GPEs which are relatively good with organic solvents due to less crystallization tendency in the gel systems protecting cell deterioration (Kumara et al., 2002; Štangar et al., 2002).

1.2 Problem statement

Proper choice of polymer, organic salt and ionic liquid combination and optimization of their composition for the development of a noble gel polymer electrolyte, which would be competent in terms of electrochemical performance as well as DSSC efficiency, is a great challenge. It is unclear yet how the chain length of quaternary ammonium iodide salt and imidazolium iodide ionic liquid in the PAN based GPEs affect the DSSC performance. Investigation of PAN based GPEs with TPAI and TBAI is to find the better choice of salt (TPAI or TBAI) and to optimize their concentrations. After optimization of better salt concentration, and to improve the DSSC efficiency, PMII and BMII are the choices of IL added.

1.3 Objectives of the Thesis

The objectives of this study are:

- to produce gel polymer electrolytes (GPEs) based on PAN:EC:PC:TPAI:I₂ and PAN:EC:PC:TBAI:I₂ complexes with high conductivity.
- to enhance PAN:EC:PC:TPAI:I₂ GEPs with highest conductivity by incorporating an ionic liquid (PMII and BMII).
- to determine and analyze the electrochemical and electrocatalytic properties of the PAN:EC:PC:TPAI:I₂ and PAN:EC:PC:TBAI:I₂ GPEs.
- to examine the suitability of the GPEs for DSSC application.
- to study the influence of the alkyl group chain length in the salts and in the imidazolium ionic liquids on the performance of DSSCs.
- to study electron transport properties of the DSSCs fabricated with these GPEs.

1.4 Scope of the Thesis

The whole thesis comprises nine chapters. The first chapter initiates with an introduction towards the scope of research. Chapter two presents a literature review covering the the corresponding state-of-the art of the GPEs prepared and the corresponding DSSCs fabricated. Chapter 3 describes the details of research methodology such as sample preparation as well as their characterizations, which include impedance spectroscopy (EIS), linear sweep voltammetry (LSV), X-ray diffraction spectroscopy (XRD) and DSSC fabrication and characterizations.

Chapter 4 describes the results obtained from characterization of PAN:EC:PC:TPAI:I₂ gel polymer electrolyte system. From impedance spectroscopy studies, the composition giving the highest ionic conductivity can be determined. From the temperature dependence of ionic conductivity, activation energy for ion conduction can be estimated. Limiting current can be determined using the LSV data from which tri-iodide diffusion

is calculated. Tafel polarization curves give exchange current density. The XRD data provide crystalline/amorphous nature of the GPEs. *J-V* characteristics of DSSCs are also presented in this chapter. Intensity Modulated Photocurrent Spectroscopy (IMPS) and Intensity Modulated Photovoltage Spectroscopy (IMVS) experiments provide electron transport characteristics such as electron transfer time, electron recombination rate, charge collection efficiency, electron diffusion rate and electron diffusion length of the DSSCs. Similarly, Chapters 5, 6 and 7 presents the results obtained from the PAN:EC:PC:TBAI:I₂ PAN:EC:PC:TPAI:PMII:I₂ and PAN:EC:PC:TPAI:BMII:I₂ gel polymer electrolyte systems and their corresponding DSSCs, respectively.

Chapter 8 discusses all results obtained in the experiments and Chapter 9 concludes the thesis with some suggestions for future work that will help to enhance the knowledge in the immense literature on polymer electrolytes and DSSCs.

CHAPTER 2: LITERATURE REVIEWS

2.1 Introduction of the chapter

The review chapter deals with discussion on DSSCs and polymer electrolytes. The properties of materials used in this study and the choice of these materials are explained. This chapter describes the basic working principle of DSSCs, factors affecting the gel polymer electrolytes and tactics to enhance performance of the DSSCs and GPEs.

2.2 Solar cells

In the present world, we are mostly consuming conventional fossil fuels which is neither unlimited nor environmental friendly. Even if use the conventional fuels with austerity, it will sooner or later be depleted (Bella et al., 2014). Thus, to fulfill future energy demands and to save our planet, much effort is necessary to find alternative renewable energy sources and to develop sustainable techniques for making these energies useable. This challenge calls for the contribution of scientists and engineers worldwide. The world political leaders and policymakers also agree that the energy policy needs to be revamped for the survival of our planet. Nowadays, the direct solar energy into electricity conversion has become a promising renewable energy technology. Solar cell technology is also known as photovoltaic (PV) technology.

Michael Gratzel had quantified that in one year, the energy from the sun reaching the earth surface is about 174×10^3 TW (O'Regan & Gratzel, 1991). The report appeared in Nature. This energy is ten thousand times greater than the world energy consumption. If we could use 0.1 % of sun's energy by 10 % efficient solar cells, it would be more than sufficient to fulfill the energy demands of the earth population (O'Regan & Gratzel, 1991). According to quantum theory, sunlight is composed of tiny massless particles called photons. These photons strike the semiconducting materials (e.g. silicon) in the solar panel. Electrons in the solar panel accept this energy and are excited. The electrons

escape from the doped semiconductor atoms and form “holes” which must be filled by other electrons (Li et al., 2006).

Generally, an n-type silicon has more electrons than a p-type silicon, which has more holes. When the p-type and n-type semiconductors come into contact, a p-n junction is formed, and an electric field is created. The extra unbound electrons in the n-type semiconductor flow to the p-type and holes are created in the n-type semiconductor. An electric field is thus developed at the interface between the p- and n-semiconductor. The electrons from the bulk of the semiconductor hop towards the interface. These electrons can flow through the external electrical circuit powering the external loads. The holes created due to the electron flow will be filled by other electrons (Li et al., 2006). Thus, in a p-n junction solar cell an electric field is generated. For developing voltage, external load such as an LED, electric field etc are necessary. However, in DSSCs, a redox electrolyte is placed in between the photoanode and the counter cathod. Photons strike the sensitizer releasing electrons which transfer to the TiO_2 from which they go to the outer circuit and come back to the counter electrode. A summary of the different types of solar cell is shown in Figure 2.1.

- Multijunction Cells ($\eta = 31\text{-}44\%$) – Multi-layer cells with different technologies built within. Costly and for research.
- Single-Junction GaAs ($\eta = 29\text{-}34\%$) – Made with Gallium Arsenide. Expensive due to costly raw materials. Used in high-end applications e.g. satellites.
- Crystalline Si Cells ($\eta = 20\text{-}27\%$) – Made with slices of silicon. Most common. Good pricing and easily installed.
- Thin-Film Technologies ($\eta = 13\text{-}23\%$) – Made by depositing a layer of high electrical performance material such as silicon. Compared to other types of cells, it is thinner and cheaper. Not so popular due to low performance.

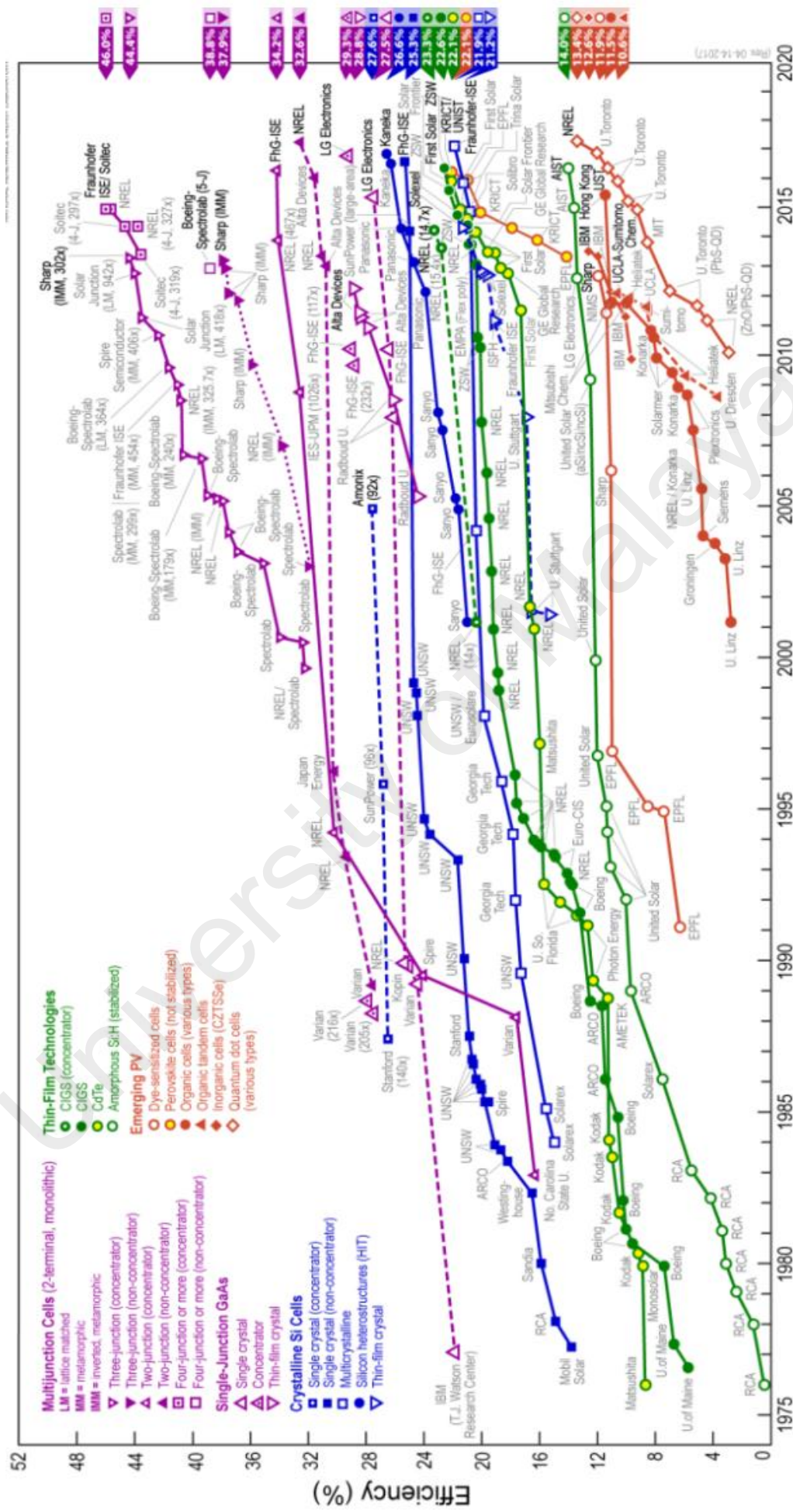


Figure 2.1: Research-cells efficiencies (source: National Renewable Energy Laboratory, NREL).

- Emerging PV ($\eta = 9-14\%$) – These cells are still under research. Performance is low but is being improved.

Crystalline silicon solar cell has become commercially available. However, dye-sensitized solar cell technology is promisingly cheaper and approaching the market. DSSCs is the focus of this research.

2.3 Dye-Sensitized Solar Cells

The success of a photovoltaic technology is its ability to enter the market. Although the cost of conventional silicon crystalline solar panels per watt has fallen a great deal over the years, they still could not compete with electricity generated from fossil fuels. Therefore, it is essential to search for photovoltaic devices, which could be more inexpensive and efficient enough for household and industrial use.

DSSCs are emerging as potential solar to electricity conversion device after the invention by O'regan and Gratzel in 1991. They developed used nanocrystalline TiO_2 as the photoanode. The efficiency of DSSCs has reached around 13 % at 1 Sun and is cost effective (Mathew et al., 2014). In 2013 a cell with efficiency 14.1 % was certified by the accredited photovoltaic calibration laboratory (Burschka et al., 2013). Figure 2.2 displays the National Renewable Energy Laboratory (NREL) research cell efficiency records.

2.3.1 Benefits of using DSSCs

It has been repeatedly mentioned by researchers that the DSSCs could compete with crystalline silicon solar cells in terms of pricing. Materials used in DSSCs are cheap and easy to process. DSSCs do not require materials that are highly pure e.g. crystalline silicon necessary for the silicon solar cell. Even though the efficiency of DSSCs is lower than many thin-film cells, DSSCs have higher price-to-performance ratio (Rhee et al., 2014).

2.3.2 Basic Principles of DSSCs

The structure and working principle of a typical DSSC is shown in Figure 2.3. A DSSC is made of four main components (Wei, 2011):

- Photoelectrode - A thin layer of nanostructured wide band-gap semiconductor (usually TiO_2 , ZnO , SnO_2 , etc) coated on a transparent conducting oxide (TCO) substrate (usually fluorine-doped tin dioxide, FTO or Indium-doped tin oxide, ITO).
- Dye – A light sensitive substance that adsorbed on the semiconductor surface.
- Electrolyte – A medium that contacts only ions with a redox couple (usually I^-/I_3^-).
- Cathod – A highly conducting layer with good catalytic activity for I_3^- reduction into I^- (platinum, Pt is commonly used) coated on a TCO.

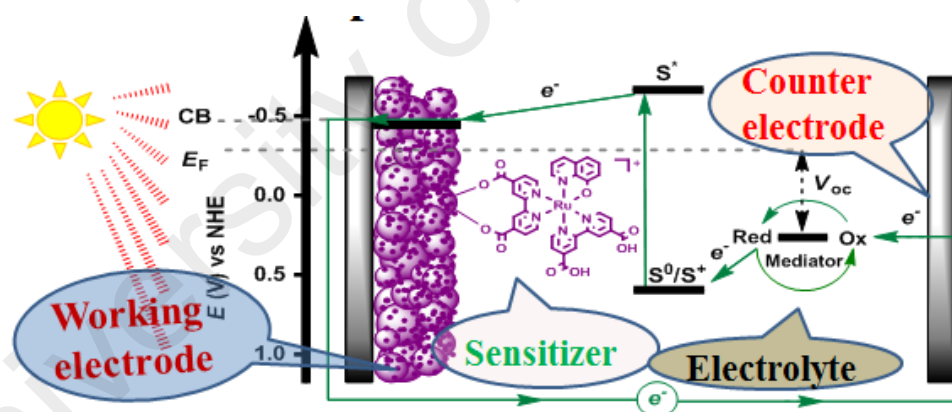


Figure 2.3: General configuration and operational principal of a DSSC.

Under sunlight, the dye molecules will absorb photons and thus, excited. The photoexcited molecules inject electrons into the TiO_2 layer leaving them oxidized (left with holes). Thus, charge separation occurs as the electrons enter the TiO_2 and a “hole” inside the dye molecules. In the absence of recombination, the electrons will percolate through the porous TiO_2 network and reach the back of the photoanode where electrons enter the external circuit. Through the external circuit the electrons pass through a load

and finally reach the counter electrode. Here I_3^- ions in the redox couple is reduced and become I^- ions. The iodide ions diffuse to the photo anode or working electrode and release electrons to the holes in the oxidized dyes and the circuit completed. The iodide ions get oxidized into tri-iodide ions and the redox cycle repeats. This process repeats itself and electrical current is created from the impinging sunlight (Li et al., 2006).

Electron transport in TiO_2 is occurred by a multiple trapping/detrapping (Figure 2.4) processes where the electron in the conduction band (CB) falls in the shallow traps and then thermally detrapped from the sub-bandgap states to the CB. The trapping/detrapping processes determines the effective electron lifetime, τ_n , and the effective electron diffusion coefficient, D_n . (Bisquert et al., 2004; Bisquert & Vikhrenko, 2004; Nguyen et al., 2009; Peter, 2007).

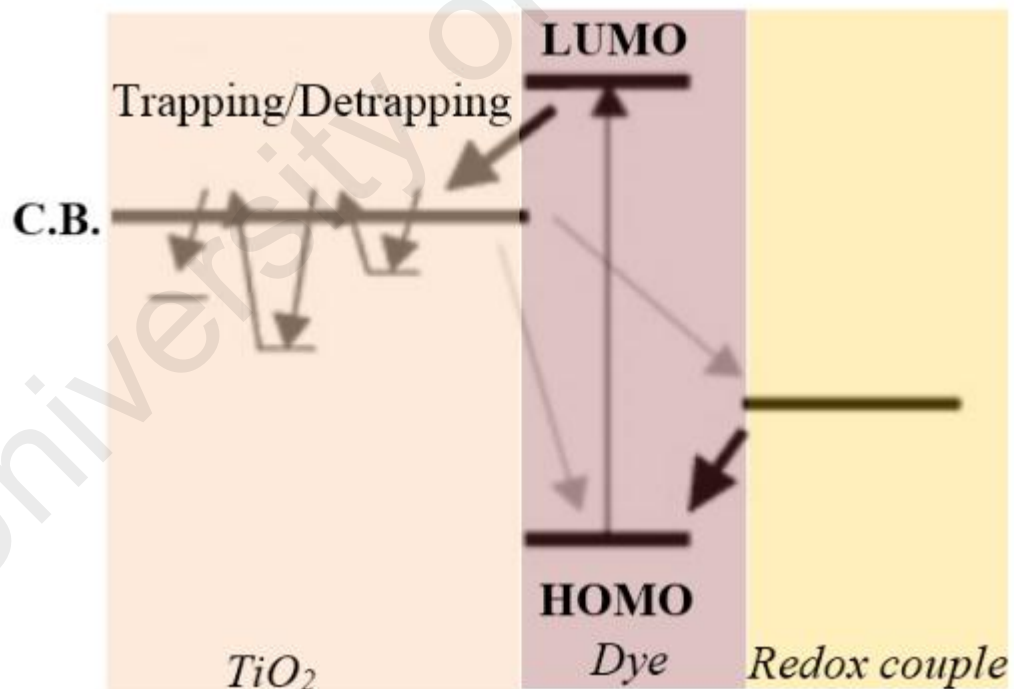


Figure 2.4: Electron trapping/detrapping model.

The DSSC performance is also governed by other processes that include light harvesting, electron injection and transport and electron loss by back reaction with I_3^- . It has been accepted that electron trapping/detrapping manages both electron forward and

back transport in DSSCs (Nguyen et al., 2009). Also, the greater portion of the electrons in a DSSC is trapped (Boschloo & Goossens, 1996; Schwarzburg & Willig, 1991; Zhu et al., 2006). The trapped electrons density depends on trap occupancy and can be determined by electrical techniques such as impedance measurements (Fabregat-Santiago et al., 2006) and charge extraction (Bailes et al., 2005; Duffy et al., 2000). The trapped electrons spend time in the traps and returns to the CB on thermal excitation. This process is called multiple trapping model (Nguyen et al., 2009). The photoinjected electrons collection efficiency, which is a vital factor in device performance, is governed by competition between transport of electrons to the anode and transfer of electrons to I_3^- ions in the electrolyte. This process is determined by the electron diffusion length $L_n = (D_n\tau_n)^{1/2}$ which depends on the diffusion coefficient D_n and lifetime τ_n of the free electrons. In cells of high efficiency, L_n values should be considerably higher than the TiO_2 film thickness. It has been demonstrated that the microstructure (e.g. crystal structure, morphology, etc.) of the TiO_2 film has a profound impact on both τ_n and D_n of DSSCs (Adachi et al., 2004; Ghadiri et al., 2010; Qiu et al., 2010; Sauvage et al., 2010; Shankar et al., 2008). The D_n of DSSCs based on conventional mesoporous TiO_2 films consisting of an interconnected nanoparticle network is 2–3 orders of magnitude lower than that of bulk material owing to the large amount of grain boundaries and defects (Fisher et al., 2000; Peter, 2007; Peter et al., 2006) .

The “parasitic” reactions resulting in reduction of cell efficiency can also occur. The parasitic reactions include recombination of injected electrons with either holes in the oxidized sensitizer (Equation 2.1) or with the oxidized redox couple i.e. I_3^- at the TiO_2 surface (Equation 2.2).



Hence, charge transfer at the electrode/dye/electrolyte interfaces must be controlled in order that photo-injected electrons be prevented from recombining with acceptors, but are sent to an external load (Nakade et al., 2005). Electron injection occurs in picoseconds (Asbury et al., 1999; Tachibana et al., 1996). The injection yield depends on TiO₂ surface condition (Benkő et al., 2003) and concentration of the cations in the electrolytes (Tada et al., 1999). The recombination of electrons with dye cations takes between tens of nanoseconds and a millisecond, depending on the electron density in TiO₂, (Haque et al., 2000) while the reduction of the dye cation by the I⁻ ions occurs in a few to tens of microseconds, depending on the concentration and the cations species (Pelet et al., 2000). Under short-circuit condition, recombination of electrons with I₃⁻ ions occurs predominantly particularly in electrolytes with high redox couple concentration. The electron lifetime as measured by various groups, ranges between a few milliseconds to more than one second with $I_e^{-a}(\lambda)$, where I_e is the light intensity and 'a' is a constant, ~ 0.5 (Fisher et al., 2000; Nelson et al., 2001; Schlichthörl et al., 1997).

2.3.3 The components of the DSSCs

DSSC is constituted with four basic components such as transparent conducting glass substrate, working electrode, electrolyte, sensitizing dye and counter electrode.

2.3.3.1 Transparent conducting films (TCFs)

Transparent conducting films or TCF is a very important component in DSSCs. They are thin layers of conducting materials coated on some substrates. Examples are indium tin oxide (ITO), fluorine doped tin oxide (FTO) conducting polymer layers, carbon nanotubes, and graphene. TCF consists of organic and inorganic materials. The most popular TCF used in the DSSCs is in the form of indium tin oxide (ITO), fluorine doped tin oxide (FTO) or the sulfur doped zinc oxide (ZnO).

2.3.3.2 The working electrodes

The working electrodes in a DSSC normally consist of a wide band-gap nano-semiconductor deposited on a transparent conducting substrate. One of the most popular semiconductor materials used is TiO_2 , with band gap of 3.2 eV. Other semiconductor materials used are ZnO , SnO_2 and NiO . TiO_2 is inexpensive, non-toxic, plentiful and easily obtainable (Bandara et al., 2012).

The size of the semiconductor nanoparticles (NPs) in the working electrode range from 15 to 30 nm. They would appear transparent or semi-opaque with porosity around 50-60 % and film thickness around 8 to 15 μm (Alkire et al., 2015). The semiconductor NPs can be deposited by screen-printing and doctor-blading. Both methods involve viscous colloidal TiO_2 paste to be deposited onto the conducting substrate. In doctor-blading a smooth glass rod or a thin glass slide is used to spread the colloidal paste on the TCO glass to a specific thickness with the help of a tape frame that will be removed after the solvent has evaporated. After deposition, the working electrodes will be sintered at 450 - 500 $^\circ\text{C}$. After sintering the TiO_2 semiconductor will be immersed in a dye solution. (Wang et al., 2007). The porous nature of the working electrode enables more dye solution to be adhered to a larger surface area enabling more light to be harvested compared to non-porous electrodes.

The DSSCs perform better with minimal charge recombination at the TiO_2 /sensitizer and FTO/ TiO_2 interfaces (Green et al., 2005; Haque et al., 2005; Ni et al., 2006). The sensitizer (dye) regeneration by I^- is faster than the charge transfer from TiO_2 to the oxidized dye i.e., the charge recombination at the interface of TiO_2 /sensitizer is negligible (Ito et al., 2005). The charge recombination will cause a considerable reduction of DSSC photoelectron conversion efficiency into electricity. Therefore, photo-injected electron recombination with triiodide ions must be stopped. To mitigate this issue, the FTO substrate is deposited with a thin compact TiO_2 layer of smaller size before printing the

TiO₂ semiconductor porous layer (Burke et al., 2008). This can lessen the contact surface area between the TCO substrate and electrolyte (Cameron & Peter, 2005; Cameron et al., 2005; Hore & Kern, 2005; Palomares et al., 2003; Peng et al., 2004). Besides blocking electron recombination, the compact layer can also improve FTO/TiO₂ interfacial adhesion, which will generate more electron passing channels from the porous TiO₂ layer to FTO for photo-induced electrons and successively rise the electron transfer efficiency (Noh et al., 2008; Yu et al., 2009).

Also, by depositing a compact TiO₂ layer on the FTO glass substrate before applying the mesoporous TiO₂ layer, the dye itself acts to screen electrons in the FTO from the I₃⁻ species in the electrolyte. *ab initio* calculations have shown that for standard ruthenium dyes, the highest occupied molecular orbital (HOMO level) is actually shared by the ruthenium metal center and the isothiocyanate (NCS) ligands. This implied that the positive charge is distributed between the metal center and the NCS ligands (Hagfeldt & Gratzel, 2000). Due to the large size of the ruthenium complex and the fact that the bis-2,2'-bipyridine-4-carboxylic acid moiety interacts strongly with the FTO surface, the injected electrons and the I₃⁻ ions in the electrolyte are physically separated. Here, distance appears to play a significant role in the probability of electron transfer from the FTO to the electrolyte.

2.3.3.3 The sensitizing dyes

One of the most important materials in DSSCs is the sensitizer. It harvests sunlight or photons into the DSSCs. Many types of dyes both ruthenium-based and metal-free organics (MOFs) have been deeply studied for better efficiency of the DSSCs (Marinado, 2009). Ruthenium-based complexes are preferred because they have exhibited DSSCs with 11-12 % efficiency. Some superior ruthenium dyes include N3, N719 (Nazeeruddin et al., 1999) and black dye (Nazeeruddin et al., 1997). N3 is the pioneering dye reported

in 1993 by Nazeeruddin et al (Nazeeruddin et al., 1993). The structures of these dyes are shown in Table 2.1.

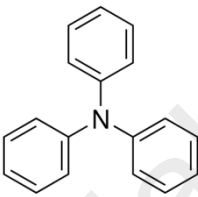
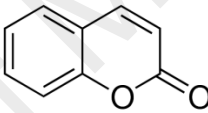
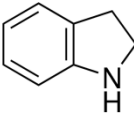
Table 2.1: Ru-based synthetic dye and their chemical structure which are used in DSSCs.

Dye	Chemical name	Chemical structure
N3 dye	Cis-Bis(isothiocyanato) bis(2,2'-bipyridyl-4,4'-dicarboxylato) ruthenium(II)	
N749 Black Dye	Di-tetrabutylammonium cis-bis(isothiocyanato)bis(2,2'-bipyridyl-4,4'-dicarboxylato)ruthenium(ii)	
Z907 dye	Cis-Bis(isothiocyanato)(2,2'-bipyridyl-4,4'-dicarboxylato)(4,4'-di-nonyl-2'-bipyridyl)ruthenium(II)	

The efficiency of organic dyes based DSSCs have increased over the years and receiving additional attention in the researchers' community. The benefits of organic dyes are easy modification as they have simple synthesizing paths and they have higher extinction coefficients in comparison with the inorganic dyes. The absorption bands of

organic dyes are shorter compared to the inorganic dyes which lowers the power conversion efficiency of the DSSCs fabricated with organic dyes (Marinado, 2009). There are some well-known organic dyes such as triphenylamine (TPA), coumarin and indoline the structures are presented in Table 2.2.

Table 2.2: The structures of triphenylamine (TPA), coumarin and indoline.

Chemical name	Chemical structure
Triphenylamine	
Coumarin	
Indoline	

2.3.3.4 The counter electrodes

The counter electrode (CE) is another vital element of DSSCs. It collects electrons coming through the external circuit. The CE works as an electro-catalyst for reduction of redox couple species, which pushes electron to the oxidized dye (sensitizer) for its regeneration. Furthermore, the CE plays an important role to collect hole generated in the hole-transporting materials of the solid state DSSCs. Platinum (Pt), gold (Au) and silver (Ag) are the commonly used materials for preparing good CE. For the liquid electrolyte based DSSCs, Pt shows better performance in reducing the tri-iodide species whereas Au and Ag are superior for solid electrolytes as they have outstanding hole transfer abilities.

Even though these materials are better as CE, they are expensive due to their low presence in the earth.

Generally, ultra-micro thin layer of Pt is coated on FTO glass and applied as a CE in DSSCs. Modification of CE materials can enhance the fill-factor of the DSSC which is essentially governed by the cell's series resistance (R_s). Researchers are trying to find alternative naturally abundant cheaper materials to serve as CEs. These are listed below (Ye et al.):

- Carbon materials: Carbon is cheap and abundant material in the Earth which can provide good performance in DSSC. Their corrosion resistance and thermal stability are high.
- Inorganic compounds: Although these materials are cheap and abundant, their performance is low, and they are less stable. For practical application in DSSCs, the inorganic materials need huge improvement. CoS_2 , TiC, TiN and metal oxides are some examples of inorganic materials.
- Conductive polymers (CPs): These are potential materials to replace Pt as CE. The DSSCs employing them exhibit good performance. The conductive polymers are very stable and transparent, which make them lucrative in DSSC application. There are some examples of CPs such as polyaniline (PANI) and poly(3,4-ethylenedioxythiophene) (PEDOT). PEDOT is widely used in DSSCs. Incorporation of salts such as LiI, TPAI, TBAI, TBP etc. improves its performance.
- Composites: These types of materials constitute of two or more different components. An example is graphene-Pt/TaON/ NiS_2 /NiO//TiN/PPy composite. In the present work, we used conventional Pt-counter electrode as our research focuses on electrolytes.

2.3.3.5 The electrolytes

The electrolyte is also one of the vital components of DSSCs. It prevents aggregation of the salt made up of a polymer, salts (in this case a halide salt) additives that help dissociate and prevent aggregation of ions and a redox couple. The redox couple is formed via an iodide ion interaction with iodine that was added with the basic electrolyte components (about 10 wt % of salt mass). The iodide/triiodide redox couple is widely used and most effective redox mediator. The iodide/triiodide diffusion processes govern the transport of electrons and completes the electric circuit. At the Pt-counter electrode, the tri-iodide ion is reduced to an iodide ion, which then travels towards the photoanode where the iodide ion reduces the oxidized dye and in doing so it is oxidized again into an I_3^- ion that will diffuse to the CE. The cycle repeats. Usually, electrolytes with an iodide/tri-iodide redox mediator contains iodide salt(s) and some iodine crystals. The salt(s) will dissociate into a cation (depending on the type of salt) and an iodide ion. The reaction between the iodide ions and iodine produces the tri-iodide ions and hence the iodide/tri-iodide redox couple. Examples of iodide salts used include LiI, NaI, tetrapropylammonium iodide (TPAI) and tetrabutylammonium iodide (TBAI) etc. 4-tert-butylpyridine (4-TBP) and guanidiniumthiocyanate (GuSCN) are the widely used additives in DSSC electrolytes (Bella et al.). 4-TBP can enhance the open-circuit voltage, V_{oc} but maintains the short-circuit current density, J_{sc} . GuSCN can increase J_{sc} and maintains V_{oc} . Hence optimizing J_{sc} and V_{oc} can increase the DSSC efficiency, η . For efficient dye regeneration, the redox potential must be less positive than the ground state of the dye. In this work, we use gel polymer electrolytes (GPEs). We now focus on GPEs.

2.4 Gel Polymer Electrolytes

As already mentioned, although DSSCs with LEs have high photovoltaic efficiencies of 13 % (Mathew et al., 2014), they suffer from some drawbacks due to the use of liquid electrolytes. Accordingly, common problems such as electrolyte evaporation, leakages,

desorption, photo degradation of the dye and corrosion of the platinum secondary electrode are observed (Hsu et al., 2013; Tiautit et al., 2014; Vittadello et al., 2011). Efforts to find alternatives for the liquid electrolytes have been carried world-wide. The efforts have resulted in the all-solid, quasi-solid and ionic liquid types of electrolytes (Benedetti et al., 2008; Freitas et al., 2008; Longo & Paoli, 2003; Nogueira et al., 2004; Nogueira & Paoli, 2000; Nogueira et al., 2001; Nogueira et al., 2006; Priya et al., 2008; Ren et al., 2002; Tan et al., 2004). The blend of coordinating polymer and an appropriate salt is advantageous in their conductive properties in the solid state. Nevertheless, the increased viscosity results in low and limited ionic transport (Nakade et al., 2005) and an inadequate filling of the mesoporous titania in the photoelectrode by the electrolyte (Freitas et al., 2009). The DSSCs with pure polymer electrolyte showed lower current, fill factor and efficiency when compared to DSSC with liquid electrolytes.

Researchers have discovered gels, which are neither liquid nor solid electrolytes to uphold the beneficial characteristics of both types of electrolytes. The GPEs or quasi-solid type of electrolytes have emerged as a potential component in DSSC due to its considerably high electrical conductivity and excellent long term stability (Lan et al., 2010; Li et al., 2014). Gel polymer electrolyte (GPE) is the homogenous blend of a polymer host, solvents, salt and additives. Generally, a significant amount of organic solvent can be trapped inside the polymer host. This may compensate the solvent leakage and solvent volatility. GPEs have excellent contacting properties with electrodes (Khanmirzaei et al., 2015), high ionic conductivity (Hu et al., 2016), reasonably high photovoltaic performances and high thermal and mechanical stability (Wang, 2009). Classical GPEs consist of small portions of low molecular weight polar polymer host in large amounts of organic plasticizer such as ethylene carbonate (EC) and/or propylene carbonate (PC) and polar aprotic organic solvent (e.g. ACN, THF). The plasticizer decreased the polymer's glass transition temperature by disrupting some of the crystalline

phase, increasing the polymer's segmental mobility and its free volume (Nogueira et al., 2004). In addition, the GPEs are advantageous in the manufacturing view point (Lan et al., 2008). Poly(ethylene oxide) (PEO) has been comprehensively dealt. The incorporation of the liquid plasticizers EC in the electrolytes can decrease the PEO crystallinity resulting in enhancement of polymer segmental mobility. This will lead to arise of ionic conductivity. Polymers typically play the role for providing dimensional stability in the GPE matrix. Along with other electrolytes, GPEs based on PAN have been developed and studied. Authors reported good ionic conductivity that may be due to the low crystallinity of the polymer.

The GPEs are essentially found to be well-suited with the DSSCs applications. The liquid electrolyte is entrapped in them. The GPEs have negligible evaporation rate, free of leakage and high temperature resistance. Some GPEs are also sticky making good contacts with the electrodes. These lucrative features of GPEs solve some problems associated with LE based DSSC. With the aim of achieving high quantum efficiency of DSSCs, high ionic conductive electrolytes are compulsory as high ionic conductive electrolytes could increase the short circuit current (J_{sc}) of a DSSC. Upon comparing the corresponding parameters of the DSSCs using GPE and liquid electrolyte (LE), it is evident that the open circuit voltage (V_{oc}) increased for GPE-based DSSCs due to the dark current suppression by the polymer chains shielding the TiO_2 electrode surface. This may lead to high quantum efficiency of the DSSCs, which could be better or at least comparable to the DSSCs using LEs (Wang, 2009).

Although, GPEs have numerous advantages, there are still other problems. Wang (Wang, 2009) reported that the V_{oc} for GPE-based DSSCs is higher than DSSCs with LEs, but the performance of DSSCs with GPEs is less than with LEs. The polymer network, which forms gel, could restrict the movement of the charge carriers in the GPEs. The

polymer may react with the salt(s) and additives used. For this reason, several approaches were undertaken to improve the performance of GPEs and DSSCs using these GPEs. Nevertheless, it is essential to comprehend what are the factors governing the GPE transport properties such as ionic conductivity and eventually the DSSCs performance. Table 2.3 displays the list of some PAN based GPEs with their DSSCs characteristics parameters.

Table 2.3: List of GPEs based on PAN applied in DSSCs and corresponding parameters: conductivity (σ), open circuit voltage (V_{oc}), short circuit current (J_{sc}), fill factor (FF) and efficiency (η %).

GPEs	σ (mS cm ⁻¹)	V_{oc} (mV)	J_{sc} (mA cm ⁻²)	FF	η %	Ref
PAN:EC:PC:Pr ₄ N ⁺ I: I ₂	2.95	690	3.73	0.535	2.99	(Dissanayake et al., 2002)
PAN:EC:PC:PSQAS: I ₂	1.43	565	7.00	0.65	4.30	(Wang et al., 2004)
PAN:LiBOB:BMII: I ₂	120	540	2.04	0.38	1.40	(Arof et al., 2013)
PAN:EC:PC:He ₄ N ⁺ I: I ₂	210	696	9.37	NA	2.80	(Bandara et al., 2012)
PAN:EC:PC:BMII:Pr ₄ N ⁺ I: LiI: I ₂	393	500	20.61	0.53	5.54	(Bandara et al., 2015)
PAN:EC:PC:TBAI:TBP: I ₂	433	751	15.96	0.616	7.27	(Ileperuma et al., 2011)

Dissanayake et. al. (Dissanayake et al., 2002) reported PAN:EC:PC:Pr₄N⁺I: I₂ GPE with conductivity $\sigma = 2.95$ mS cm⁻¹ applied in DSSC and obtained the efficiency 2.99 %. In another report the GPE with PAN:EC:PC:PSQAS: I₂ combination shows the conductivity of 1.43 mS cm⁻¹ and the DSSC based on this electrolyte shows the efficiency 4.3 % (Wang et al., 2004). They used polysiloxane quaternary ammonium side groups (PSQAS) which comprises of a bulky polycation and anions acting as an organic salt for enhancing the ionic conductivity. The addition of BMII in PAN:LiBOB:BMII: I₂ gel type

electrolyte by Arof and co-workers (Arof et al., 2013) exhibited $1.2 \times 10^{-2} \text{ S cm}^{-1}$ ionic conductivity and DSSC efficiency of 1.40 %. Bandara et. al. (Bandara et al., 2012) also reported PAN based GPE such as PAN:EC:PC:He₄N⁺I₂. They observed the ionic conductivity of 2.10 mS cm^{-1} along with 2.8 % DSSC efficiency. A combined effect of RTIL and quaternary ammonium iodide salt along with an inorganic salt (LiI) was in PAN based GPE observed by the work of Bandara et. al. (Bandara et al., 2015). They reported σ as $3.93 \times \text{mS cm}^{-1}$ and the efficiency of DSSC, 5.54 %. Furthermore, using t-butyl phosphate (TBP) in the PAN:EC:PC:TBAI:TBP:I₂ gel polymer electrolyte, Ileperuma and co-workers (Ileperuma et al., 2011) obtained higher conductivity 4.33 mS cm^{-1} and higher efficiency (7.27 %) of DSSC. Jayathilaka et al. have also prepared PAN:LiTFSI:EC:PC GPE with ionic conductivity 2.50 mS cm^{-1} that could be applied in the electrochemical devices (Jayathilaka, Dissanayake, Albinsson, & Mellander, 2003). PMMA is another popular polymer, which can be used to prepare polymer electrolytes with good ionic conductivity (Stephan & Thirunakaran, 1999). However, as it is mechanically not so strong, its application in GPEs is limited. To increase the mechanical strength of PMMA based GPEs, poly(vinyl chloride) (PVC) has been used as additive. In addition, PVC and PVDF are also prospective polymers for use in GPEs.

From the extensive literature survey, it has been found that only Bandara et. al. reported PAN:EC:PC based GPEs with various quaternary salts such as TPAI, TBAI, and also BMII ionic liquids (Bandara et al., 2015; Bandara et al., 2012; Bandara et al., 2013) in which they tried to understand the cation size effect on the electrochemical properties as well as DSSC performances. Nonetheless, the systematic optimization of the salt concentration in the GPE systems are absent in their study. Furthermore, there is no report on structural characterization and electrocatalytic performance of the GPEs as well as cell performance in terms of IPCE. The electrokinetic mechanism of the DSSCs operation is also missing. There is also no report concluding the best choice of RTILs (either PMII or

BMII) with this GPE for electrochemical device applications. Therefore, in the present work, we will use polyacrylonitrile (PAN) as polymer framework material and EC/PC as plasticizers to formulate RTIL [1-propyl-3-methyl imidazolium iodide (PMII) and 1-butyl-3-methyl imidazolium iodide (BMII)]-based gel polymer electrolytes for better electrochemical performance of DSSCs. The organic cations may form coordination with PAN polymer chains in the gel electrolyte offering channels to transport the I^- anion freely. In this study we will employ organic cationic iodide salt, tetra-propylammonium iodide (TPAI) room temperature ionic liquid PMII and BMII in separate GPEs with organic solvents due to less crystallization tendency in the gel systems protecting cell deterioration (Kumara et al., 2002; Štangar et al., 2002)

2.4.1 Factors affecting the ionic conductivity of GPE and DSSC performance

2.4.1.1 Polymer concentration

In the GPE matrix, if the polymer concentration decreased, the ionic conductivity increased since the viscosity decreases with polymer concentration. In polyblend gel electrolytes, ionic conductivity of the GPE rises with declining contents of polymer with higher viscosity at fixed salt concentration. For instance, the ionic conductivity of the polyblend P(MMA-co-MAA)/PEG reduced with reducing amount of PEG (Li et al., 2007). This is because of:

(i) The complex of PEG and salt has higher conductivity than those of P(MMA-MAA)-salt complexes at the same salt concentration.

(ii) With increasing the PEG amount, viscosity is decreased causing increased segmental mobility that results in higher conductivity of the polyblend GPE.

2.4.1.2 The iodide salts

The incorporation of salts into the polymer host is important for enhancing of the GPE's ionic conductivity. Some examples of the salts used for this purpose are LiTf, LiTfSI, and LiBOB. For the functioning of DSSCs, i.e. the process of converting photon absorption to electricity the electrons injected into the CB of the TiO₂ semiconductor on light absorption must be sent back to the holes in the dye molecules. If the electrolyte contains an I⁻/I₃⁻ redox couple the I⁻ regenerates the dye by acting as a mediator to carry the electrons to the holes in the dye. That is why, the use of iodide salts for example KI, NaI, TPAI, TBAI etc. have been established for electricity production from DSSCs. Incorporation of iodide salts can influence the conductivity of iodide ion in the GPE resulting in enhancement of the DSSCs' short circuit current density which also contributes to efficiency (Wang, 2009).

2.4.1.3 The concentration of the iodide salts.

It is very important to choose the appropriate iodide salts as well as their suitable concentrations for better efficiency of DSSCs. The number density species-carrying charge increases with increase of iodide salt(s) concentration and declines after attaining an optimum salt(s) concentration. The increase in viscosity on addition of more salt after the optimum concentration have been used to explain such dropping conductivity. The increase in viscosity resulted from the binding of the cations and the polar atoms of the polymers, which could reduce the polymer chain's segmental motion and reduces ionic conductivity. Besides, the solubility of the salts could be restricted by the solvents and the equilibrium of the salt dissociation reaction could shift to left. If added salt concentration exceeds the solubility limit, the ions would be reassociated rather than dissociated in the solution. This could lead to the recurrence of crystalline phase in the GPEs and results in the decrease of the ionic conductivity of the GPEs (Li et al., 2007). This phenomena can also be explained using the pair-ion theory (Price & Weingaertner,

1991) and the disengagement of phases (Mover & Dowell, 1981) of polymer matrix and liquid electrolyte caused by the influence of the ions. Figure 2.5 presents the state of ions in solvent according to pair-ions model. Small amount of salt added in the GPE system can be dissociated completely and form homogeneous solution or system under vigorous stirring.

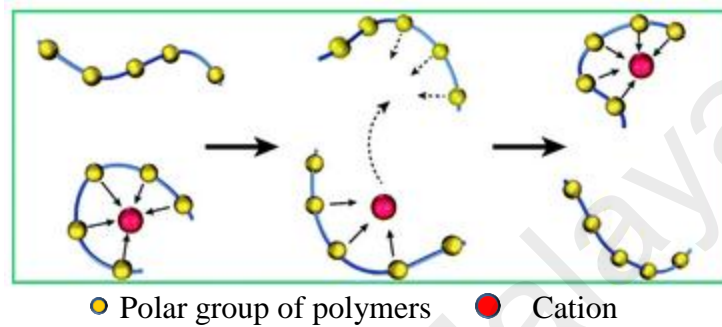
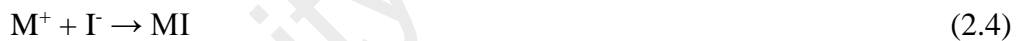


Figure 2.5: State of ions in solvent according to pair-ions model (Wang, 2009).

The reactions involved in the dissociation of salts are as follows:



In this process, reaction (Equation 2.3) usually dominates over reaction (Equation 2.4) when the salt concentration is low and ionic conductivity can still increase with salt concentration until an optimized condition. In this example, MI is metal iodide. Nevertheless, in the high salt concentration GPEs, the solvated ions could form contact ions. In this case, the equilibrium shifts from right to left i.e., the reaction (Equation 2.4) dominates over the reaction (Equation 2.3). Contact ions are disadvantageous in the GPEs as they cannot move freely, and they do not contribute to ionic conductivity. Therefore, it diminishes the GPE performance resulting in reduced DSSC efficiency. The high concentration of salts in the GPE also lead to reduced mobility of polymer chains movement and phase disengagement of polymer and liquid electrolytes that results in the ions to remain static in the liquid electrolyte instead of in motion.

2.4.1.4 Size of the inorganic cation of iodide salts

Some researchers studied to find the best salt candidate for the electrolytes by altering the cation (Shi et al.). They investigated influence of the cations with various charge densities such as lithium, sodium, potassium on the photo-voltaic performance of DSSCs. They found that the photo-voltage of the cells increased with the decrease of cationic charge density which is mainly related with the negative shift of the conduction band edge of TiO₂. It is established that the conductivity mainly depends on the ionic strength. In GPEs, the ionic size as well as their charge density have intense effects on both the ionic strength and conductivity. Shi and co-workers (Shi et al.) studied a series of GPEs with five different alkali metal iodide salts (LiI, NaI, KI, RbI and CsI) and applied in DSSCs to understand the effect of cation size on DSSCs performance. The ionic conductivity of the electrolytes with larger cations, K⁺, Rb⁺ and Cs⁺, showed higher values and basically constant (around 2.6 mS cm⁻¹ at 20 °C) (Bandara et al., 2016) whereas for the other smaller cations (Na⁺ and Li⁺) lower conductivity was exhibited for the PAN based GPEs.

2.4.1.5 Length of side chains of the organic iodide salts

The chain length of the organic cations of the salts is essentially important for the ionic conductivity. The ionic conductivity of the GPEs could drop if the organic cationic chain length is increased (Mortazavi et al., 2013). This is because the longer chain length of the salt cation can increase the viscosity, the van der Waals forces of attraction and reducing ion diffusion. It can be expected that DSSCs with GPEs containing long chain length cation exhibit lower efficiency (Mortazavi et al., 2013). In GPEs with long chain salt cation, the electron lifetime could be increased and thus the electron diffusion coefficient could decrease. Suryanarayanan et. al. reported the PVDF-HFP based GPEs composed of imidazolium ionic liquids (IILs) with different carbon chain lengths containing DSSCs where the performance of DSSCs was observed to decrease with increase in carbon chain

lengths (C_3 to C_7) of ILs (Suryanarayanan et al., 2007). Table 2.4 shows some imidazolium based ILs with their chemical structures.

Table 2.4: some ILs with their chemical structures.

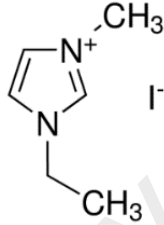
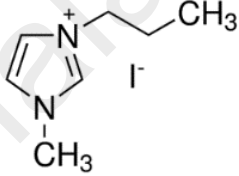
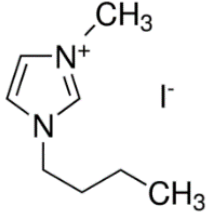
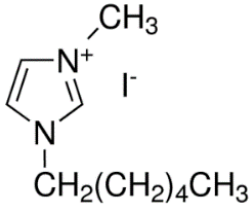
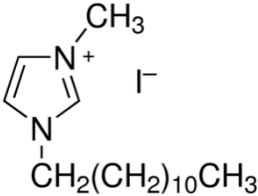
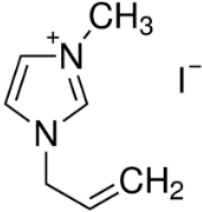
Chemical name	Chemical structure
1-Ethyl-3-methylimidazolium iodide	
1-Propyl-3-methylimidazolium iodide	
1-Butyl-3-methylimidazolium iodide	
1-Hexyl-3-methylimidazolium iodide	
1-Dodecyl-3-methylimidazolium iodide	

Table 2.4, continued.

Chemical name	Chemical structure
1-Allyl-3-methylimidazolium iodide	

2.4.1.6 Organic solvent

The solvent is an important component of electrolytes for the electrochemical devices such as DSSCs, Li⁺ ion batteries etc. It is significantly essential to study the influence of solvents on the DSSCs' photovoltaic performance either in liquid electrolyte or in gel electrolyte developed by solidification of liquid electrolyte with polymer materials (Fukui et al., 2006; Hara et al., 2000; Wu et al., 2006). Lewis acid-base type of interaction occurred between the polymer/solvent and salts in the polymer electrolyte matrix which is the determining factor for ionic conductivity of GPEs that governs the DSSCs' photovoltaic performance in terms of V_{oc} , J_{sc} and FF .

Wu and co-workers (Wu et. al., 2012) reported poly(acrylic acid)-oligo-(ethylene glycol) polymer based N-methyl pyrrolidone- γ -butyrolactone based GPEs with 0.5 M NaI and 0.05 M I₂. The ionic conductivity was 4.45 mScm⁻¹. Subsequently, adding another 0.4 M of the pyridine additive, the electrolyte showed DSSCs' efficiency of 4.74 % (AM 1.5) (Wu et al., 2007).

2.4.1.7 Temperature

Generally, the ionic conductivity rises with the rise of temperature. The Arrhenius equation can represent dependence of conductivity on temperature following:

$$\sigma = A \exp(-E_a/RT) \quad (2.5)$$

where, E_a , R , A and T are the activation energy, molar gas constant, constant and absolute temperature.

The conductivity change is the function of the ions' thermal hopping frequency at which an ionic mobility involves intermolecular ion hopping (Baskaran et al., 2006). The conductivity-temperature relationship of the GPEs is also dependent on the free-volume model in which the polymer matrix has large amorphous phase free-volume cages. At higher temperature, more spaces are created due to the increased kinetic motion leading to more movable ions and results in higher ionic conductivity in the GPEs.

2.4.1.8 Addition of room temperature ionic liquid (RTIL)

Paul Walden synthesized ionic liquids or molten salts in 1914. It was done by neutralizing ethylamine with concentrated nitric acid. The yield was ethylammonium nitrate ([EtNH₃][NO₃]). One of the popular IL cations used is the imidazolium ion first synthesized in the eighties by Hussey and coworkers. However, these imidazolium ionic liquids were very sensitive to moisture, which would react with its main component, chloroaluminate (AlCl₃). The stable imidazolium ILs to air and moisture were first synthesized in 1992, using nitrate, tetrafluoroborate and acetate anions. Due to the effort of these researchers, more stable ionic liquids are now available. Nowadays, the ionic liquids were synthesized with fluorinated anions such as hexafluorophosphate (PF₆) and bis(trifluoromethylsulfonyl)imide (N[CF₃SO₂]₂⁻ or TFSI). These anions could largely reduce water solubility. However, some of these ILs still absorb moisture. Table 2.5 and Table 2.6 show some cations and anions of ILs, respectively.

Table 2.5: Commonly used cations that comprise ionic liquids Common Cations Structures.

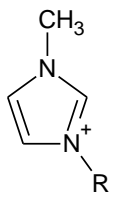
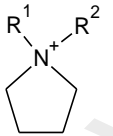
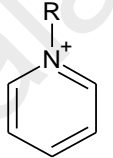
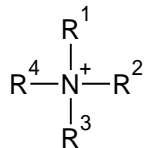
Name of Cations	Chemical structures
1-alkyl-3-methylimidazolium	
N-alkyl-N-methylpyrrolidinium	
N-alkyl-pyridinium	
Tetra-alkyl-ammonium	

Table 2.6: Commonly used anions that comprise ionic liquids Common Anions Structures

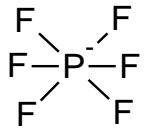
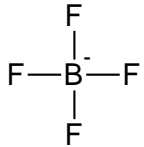
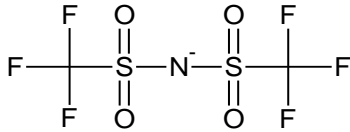
Chemicals	Structural formula
Hexafluorophosphate	
tetrafluoroborate	

Table 2.6, continued.

Chemicals	Structural formula
Bis(trifluoromethylsulfonyl)imide	
Other halogens	X ⁻

Generally, the IL has low melting point. This is typically because of having large anionic size in the ILs. The anions are large with very flexible organic groups and largely delocalized charges. These phenomena cause minor lattice energy exchange for crystallization as well as the melting entropy change is much larger. For this reason, the preferable state is liquid. On the other hand, the metal salts such as KI, LiI etc. have small sized anions which can easily be packed into the crystal lattice results high charge density and very strong electrostatic force of attractions between anions and cations. That is why metal salts prefer solid like structure. Many authors reported that the performance of the polymer electrolytes especially in terms of ionic conductivity could be improved if IL is incorporated. Costa and co-workers observed that that the BmImPF₆ IL enhanced the ionic conductivity of PEGdME from $8 \times 10^{-6} \text{ S cm}^{-1}$ to $3 \times 10^{-4} \text{ S cm}^{-1}$ (Costa et al., 2007). The improvement of electrochemical performance of the polymer electrolytes could lead to boost of the electrochemical device performance. For example, Liew et al has used PVA blended with BmImBr in super capacitor and achieved enhancement of the voltage and the life cycle of the device (Liew et al.). Furthermore, ionic liquids incorporation can also stabilize the lithium metal reduction in Li⁺ ion battery which improves the ionic conductivity and shelf lifetime. Thus, since ILs can enhance the performance of different electrochemical applications we would expect that incorporating the ILs into our GPEs could also improve the DSSCs performances. Other than the high ionic conductivity, IL can widen the electrochemical window and improve thermal stability. For example, Nath

and co-workers used ionic liquid into the polymer electrolytes for enhancing thermal stability (Nath & Kumar). In addition, some studies show that addition of IL into the electrolytes could improve the electrolyte-electrode interfacial reactions.

2.5 Summary of the chapter

In this chapter, the current literatures associated with solar energy, solar cells, dye-sensitized solar cells (DSSCs), liquid electrolytes, polymer electrolytes, solid polymer electrolytes, gel polymer electrolytes, room temperature ionic liquid electrolytes and incorporation in electrolytes etc. have been discussed. It has also discussed the development of DSSCs. The chapter has also discussed factors that could affect ionic conductivity and the photovoltaic performance of DSSCs.

University of Malaysia

CHAPTER 3: METHODOLOGY

3.1 Introduction to the chapter

This chapter will discuss on the materials and chemicals used in this work in its first part. After that, the GPEs preparation technique, working and counter electrodes development procedure will be described. Subsequently, the fabrication procedure of DSSC will be discussed. Then it will proceed on discussing the characterizations of GPEs such as electrochemical impedance spectroscopy (EIS), linear sweep voltammetry (LSV), structural studies (XRD) etc. Finally, DSSCs characterizations such as photovoltaic (J-V) characterization, quantum efficiency or incident photon to electron conversion efficiency (IPCE) measurement, intensity modulated photocurrent spectroscopy (IMPS) and intensity modulated photovoltaic spectroscopy (IMPS) will be discussed.

3.2 Materials

All the materials used in this research are listed in Table 3.1.

Table 3.1: Chemical structures of materials used in the research.

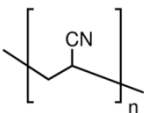
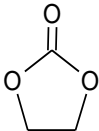
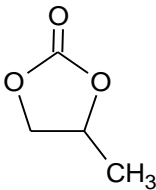
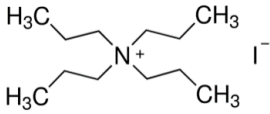
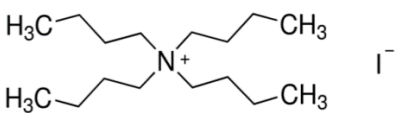
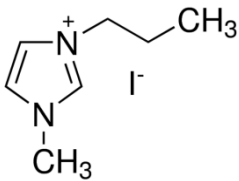
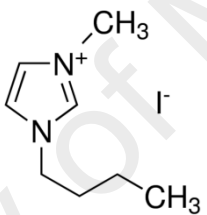
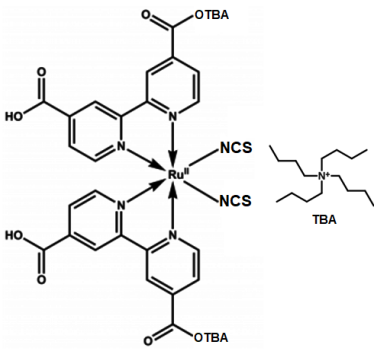
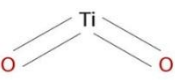
Chemicals	Chemical structures	Company
Polyacrylonitrile (PAN)		Sigma-Aldrich
Ethylene carbonate (EC)		Merck
Propylene carbonate (PC)		Merck

Table 3.1, continued.

Chemicals	Chemical structures	Company
Tetrapropylammonium iodide (TBAI)		Sigma-Aldrich
Tetrabutylammonium iodide (TBAI)		Sigma-Aldrich
1-Propyl-3-methylimidazolium iodide		Sigma-Aldrich
1-Butyl-3-methylimidazolium iodide		Sigma-Aldrich
Iodine	I-I	Friendemann Schmidt
Di-tetrabutylammonium <i>cis</i> -bis(isothiocyanato)bis(2,2'-bipyridyl-4,4'-dicarboxylato)ruthenium(II)		Sigma-Aldrich
Titanium dioxide		Degussa Germany

3.3 Research layouts

The research began with the optimization of the organic salt tetrapropylammonium iodide composition in the PAN:EC:PC:TPAI:I₂ GPEs systems. This led us to wanting the understanding of the polyacrylonitrile (PAN) based TPAI incorporated and subsequently RTILs blended GPEs through electrochemical, ion conduction, electro-catalytic and crystallographic studies (XRD). It is hoped that these studies will help to design DSSCs and determine their characteristics via current density-voltage relationship (*J-V*), incident photon-to-current efficiency (IPCE), intensity-modulated photocurrent spectroscopy (IMPS) and intensity-modulated photovoltage spectroscopy (IMVS). Then the TPAI salt was replaced by tetra-butylammonium iodide (TBAI) salt to observe the effect of alkyl chain length attached to the N-atom of quaternary ammonium iodide salt on the GPEs as well as DSSCs performances. To enhance the efficiency of DSSC further, room temperature ionic liquid propyl-methyl-Imidazolium iodide (PMII) was incorporated into the GPEs and optimized the proper ratio by the way of ionic conductivity measurements. Finally, the PMII was replaced by butyl-methyl-Imidazolium iodide (BMII) to check whether the size of alkyl chain length of ILs have any influence on the GPEs and DSSCs.

The following systems of gel polymer electrolytes have been prepared and studied

1. PAN:EC:PC:TPAI:I₂
2. PAN:EC:PC:TBAI:I₂
3. PAN:EC:PC:TPAI:PMII:I₂
4. PAN:EC:PC:TPAI:BMII:I₂

3.4 Preparation of Gel Polymer Electrolytes

The GPEs were prepared following the composition tabulated in Tables 3.2 to 3.5 for four different sets of polymer systems. The ratio of the solvent/plasticizer: EC (1.5 g)/PC (1.5 g) was kept constant (1:1). The ratio of iodide salt to iodine in molar weight was taken as 10:1. In order to gelatize PAN, EC and PC were used as plasticizer. These were

heated with constant stirring. I₂ was added to create the redox mediator. The EC and PC were mixed and stirred in a glass bottle and heated between 110 and 120°C. PAN polymer was then added with continued stirring and heating. After obtaining a homogenous solution, salt was added and stirring at the same temperature was continued for another 4 to 6 h until homogenous. The solution was then kept without agitation for cooling and PAN:EC:PC:TPAI (or TBAI) gel formation. Once the GPE has formed, an appropriate amount of I₂ was added to the mixture for providing the I⁻/I₃⁻ redox mediator. Stirring was again continued at 60 °C to get a homogenous mixture. The sample was then cooled to room temperature and kept undisturbed for gel formation. The final GPEs were used for further studies. For the formation of IL blended GPEs, the calculated amount of IL was added before I₂ addition and the same procedure was followed. Figure 3.1 presents the step by step preparation procedure of GPEs and Figure 3.2 shows a set of prepared GPEs. Once the GPEs were prepared, all the characterizations were performed. The DSSCs were then fabricated based on these GPEs and device characterization carried out.

Table 3.2: Composition of the PAN:EC: PC: TPAI:I₂ gel polymer electrolytes.

% TPAI	PAN (g)	EC (g)	PC (g)	TPAI (g)	I ₂ (g)
10	0.51	1.92	1.92	0.50	0.034
20	0.35	1.30	1.30	0.75	0.052
30	0.27	1.02	1.02	1.00	0.069
40	0.22	0.84	0.84	1.25	0.086

Table 3.3: Composition of the PAN:EC: PC: TBAI:I₂ gel polymer electrolytes.

% TBAI	PAN (g)	EC (g)	PC (g)	TBAI (g)	I ₂ (g)
10	0.51	1.92	1.92	0.50	0.034
20	0.35	1.30	1.30	0.75	0.052
30	0.27	1.02	1.02	1.00	0.069
40	0.22	0.84	0.84	1.25	0.086

Table 3.4: Composition of the PAN:EC:PC:TPAI:PMII:I₂ gel polymer electrolytes.

wt % PMII	PAN (g)	EC (g)	PC (g)	TPAI (g)	PMII (g)	I ₂ (g)
4	0.27	1.02	1.02	1.00	0.14	0.069
6	0.27	1.02	1.02	1.00	0.21	0.069
8	0.27	1.02	1.02	1.00	0.29	0.069
10	0.27	1.02	1.02	1.00	0.37	0.069
12	0.27	1.02	1.02	1.00	0.46	0.069

Table 3.5: Composition of the PAN:EC:PC:TPAI:BMII:I₂ gel polymer electrolytes.

wt % BMII	PAN (g)	EC (g)	PC (g)	TPAI (g)	BMII (g)	I ₂ (g)
4	0.27	1.02	1.02	1.00	0.14	0.069
6	0.27	1.02	1.02	1.00	0.21	0.069
8	0.27	1.02	1.02	1.00	0.29	0.069
10	0.27	1.02	1.02	1.00	0.37	0.069
12	0.27	1.02	1.02	1.00	0.46	0.069

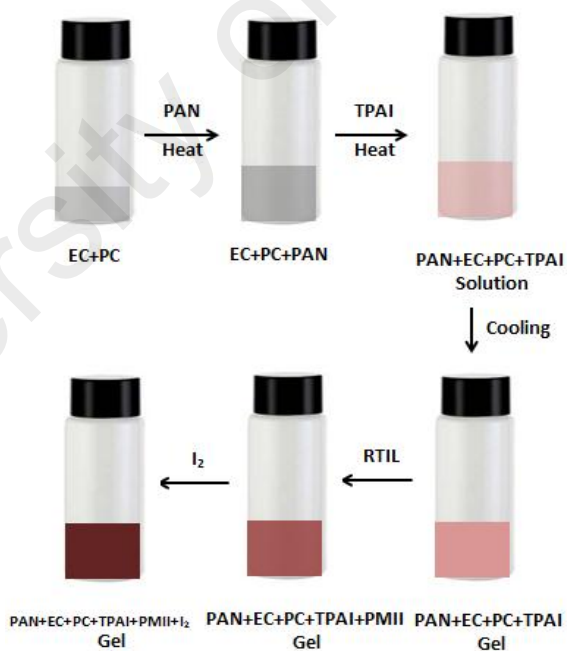


Figure 3.1: Schematic diagram of GPEs preparation.



Figure 3.2: Gel polymer electrolytes.

3.5 Characterization of the Gel Polymer Electrolytes

After the preparation of the GPEs different characterizations have been performed. The techniques that have been employed for characterization are as follows:

1. Electrochemical Impedance spectroscopy (EIS)
2. Linear sweep voltammetry (LSV)
3. X-ray Diffraction spectroscopy (XRD)

3.5.1 Electrochemical Impedance Spectroscopy (EIS)

The HIOKI 3532-50 LCR Hi-Tester was used to measure impedance of the GPEs from 50 Hz to 1 MHz from room temperature 30 °C to 100 °C. To measure the current, a small sinusoidal potential was applied across the samples. The applied voltage was as small as 10 mV. The GPEs were placed between two stainless-steel blocking electrodes. Negative imaginary impedances were plotted against real impedance in a Nyquist diagram. For each single frequency, there is a corresponding set of complex impedance, Z^* values. From the values of Z^* , real impedance, Z' and imaginary impedance, Z'' were acquired.

The Z' and Z'' values were estimated using the following equation

$$Z' = |Z(\omega)|\cos\theta \quad (3.1)$$

$$Z'' = |Z(\omega)|\sin\theta \quad (3.2)$$

The complex impedance data, Z^* can be defined by its real, Z' and imaginary, Z'' part by the following equation:

$$Z^* = Z' - iZ'' \quad (3.3)$$

where, i is $\sqrt{-1}$.

3.5.1.1 Ionic Conductivity measurement

The bulk resistance, R_b , was acquired from the intercept of the Nyquist plot to the real impedance axis. The following equation was used to calculate electrical conductivity, σ , of the samples (Wen et al., 2002):

$$\sigma = \frac{t}{A \times R_b} \quad (3.4)$$

Here, t is the sample thickness and A is the electrode–electrolyte contact area.

3.5.1.2 Calculation of activation energy (E_a) for ion conduction

The plot of $\ln\sigma$ versus $1000/T$ shows a straight line following equation (3.5) with negative slope for all the GPEs in this study. The equation is a Arrhenius type equation of the form:

$$\ln\sigma = -\frac{E_a}{RT} + \ln C \quad (3.5)$$

where, σ represents ionic conductivity, E_a activation energy, R molar gas constant, T absolute temperature and C the pre-exponential factor.

3.5.2 linear sweep voltammetry (LSV)

Linear sweep voltammetry as well as cyclic voltammetry is a potential technique to characterize electrocatalytic activity of electrocatalysts (Wu et al., 2012). A symmetrical thin-layer dummy cell with 53 μm thickness was used for the measurement of limiting current (steady state current) densities, which was constituted of two platinized counter electrodes separated by Scotch tape of 53 μm (Kontos et al., 2006; Zheng et al., 2013). Linear sweep voltammetry (LSV) technique can be used to measure the apparent diffusion

coefficient of triiodide (I_3^-) ion, $D_{I_3^-}^*$. From the LSV data, the following parameters can be obtained.

1. Limiting current density, J_{lim} : The maximum current density that can be used to get a desired electrode reaction without undue interference, such as may come from polarization.
2. Exchange current density, J_0 : The exchange current density is the current in the absence of net electrolysis and at zero overpotential. The exchange current can be thought of as a background current to which the net current observed at various overpotentials is normalized.

3.5.2.1 Limiting current density, J_{lim}

In this experiment the applied voltage was swept from - 0.6 V to 0.6 V at the slow rate of 10 mV/s for capturing the LSV data. The $D_{I_3^-}^*$ was determined by measuring the diffusion-limited current, J_{lim} . The electrochemical reaction at the Pt/electrolyte interface due to the application of potential is:



Figure 3.3 is a schematic diagram of linear sweep voltammetry curves. It is to be noted that the limiting current is for triiodide ions as iodide concentration is greater than the concentration of I_2 in the mixture (Papageorgiou et al., 1996). Hence, limiting current densities (J_{lim}) can only be used to determine the apparent diffusion coefficient of triiodide, $D_{I_3^-}^*$ according to the following relation:

$$J_{lim} = \frac{2nFC_0D_{I_3^-}^*}{d} \quad (3.7)$$

where $n = 2$ is the number of electrons required for the reduction of a triiodide ion to iodide. C_0 is the initial triiodide ion concentration. The thickness of the cell is d (53 μm) and F is Faraday's constant.

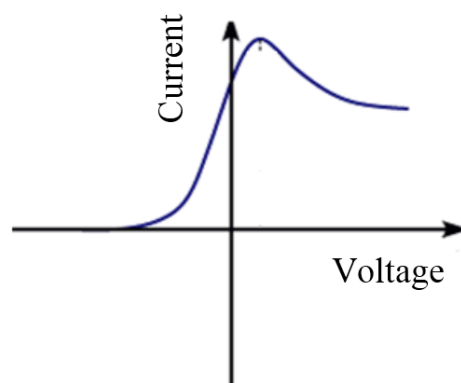


Figure 3.3: Schematic diagram of a linear sweep voltamogram.

3.5.2.2 Exchange current density, J_0

From the LSV measurements, the exchange current density, J_0 has also been estimated using Tafel polarization technique. The linear sweep voltammetry (LSV) curves obtained from symmetrical cells have been converted to logarithmic current-voltage ($\text{Log } J$ - V) Tafel polarization curves (Figure 3.4) (Bard et al., 1980). Tafel curves have been divided into three zones: (1) polarization region, $V < 120$ mV, (2) Tafel zone, 120 mV < 400 mV and (3) diffusion zone, $V > 400$ mV (Bard et al., 1980) as shown in Figure 3.4. The J_0 can be obtained by extrapolating the anodic or cathodic curves in its Tafel zone and the cross point at 0 V.

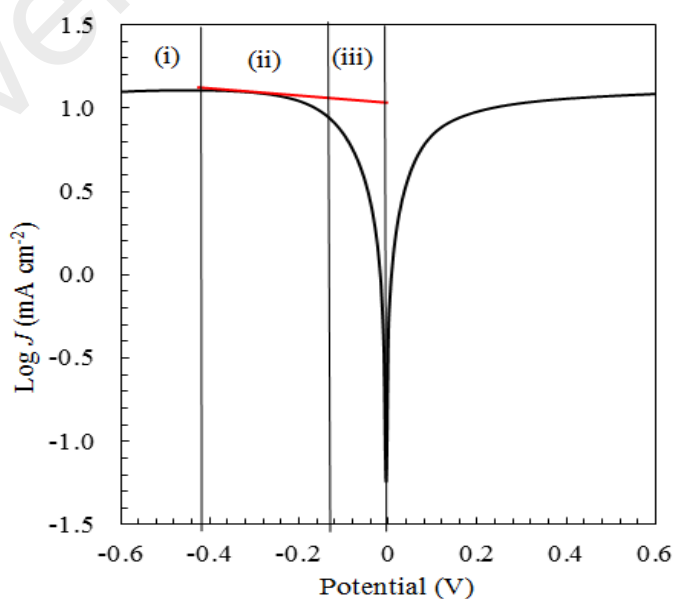


Figure 3.4: Tafel polarization curve.

3.5.3 X-ray Diffraction (XRD) study

X-ray scattering technique is a non-destructive analytical technique that unveils information about the crystal structure, chemical composition, and physical properties of materials and thin films. In XRD one can observe the scattered intensity of an X-ray beam hitting a sample as a function of incident and scattered angle, polarization, and wavelength or energy. The cathode ray tube generates X-rays which is filtered by a monochromator producing monochromatic radiation that will be focused toward the sample after collimation. If the Bragg's Law ($n\lambda=2d \sin\theta$) is satisfied, interaction between the impinging rays and the sample yields constructive interference as well as a diffracted ray. The Bragg's Law expresses the relationship between of wavelength of electromagnetic radiation, diffraction angle and the lattice spacing in the crystalline material. All possible lattice diffraction directions of the material can be obtained by scanning the sample within a range of 2θ angles. The material can be identified by transferring the diffraction peak to d-spacing as each material has a set of peculiar d-spacing which is compared with standard reference patterns.

3.6 Fabrication of DSSC

Before assembling the DSSC, some components must be prepared. These include preparation of working electrode, counter electrode and electrolyte are major tasks. Detailed description for the preparation of working electrode and counter electrode will be presented here.

3.6.1 Preparation of the working electrodes

Fluorine doped tin oxide (FTO) conductive glass was utilized to prepare both working electrodes (photoanode) and counter electrode. For the working electrode, nanocrystalline TiO_2 particles were coated on the FTO glass in two thin layers. According to the Lu et al. (Lu et al., 2015) the optimum thickness of compact layer (c- TiO_2) is 10

nm. The first layer is a compact layer with thickness $\sim 8\mu\text{m}$ and on top of this a mesoporous layer with thickness $\sim 10\mu\text{m}$ is decorated (Hagfeldt et al., 2010). Prior to use, the FTO glasses were cleaned with distilled water followed by ethanol. To prepare a thin TiO_2 compact layer, TiO_2 (P90) paste was spin-coated at 2650 rpm for 60s on the conducting surface of FTO. For the paste preparation, 0.5 g of P90 TiO_2 powder was ground well for ~ 30 min with ~ 2 ml of HNO_3 (pH=1) in an agate mortar. During the spin-coating a part of the glass plate was covered with adhesive tape to prevent coating TiO_2 on the part needed for electrical contacts. After drying in air for ~ 30 min, the coated substrate was sintered at 450°C for ~ 30 min. The second layer of TiO_2 (P25) paste was prepared by mixing 0.5 g of TiO_2 (P25) powder with 2 mL HNO_3 (6N), 0.1 g carbowax and 1-2 drops of surfactant through 30 min grinding. The paste was doctor-bladed on the compact layer followed by sintering at 450°C for 30 min. Sometimes polyethelenglycol (PEG) was used in the paste to get crack free photoanode (Dhungel & Park, 2010; Mistler & Twiname, 2000; Zulkifili et al., 2015). Figure 3.5 displays some steps of working electrode preparation.

TiO_2 (P25) is as anatase: rutile mixture with ratio (80:20). The crystallite size of an anatase NPs is 17.9 nm and that of rutile is 1.8 nm. Specific surface area is $50\text{ m}^2/\text{g}$ (Haque et al., 2005; Hidalgo et al., 2002; Peiró et al., 2006). Similarly, TiO_2 (P90) is the mixture of anatase and rutile forms with ratio (92:8). The crystallite size of anatase is 10.4 nm and that of rutile is 53.4 nm. Specific surface area is $91\text{ m}^2/\text{g}$ (Peiró et al., 2006) (Chen et al., 2011).

The TiO_2 photoanode immersed in 0.3 mM ethanol solution of N719 [Di-tetra-butylammonium *cis*-bis(isothiocyanato)bis (2,2'-bipyridyl-4,4'-dicarboxylato) ruthenium(II)] dye for 24 h. The Pt counter electrode was prepared by spin-coating

chloroplatinic acid (1 mM) ($\text{H}_2\text{PtCl}_6 \cdot 6\text{H}_2\text{O}$, Aldrich, 99.9 %) in 2-propanol (Aldrich, 99.7 %).

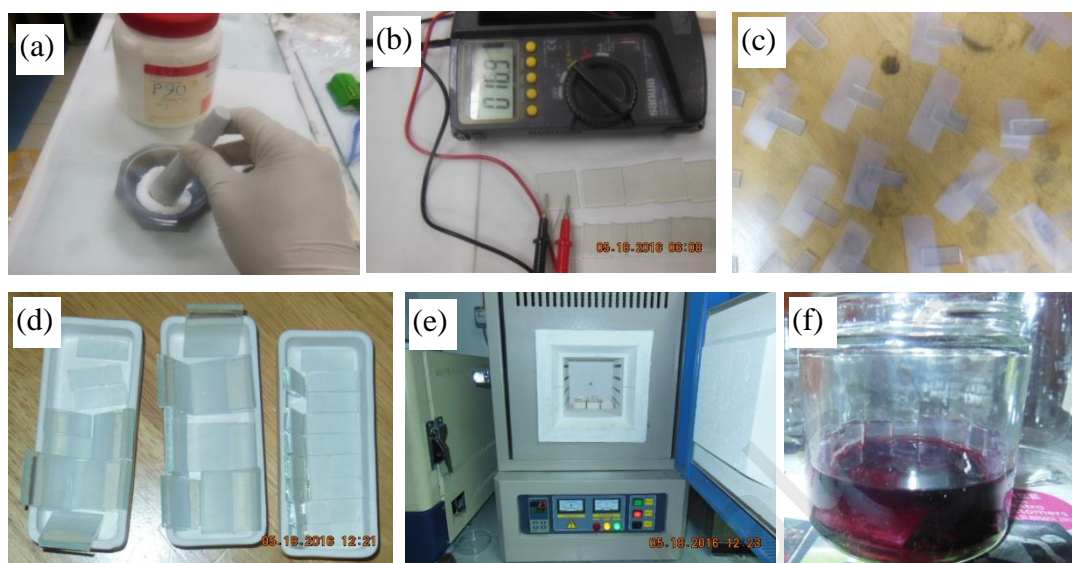


Figure 3.5: Preparation of working electrode (a) grinding of TiO_2 powder, (b) checking conducting side of the FTO glass, (c) partial masking of FTO glass, (d) dried TiO_2 coated FTO glass, (e) TiO_2 coated FTO glass into the furnace for sintering and (f) soaking of TiO_2 coated FTO glass into dye solution.

3.6.2 Preparation of the counter electrodes

For the preparation of Pt-counter electrode, chloroplatinic acid solution (H_2PtCl_6) and isopropyl alcohol ($\text{C}_3\text{H}_7\text{OH}$) were mixed in the weight ratio of 1:1. The solution ($\text{H}_2\text{PtCl}_6 + \text{C}_3\text{H}_7\text{OH}$) was dropped on the cleaned FTO glass substrate surface and air-dried. Then, the coated FTO glass was sintered at $100\text{ }^\circ\text{C}$ for 5 minutes and followed by $500\text{ }^\circ\text{C}$ for another 30 minutes. After sintering, the Pt-counter electrode was gently washed with ethanol. For thicker Pt-cathod the procedure was repeated 3 to 4 times.

3.6.3 Fabrications of the DSSCs

Utilizing these TiO_2 working electrode, GPEs and Pt-counter electrode, the DSSC was assembled which is shown in Figure 3.6. Figure 3.7 (a) displays a complete DSSC. The GPE was coated on dye-sensitized TiO_2 layer followed by sandwiching together with the Pt-counter electrode. The sandwich type DSSC was assembled with binder clips. The

active area of DSSC was 0.2 cm^2 . The configuration of the cell prepared in this study was FTO/TiO₂/N719/GPE/Pt/FTO. Excess GPEs were removed. Then, characteristic photophotocurrent density-voltage (J - V) of the DSSC was performed using Metrohm AUT 85988 advanced electrochemical system (Metrohm Autolab B.V. PGSTAT 128N Netherlands) under illumination of 100 mW cm^{-2} (AM 1 sun) from a xenon lamp. For confirming the experimental reproducibility, three different replicated DSSCs with same material composition were examined and average the results were reported.

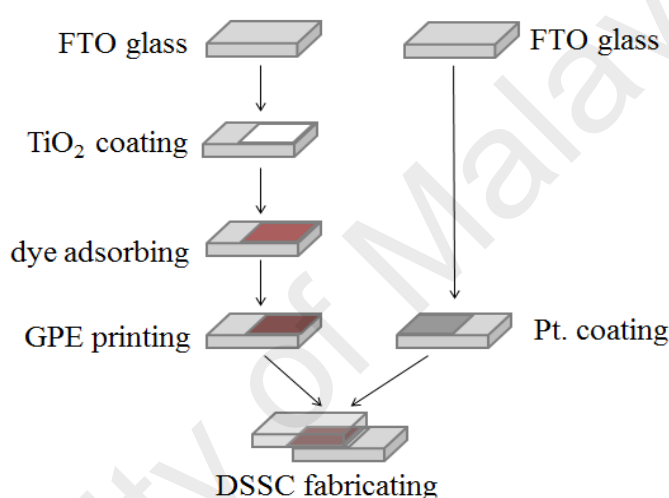


Figure 3.6: Flow chart of DSSC fabrication.



Figure 3.7: Dye-sensitized solar cell (DSSC) (a) a complete DSSC, (b) DSSC under solar simulator light and (c) DSSC characterization by AutoLab station.

3.7 DSSC characterization

DSSC characterization can be performed using various techniques. In this study the following techniques have been applied for DSSC characterization

1. Photovoltaic (J - V) characteristics

2. Incident photon-to-current conversion efficiency (IPCE)
3. Intensity-modulated photocurrent spectroscopy (IMPS) and intensity-modulated photovoltage spectroscopy (IMVS)

3.7.1 Photovoltaic (J - V) characteristics

The efficiency of DSSC was estimated from the J - V characteristics curve under the 1 sun illumination condition which is simulated as the standard solar spectrum with an intensity of 100 mW cm^{-2} . The characteristics of photophotocurrent density-voltage of DSSCs were scanned with a variable external load from zero (short-circuit condition) to infinite (open-circuit condition). The photovoltaic performance was typically demonstrated by a J - V curve as in Figure 3.8. Generally, the following parameters are estimated from the analysis of J - V plots for a DSSC.

3.7.1.1 Open Circuit Voltage (V_{OC})

The V_{OC} of the solar cell is the maximum voltage supplied by the cell which is the actual voltage without applying any load. In other words, the V_{OC} is the potential where flow of current through a solar cell is zero.

$$V_{OC} = V_{max} = V (I = 0) \quad (3.8)$$

It is a function of the semiconductor bandgap and charge recombination in the cell. It yields information on how efficiently charges are separated. For DSC the V_{oc} is given by:

$$V_{OC} = \frac{E_{CB}}{q} + \frac{kT}{q} \ln \left(\frac{n}{N_{CB}} \right) - \frac{E_{redox}}{q} \quad (3.9)$$

where, n is the number of electron in TiO_2 conduction band and N_{CB} is the effective density of states. The first two terms define the quasi-fermi level of TiO_2 and E_{redox} is the Nernst potential of the redox mediator.

3.7.1.2 Short Circuit Current (J_{SC})

J_{SC} is the maximum photocurrent of a cell per unit area (mA/cm²) when an illuminated cell is short circuited where the external output voltage is zero, that is the loading of resistance is zero. The J_{SC} yields information on how efficiently the photogenerated charges are generated. It depends on several factors such as the light intensity, light absorption, injection efficiency, regeneration of the oxidized dye, and the efficiency of charge transport in the TiO₂ film to the counter electrode. This the current measured at a free flow or $V = 0$ in the solar cell.

$$J_{SC} = J_{max} = J(V = 0) \quad (3.10)$$

3.7.1.3 Fill factor (FF)

The Fill factor (FF) is a vital parameter to estimate the overall solar cell capabilities. It expresses the solar cell's quality and perfection. It is related to the maximum power point and is often described as a measure of the "squareness" of the J - V curve and describes the degree to which the voltage at the maximum power point (V_{MP}) matches V_{OC} and that the current at the maximum power point (J_{MP}) matches J_{SC} . Fill factor is the ratio of the areas of two rectangles under the J - V curve as shown in Figure. 3.8. Moreover, its value is determined by the ratio of the maximum power ($V_{MP} \cdot J_{MP}$) to the maximum power attainable by the solar cell ($J_{SC} \cdot V_{OC}$), with a value between 0 and 1. The overall formula for the Fill Factor is:

$$FF = \frac{P_{max}}{P_{theo}} = \frac{V_{MP} \cdot J_{MP}}{V_{OC} \cdot J_{SC}} \quad (3.11)$$

V_{MP} and J_{MP} are the voltage and current of the J - V curve at which the generated power is the maximum. The FF can also be shown by the rectangles in a J - V curve (Figure 3.8). Figure 3.8 demonstrates a schematic illustration of J - V curve.

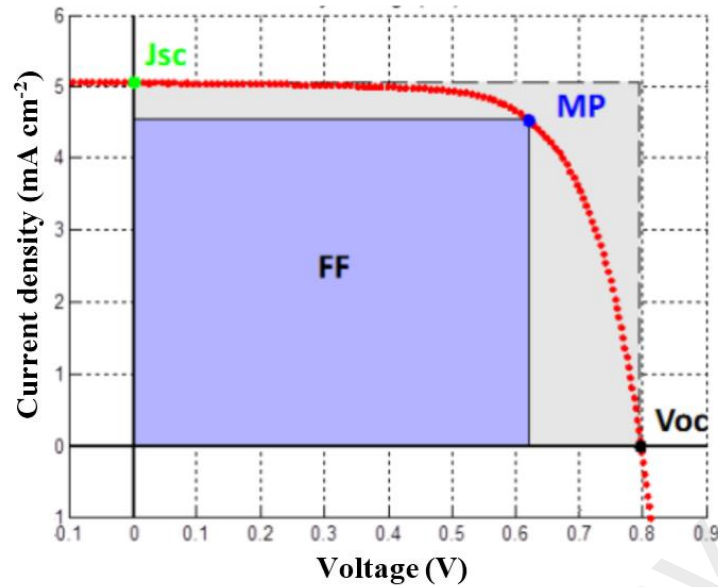


Figure 3.8: Schematic illustration of J - V curve of dye-sensitised solar cell.

In the ideal situation, the J - V curve is a rectangle (green area). The maximum power is at V_{OC} and J_{SC} and the corresponding fill factor is one. Nevertheless, non-ideal conditions due to parasitic effects in the solar cell reduce the maximum power and the J - V curve rounds off. The subsequent true area in J - V curve which evaluates the power maximum (blue rectangle) becomes smaller. This area is constituted by the voltage V_{MP} and J_{MP} .

3.7.1.4 Efficiency

The overall solar energy to electric power conversion efficiency (η), the key parameter of the device, measures how much power is converted by the cell in comparison to the amount of absorbed light that reaches the device. It is given by the ratio of the maximum output power (P_{max}) to the incident solar power (P_{in}). The overall sunlight to electric power conversion efficiency of a DSSC is given by the following expression.

$$\eta = \frac{P_{max}}{P_{in}} 100 \% \quad (3.12)$$

Thus, to optimize the efficiency of a solar cell, each of these parameters, the J_{SC} , the V_{OC} , and the FF have to be maximized.

3.7.2 Incident Photon to Charge Carrier Efficiency (IPCE)

Incident photon to charge carrier efficiency (IPCE) is also denoted as Quantum efficiency (QE) (Shaheen et al., 2001). It is the ratio of the number of charge carriers collected by the solar cell to the number of incident photons of a given energy shining on the solar cell. For the understanding of the light to electricity conversion efficiency as a function of the wavelength of the light incident on the cell, the measurement of IPCE is important. A solar cell area can be determined by number of photons instead of a shading mask. The lamp house, power supply and monochromator are placed in a unit body for easy placement on a desktop.

3.7.3 Study of electron transfer mechanism in DSSCs

IMPS and IMVS are associated to electrochemical impedance spectroscopy (EIS). In EIS, a constant potential or current signal is applied to a cell which is superimposed by an AC signal and thus the frequency is modulated. The measured sinusoidal signal has the same frequency as the applied signal, but it is phase-shifted. The frequency-dependent impedance Z can be then calculated. The operation of both IMPS and IMVS is similar. Here, the modulation of the intensity of a light beam focused on a DSSC is done instead of modulating the amplitude of a current or potential signal. Figure 3.8 illustrates both techniques.

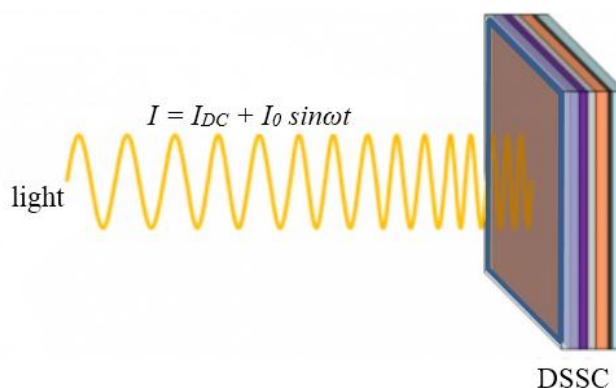


Figure 3.9: Sketch of the light signal focused on a DSSC during IMPS and IMVS.

The light beam with a base intensity I_{DC} is focused on a DSSC during IMPS and IMVS experiments. A sinusoidal waveform with amplitude I_0 is superimposed on the constant base intensity. The frequency (f) of the sine wave is changed during the experiment. The angular frequency (ω) can be expressed as $\omega = 2\pi f$. The photocurrent (IMPS) or photovoltage (IMVS) of a DSSC is measured, respectively. The resultant light signal has the same frequency as the applied signal, but its phase is shifted. By changing the frequency of the light signal, time-dependent information on various processes such as diffusion coefficients or reaction rates can be obtained.

Figure 3.9 presents J - V curves with increasing light intensity in which EIS, IMPS, and IMVS are identified. As the DSSC generated power increases with increasing light intensity, the photocurrent increases which results in a higher short-circuit current J_{SC} at 0 V. Moreover, the open-circuit potential V_{OC} also moves towards higher potentials. Normally, in photovoltaic characterization of DSSCs a constant illumination is supplied with modulating the amplitude of a current or potential signal. Only one point on a single J - V curve can be analyzed using EIS spectra. On the other hand, in IMPS and IMVS measurement, the intensity of a light beam focused on a DSSC is modulated and the cell's response as a series of J - V curves can be measured. The regions for IMPS and IMVS are highlighted in green and red in Figure 3.10.

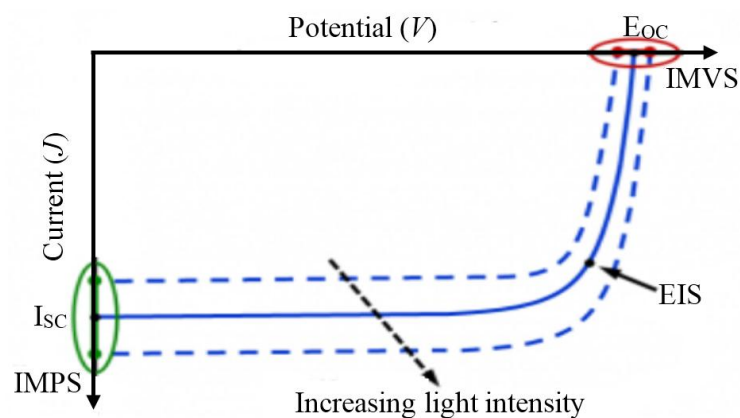


Figure 3.10: J - V curves of a DSSC showing the regions covered by EIS, IMPS and IMVS.

3.7.3.1 Intensity-modulated photocurrent spectroscopy (IMPS)

Intensity-modulated photocurrent spectroscopy (IMPS) and intensity-modulated photovoltage spectroscopy (IMVS) can provide valuable information about dye-sensitized solar cells (DSSCs). For the experiments, Metrohm AUT 85988 advanced electrochemical system (Metrohm Autolab B.V. PGSTAT 128N Netherlands) instrument was used and a red LED ($\lambda_{em} = 627$ nm) was focused on the DSSC. The base intensity of the light source has been taken as 0.03, 0.06 and 0.09 mW. The AC amplitude was set to 10 % of the applied base intensity. Frequency modulation was applied between 10 kHz and 10 mHz. During IMPS experiment, the potential of a DSSC is potentiostatically controlled and set to 0 V (short-circuit conditions) and the generated photocurrent is measured. At short-circuit conditions, the band gap between non-conductive valence band and CB of the semiconductor is maximum which results in nearly no injection of electrons into the conduction band of TiO_2 . Most reactions occurred on the back layer of the anode and electrons are migrating from the location where they are generated to the electrode's back layer. The characteristic frequency, f_{IMPS} can be obtained from the maximum point of the IMPS plot as Figure 3.11.

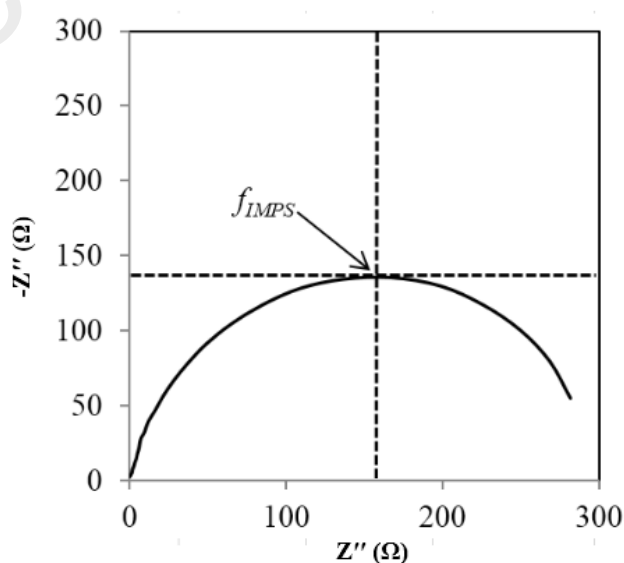


Figure 3.11: Estimation of characteristic frequency, f_{IMPS} from Nyquist type plot.

The corresponding electron transport time constant, τ_{tr} can be calculated by IMPS according to the following equation.

$$\tau_{tr} = \frac{1}{2\pi f_{IMPS}} \quad (3.13)$$

where, f_{IMPS} is the characteristic frequency which can be obtained from the Nyquist type plot of IMPS for the DSSCs.

3.7.3.2 Intensity-modulated photovoltage spectroscopy (IMVS)

Metrohm AUT 85988 advanced electrochemical system (Metrohm Autolab B.V. PGSTAT 128N Netherlands) instrument was used to perform IMVS experiments. Data have been taken under open-circuit conditions. It implies that, the cell is open and the open-circuit potential of a DSSC is measured. The open-circuit potential is the maximum potential of a DSSC before power is dissipated instead of being generated. At this point, the band gap between valence band (VB) and CB is small. Hence, the reactions on the back layer of the anode are less likely. Most of the generated photoelectrons are injected into the semiconductor's CB. Furthermore, the DSSC reaches steady-state at the open-circuit potential. This implies that the rate of electron injection into the conduction band is equal to the rate of the recombination electron. The rate of electron recombination or the electron life time τ_{rec} can be evaluated from the IMVS experimental results using the following equation.

$$\tau_{rec} = \frac{1}{2\pi f_{IMVS}} \quad (3.14)$$

where, f_{IMVS} is the characteristic frequency associated with the Nyquist type plot of IMPS for the DSSCs.

3.7.3.3 Charge-collection efficiency (η_{cc})

The time constants τ_{tr} and τ_{rec} can be used further to evaluate the charge-collection efficiency η_{cc} (Equation 3.14). This is a vital factor for the characterization of the overall performance of dye-sensitized solar cells. The higher the η_{cc} , the more efficient is the cell.

High charge-collection efficiencies can be achieved by increasing the time for electron recombination or decreasing the electron transport time.

$$\eta_{cc} = 1 - \frac{\tau_{tr}}{\tau_{rec}} \quad (3.15)$$

3.7.3.4 Electron diffusion coefficient (D)

The electron diffusion coefficient, D in the DSSC can also be estimated. At low potentials, transportation of electron is mainly restricted by its diffusion through the active electrode film with thickness L . At such low potentials, electron recombination is insignificant and only the electron transport time constant t_{tr} can be considered. Electron diffusion coefficient, D can be estimated by Equation 3.15 (Villanueva-Cab et al., 2016).

$$D = \frac{L^2}{2.54\tau_{tr}} \quad (3.16)$$

At higher potentials or in less efficient cells, electron recombination plays a crucial role. There is a competition between electron transport and recombination resulting lowering of effective electron diffusion length, L_D . The L_D can be calculated by Equation 3.16. For good efficiencies, the effective diffusion length L_D should be greater than the electrode film thickness L . This means that electrons can be efficiently collected at the electrode before they recombine.

$$L_D = \sqrt{D\tau_{rec}} \quad (3.17)$$

3.8 Summary of the chapter

This chapter has described the techniques for the preparation and characterization of GPEs. The working electrode and counter electrode development technique has been demonstrated. The DSSC fabrication procedure and related characterization are also discussed in this chapter. The results and discussion will be expressed in following chapter.

CHAPTER 4: RESULTS ON THE PAN:EC:PC:TPAI:I₂ GPE SYSTEM

This chapter describes the electrochemical, electrocatalytic and structural study of PAN:EC:PC:TPAI:I₂ GPEs. The DSSCs characteristics such as *J-V*, IPCE, IMPS and IMVS will also be discussed in this chapter.

4.1 Electrochemical impedance spectroscopy (EIS) measurement

4.1.1 Ionic conductivity study

Figure 4.1 represents the Nyquist plots showing imaginary impedance versus real impedance for PAN:EC:PC:TPAI:I₂ GPEs with varying weight percentage of TPAI (0 wt %, 10 wt %, 20 wt %, 30 wt % and 40 wt %) at different temperatures. For 0 wt % TPAI, the Nyquist plots take the form of a semicircle and GPE with TPAI salt showed only a spike in their Nyquist plots. From the Nyquist plots, the bulk resistance, R_b was estimated and used to calculate the ionic conductivity (σ) the GPEs. Table 4.1 shows the R_b and σ for the all the TPAI containing GPEs. It is evident that, the bulk impedance decreased with the increased percentage of TPAI salt showing the lowest value of 22 Ω at 30 wt % TPAI containing GPE. Consequently, σ increases with increase in TPAI concentrations and reached the highest value of 3.62×10^{-3} S.cm⁻¹ at 30 wt % TPAI and then decreased with further addition of salt.

4.1.2 Activation energy for ionic conduction

Figure 4.2 shows $\ln\sigma$ versus $1000/T$ plots, respectively for the GPEs containing different percentages of TPAI. The plot follows the Arrhenius equation (Equation 3.5). From the slope of this equation activation energy (E_a) has been calculated and tabulated in Table 4.1. The activation energy for transportation of ions decreased with TPAI percentage and is the lowest as 10.09 kJ/mol for 30 wt % TPAI containing GPE which is conceivable with the conductivity behavior.

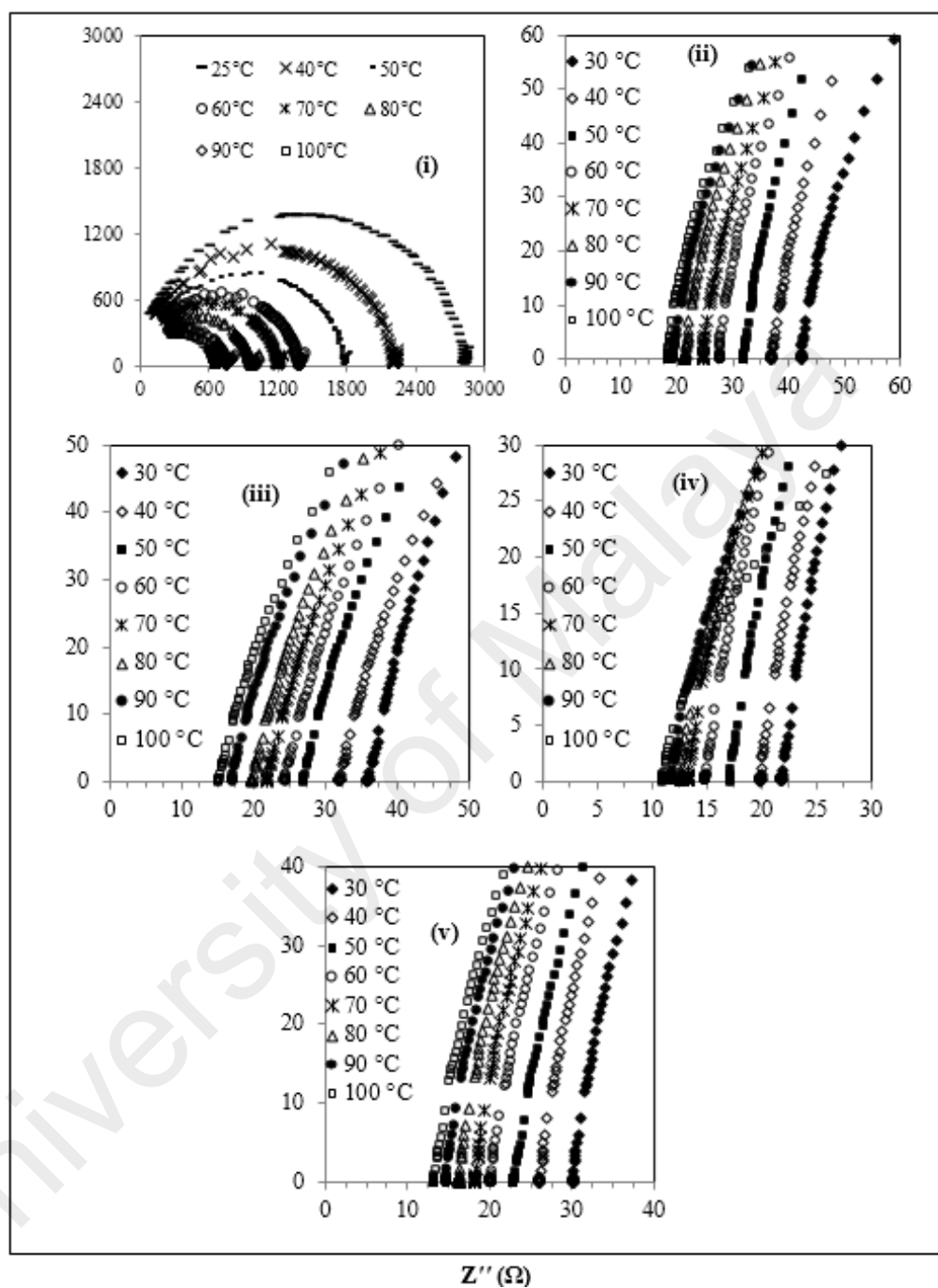


Figure 4.1: Nyquist plots for PAN:EC:PC:TPAI:I₂ GPEs: (i) 0 wt % TPAI, (ii) 10 wt % TPAI, (iii) 20 wt % TPAI, (iv) 30 wt % TPAI and (v) 40 wt % TPAI.

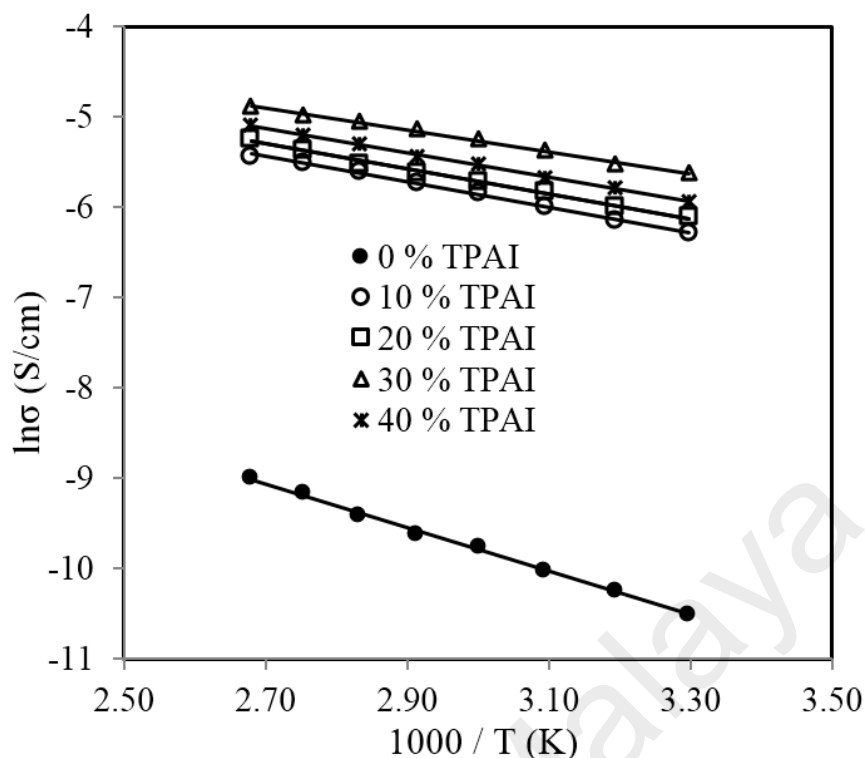


Figure 4.2: $\ln\sigma$ versus $1000/T$ graphs for different TPAI containing GPEs.

Table 4.1: Bulk impedance, R_b (ohm), ionic conductivity, $\sigma \times 10^{-3}$ (S/cm) and activation energy, E_a (eV) for ion conduction for the TPAI containing GPEs.

TPAI (wt %)	R_b (ohm)	Conductivity, $\sigma \times 10^{-3}$ (S/cm)	Activation energy	
			E_a (kJ/mol)	E_a (eV)
0	2900	0.03	19.94	0.207
10	42.00	1.89	11.73	0.122
20	36.00	2.21	11.11	0.115
30	22.00	3.62	10.09	0.105
40	30.00	2.65	11.12	0.115

4.2 Linear sweep voltammetry (LSV) measurement

4.2.1 Limiting current and I_3^- Diffusion coefficient study

Linear sweep voltammetry and cyclic voltammetry are potential techniques to characterize electrocatalytic activity of electrocatalysts (Wu et al., 2012). In the present study, we used Pt-electrode as electrocatalyst for LSV experiment. Figure 4.3 displays the characteristic linear sweep voltammetry curves for the electrolyte systems containing different compositions of TPAI. The current densities attain saturations for both polarities at above 0.3 V. The anodic and cathodic limiting current plateaus are quite similar which

indicates the equilibrium steady state conditions. It is to be noted that, as iodide salt (TPAI) concentration is greater than the concentration of I_2 , the limiting current is associated with total number of triiodide ions (I_3^-) which is equivalent to the amount of I_2 taken ($I_3^- = I_2 + I^-$) (Papageorgiou et al., 1996). All the I_2 has combined with the equivalent amount of I^- ions. Hence, limiting current density (J_{lim}) can only be used to determine the apparent diffusion coefficient of triiodide, $D_{I_3^-}^*$ according to the equation $[D_{I_3^-}^* = (J_{lim} \times d)/(2nFC_0)]$ (Equation 3.7).

The J_{lim} and $D_{I_3^-}^*$ values for TPAI containing GPE systems are tabulated in Tables 4.2. The values of J_{lim} and $D_{I_3^-}^*$ increased with increased I_2 content and were highest at 12.76 $mA\ cm^{-2}$ and $16.83 \times 10^{-7} cm^2\ s^{-1}$, respectively for 0.059g I_2 containing electrolyte with TPAI = 30 wt %. The values of $D_{I_3^-}^*$ decreased if more than 0.069g I_2 was added.

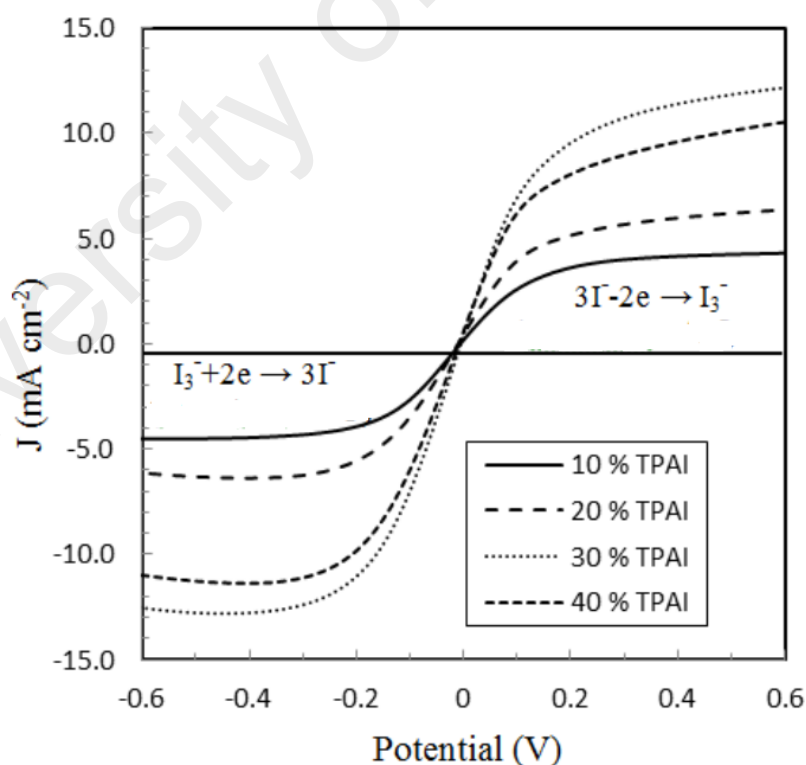


Figure 4.3: Linear sweep voltammograms (LSV) of GPEs at varying concentration of TPAI with Pt-ultramicroelectrode. Scan rate: 10 mV/s.

4.2.2 Tafel polarization curve and Exchange current density, J_0

From the LSV measurements, the exchange current density, J_0 has also been estimated using Tafel polarization technique. The linear sweep voltammetry (LSV) curves obtained from symmetrical cells have been converted to logarithmic current-voltage ($\text{Log } J\text{-}V$) Tafel polarization curves (Figure 4.4) (Bard et al., 1980). The J_0 has been obtained by extrapolating the anodic or cathodic curves in its Tafel zone and the cross point at 0 V which have been summarized in Table 4.2. The exchange current density is the current in the absence of net electrolysis and at zero overpotential. In this study, the values of J_0 are rising with the increase of TPAI concentration. At 30 wt % TPAI containing GPEs, the J_0 value is highest (11.22 mA cm⁻²).

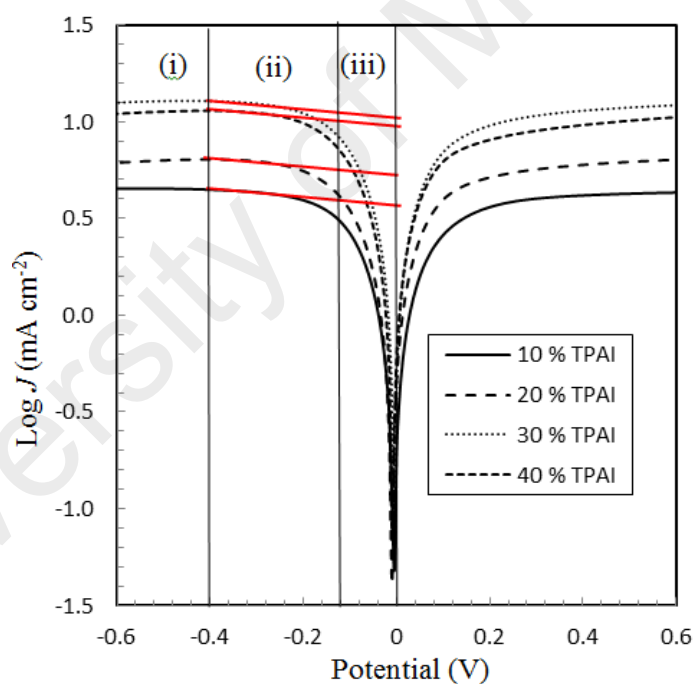


Figure 4.4: Tafel polarization curves for the electrolytes with different TPAI containing GPEs.

Table 4.2: Limiting current or steady state current (J_{lim}), diffusion coefficients of I_3^- ion ($D_{I_3^-}^*$), exchange current density (J_0) of GPEs containing different composition of iodine.

TPAI (wt %)	10	20	30	40
I_2 (g)	0.034	0.052	0.069	0.086
J_{lim} (mA cm ⁻²)	4.46	6.32	12.76	11.29
$D_{I_3^-}^*$ ($\times 10^{-7}$ cm ² s ⁻¹)	9.06	9.40	16.83	13.28
$J_0, Tafel$ (mA cm ⁻²)	3.98	5.62	11.22	10.00

4.3 X-ray diffraction (XRD) studies

To perform the structural characteristics of GPEs with different percentages of TPAI, X-ray diffraction studies were carried out. Figure 4.5 exhibits the X-ray diffraction patterns of (i) PAN and (ii) PAN:EC:PC GPE. Pure PAN has a sharp peak at $2\theta \approx 16.5^\circ$ and a broad peak at $2\theta \approx 28.7^\circ$. Figure 4.6 compiles XRD pattern of PAN:EC:PC:xTPAI: I_2 GPEs where x stands for 10 wt %, wt 20 wt %, wt 30 wt % and 40 wt %. Based on the equatorial reflections in diffraction patterns of PAN (Bohn et al., 1961; Tsai & Lin, 1991), it can be conferred that PAN has only two-dimensional order without periodicity along the chain axis. Therefore, PAN is a paracrystalline or laterally ordered polymer. PAN crystals usually show two diffraction peaks at $2\theta \approx 17$ and 29° (Herbert et al., 1993). Some authors used an orthorhombic lattice to describe the crystal structure of PAN (Colvin & Storr, 1974; Yamazaki et al., 1987). Others mentioned that dry PAN has hexagonal lattice (Tan et al., 2009). The diffraction patterns were also indexed as (010) and (300) at $2\theta \approx 17$ and 29° , respectively, on the basis of hexagonal packing of PAN molecules (Bashir, 1992, 1993). However, some authors reported that the XRD pattern of the pure PAN has semi crystalline structure and the crystalline peak at $2\theta \approx 17^\circ$ corresponds to orthorhombic (110) reflection (Rajendran et al., 2001; Sawai et al., 2000; Zhang et al., 2001).

The addition of salt (TPAI) into PAN matrix results in significant reform of XRD pattern observed in terms of (1) a systematic shifting and enlargement of the main peak

($2\theta \approx 17^\circ$) of pure PAN toward higher angle ($2\theta \approx 20^\circ$) in PAN:EC:PC: GPE and (2) generation of new peaks at $2\theta \approx 10^\circ$ and 20° for 10 %, 20 %, 30 % and 40 % TPAI containing GPEs. (Figure 4.6). An up-shifting of XRD peak is due to the increase in d-spacing of the polymer matrix which is the evidence for polymer-salt interaction due to complexation of cation (TPA^+ ion) with lone pair electron containing site ($-\text{CN}$) in the host polymer matrix. Furthermore, the addition of TPAI containing long propyl chain ($\text{CH}_3\text{-CH}_2\text{-CH}_2\text{-}$) prevents polymer chain reorganization causing significant disorder in the polymer chains that promotes the interaction between them. TPA^+ ions may break the regular arrangement of PAN polymer backbone and aggregate through non-polar hydrophobic chain initiated micellization, which severely disturbs the order of crystalline phase of polymer causing development of amorphousness in the GPEs.

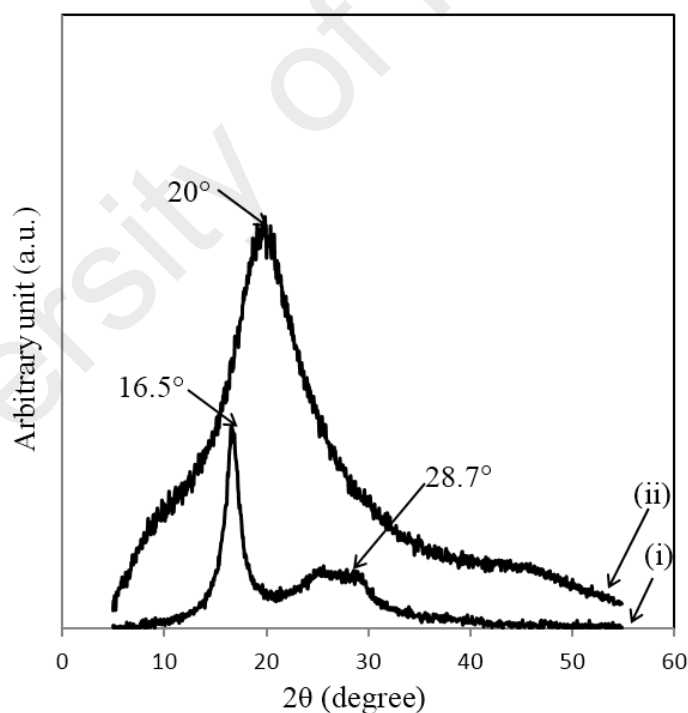


Figure 4.5: XRD pattern of (i) PAN and (ii) PAN:EC:PC GPE.

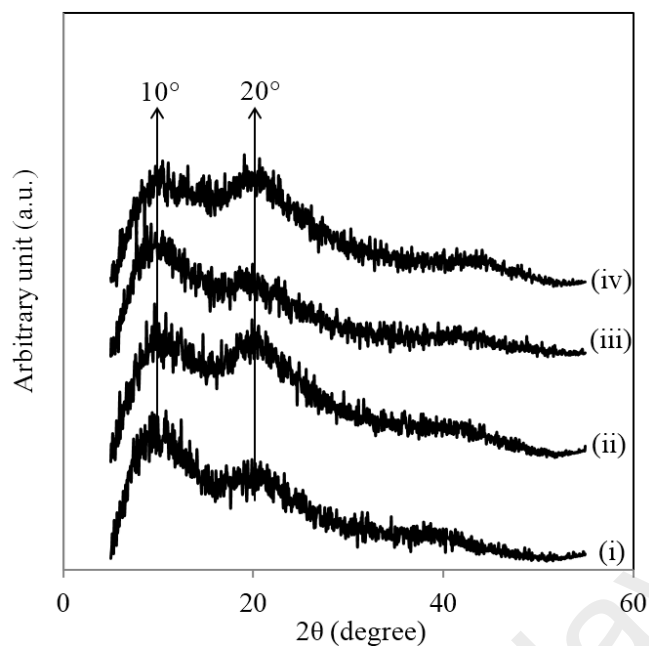


Figure 4.6: XRD pattern of (i) PAN:EC:PC:TPAI:10 wt % TPAI:I₂, (ii) PAN:EC:PC:TPAI:20 wt % TPAI-I₂, (iii) PAN:EC:PC:TPAI:30 wt % TPAI:I₂ and (iv) PAN:EC:PC:TPAI:40 wt % TPAI:I₂ GPEs.

4.4 DSSC performance analysis

4.4.1 Photovoltaic (*J-V*) characteristics

The photovoltaic characteristics, *J-V* curves for DSSCs fabricated using PAN:EC:PC gel polymer blend electrolytes with different percentages of TPAI are depicted in Figure 4.7. Table 4.3 shows the open-circuit voltage (V_{oc}), short-circuit current (J_{sc}), fill factor (*FF*) and the efficiency obtained from the *J-V* curves.

Following the similar trend of conductivity versus TPAI concentration, J_{sc} as well as efficiency (η) of DSSC increases with the addition of TPAI in the GPEs attaining the maximum of J_{sc} (19.75 mA cm^{-2}) and η (4.76 %) (Figure 4.7 and Table 4.3) for the 30 wt % TPAI and then, decrease with further addition of TPAI. The V_{oc} is also highest (553.8 mV) for 30 wt % TPAI containing GPE whereas they are almost the same for other GPEs.

Table 4.3: Photovoltaic performance of PAN:EC:PC:TPAI:I₂ with different weight contents of TPAI-added polymer electrolytes.

TPAI	J_{sc} (mA cm ⁻²)	V_{oc} (mV)	FF	η %
10 wt %	10.53	551.9	0.58	3.38
20 wt %	15.03	536.6	0.52	4.16
30 wt %	19.74	553.8	0.44	4.76
40 wt %	16.37	548.8	0.50	4.54

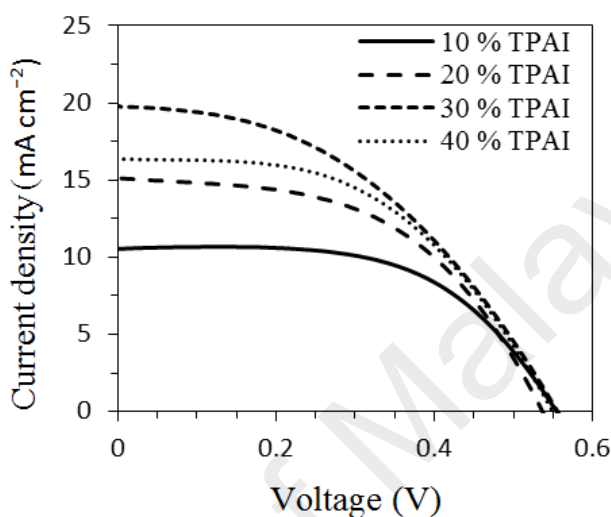


Figure 4.7: J - V curves of DSSCs for PAN:EC: PC:TPAI:I₂ GPEs systems.

4.4.2 Incident-photon-to-current efficiency (IPCE)

The incident-photon-to-current efficiency (IPCE) spectra can be used to get supporting evidence on the light-harvesting efficiency of the DSSCs. Figure 4.8 depicts the IPCE spectra as a function of wavelength from 400 to 800 nm for different DSSCs with GPEs containing various concentrations of TPAI. It is observed that the IPCE curves of the four cells display similar shape of spectrum with maximum efficiencies at 520 - 550 nm which corresponds to the absorption peak of the N719 dye (Yang Bai et al., 2012). The IPCE values for different cells follow the order as 30 wt % TPAI > 40 wt % TPAI > 20 wt % TPAI > 10 wt % TPAI at the range of visible light wavelength, which is consistent with J_{sc} order in the J - V study and conductivity trend. The DSSC fabricated using GPE with 30 wt % TPAI shows the highest IPCE value of 58.50 % among these four DSSCs.

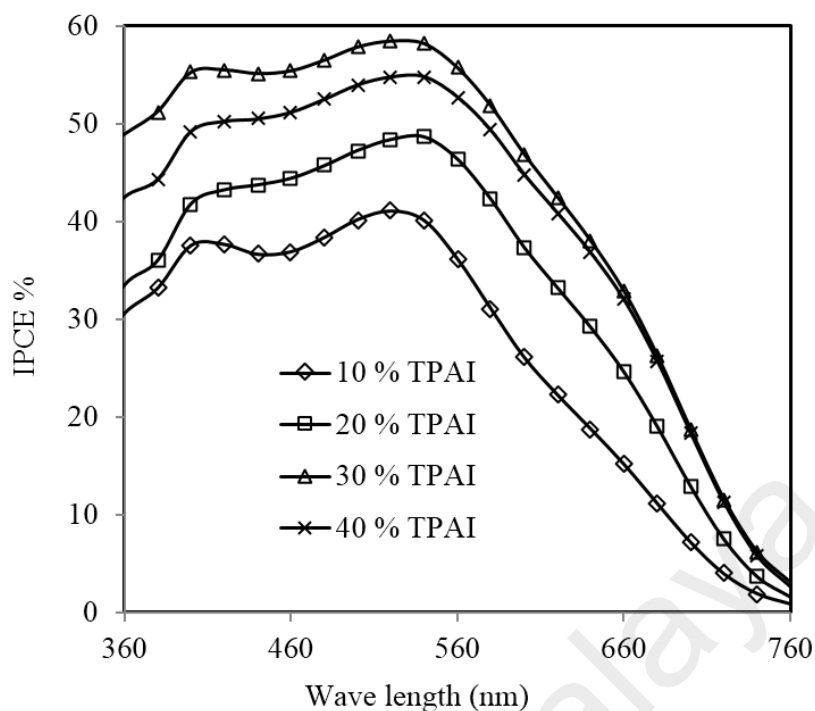


Figure 4.8: IPCE % vs. wavelength for the DSSCs with different TPAI containing GPEs.

4.4.3 IMPS and IMVS study of DSSCs

Figure 4.9 represents the IMPS results in the form of Nyquist-type plots at different base intensities (0.03, 0.06 and 0.09 mW). It is to be noted that, as the intensity increases the radius of the semicircle slightly decreases. The influence of the intensity changes on the radius of the semicircle for the IMPS is insignificant. All the curves exhibit a maximum at intermediate frequencies, f_{IMPS} which is characteristic for the electron transport through the pores of the anode to the back layer.

In Figure 4.10, IMVS experimental results have been presented as Nyquist-type plots at different base intensities (0.03, 0.06 and 0.09 mW). It is evident that, the radius of the semicircle decreases as the intensity increases. All the curves exhibit a maximum at intermediate frequencies, f_{IMVS} which is the characteristic frequency for the electron recombination causing degradation of DSSC efficiency. The values of f_{IMVS} and τ_{rec} have been tabulated in Table 4.4.

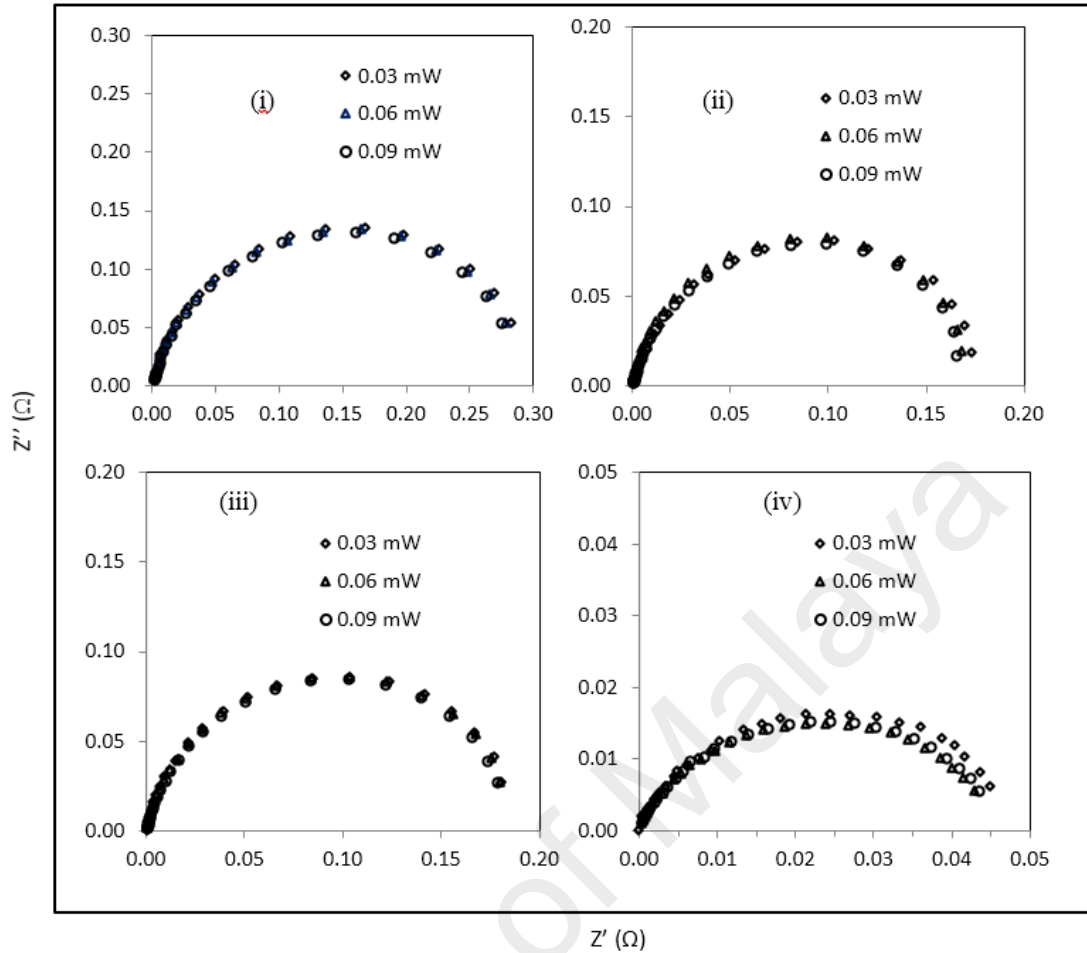


Figure 4.9: IMPS Nyquist type plots at different intensities for the DSSCs assembled with GPEs containing (i) 10 wt %, (ii) 20 wt %, (iii) 30 wt % and (iv) 40 wt % TPAI.

Among the four the one with DSSCs 30 wt % TPAI GPE show in the smallest electron transport time (τ_{tr}) value (20.05 ms) and highest recombination time (τ_{rec}) value (159.24 ms) at a given intensity which is necessary for better performance of a DSSC (Table 4.4). If $\tau_{tr} < \tau_{rec}$, the photo-excited electron is injected in to CB of TiO_2 within a very short time rather and will not undergo for recombination. The charge collection efficiencies [$\eta_{cc} = 1 - (\tau_{tr}/\tau_{rec})$] for 10 wt %, 20 wt %, 30 wt % and 40 wt % TPAI GPEs are 0.40, 0.60, 0.87 and 0.43, respectively (Table 4.5). The best charge collection efficiency η_{cc} (0.87) is observed for the 30 wt % TPAI GPE based DSSC. Furthermore, the electron diffusion coefficient (D) [$D = (L^2/2.35\tau_{tr})$] for this DSSC is also highest ($0.10 \text{ mm}^2\text{s}^{-1}$) (Table 4.5), where L stands for electrode thickness (0.07 mm). The high diffusion of electrons is relevant with the high electron diffusion length, L_D (0.13 mm).

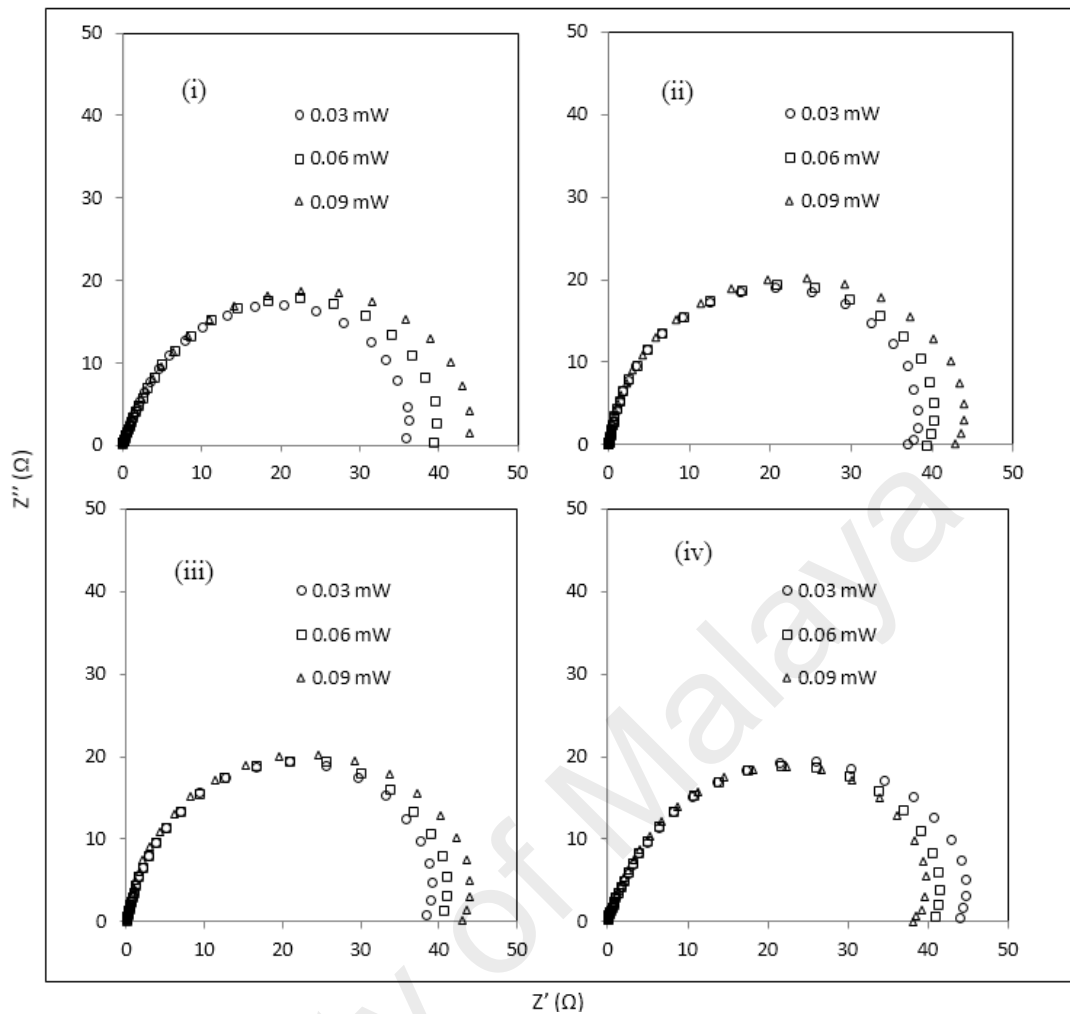


Figure 4.10: IMVS Nyquist type plots at different intensities for the DSSCs assembled with GPEs containing (i) 10 wt %, (ii) 20 wt %, (iii) 30 wt % and 40 wt % TPAI.

Table 4.4: Summary of parameters obtained from IMPS and IMVS experiments for different DSSCs fabricated with GPEs containing various percentages of TPAI.

wt % TPAI	f_{IMPS} (Hz)	τ_{tr} (ms)	f_{IMVS} (Hz)	τ_{rec} (ms)	η_{cc}	D (mm ² /s)	L_D (mm)
10	3.3160	48.02	1.9953	79.80	0.40	0.04	0.06
20	3.9811	40.00	1.5849	100.47	0.60	0.05	0.07
30	7.9433	20.05	1.0000	159.24	0.87	0.10	0.13
40	3.9811	40.00	2.2536	70.66	0.43	0.05	0.06

4.5 Summary of the chapter

- The bulk impedance decreased with increased percentage of TPAI salt showing the lowest value of 22 Ω at 30 wt % TPAI containing GPE. Consequently, σ increases with increase in TPAI concentrations and reached the highest value of

$3.62 \times 10^{-3} \text{ S cm}^{-1}$ at 30 wt % TPAI and then decreased with further addition of salt.

- The activation energy for transportation of ions decreased with TPAI percentage and is lowest (10.09 kJ/mol) for 30 wt % TPAI containing GPE.
- The value of $D_{I_3}^*$ increased with increased I_2 content and was highest at $16.83 \times 10^{-7} \text{ cm}^2 \text{ s}^{-1}$ for 0.069 g I_2 containing electrolyte and 30 wt % TPAI. The values of $D_{I_3}^*$ decreased if more than 0.069g I_2 was added.
- The values of J_0 increased with the increase of TPAI concentration. At 30 wt % TPAI containing GPEs, the J_0 value is highest (11.22 mA cm^{-2}) on the electrode which indicates the best electrocatalytic activity toward triiodide reduction among other three electrolytes.
- J_{sc} as well as efficiency (η) of DSSC increases with the addition of TPAI in the GPEs attaining the maximum of J_{sc} (19.75 mA cm^{-2}) and η (4.76) at 30 wt % TPAI and then decreased with further addition of TPAI. The V_{oc} is also highest (553.8 mV) for 30 wt % TPAI containing GPE.
- The IPCE values for different cells follow the order as 30 wt % TPAI > 40 wt % TPAI > 20 wt % TPAI > 10 wt % TPAI at the range of visible light wavelength, which is consistent with J_{sc} order in the J - V study. The DSSC fabricated using GPE with 30 wt % TPAI showed the highest IPCE value of 58.50 % among these four DSSCs.
- Among the four DSSCs, 30 wt % TPAI containing GPE showed lowest electron transport time (τ_{tr}) value (20.05 mS) and highest recombination time (τ_{rec}) value (159.24 mS) at a given intensity which is necessary for better performance of a DSSC.
- The best charge collection efficiency η_{cc} (0.87) is observed for the 30 wt % TPAI GPE based DSSC.

- The electron diffusion coefficient (D) for the DSSC with 30 wt % TPAI containing GPE is also highest ($0.10 \text{ mm}^2\text{s}^{-1}$). The corresponding effective diffusion length, L_D is greatest (0.13 mm) for the same GPE compared to other GPE which is higher than electrode thickness L ($\sim 0.07 \text{ mm}$).

University of Malaya

CHAPTER 5: RESULTS ON THE PAN:EC:PC:TBAI:I₂ GPE SYSTEM

The electrochemical, electrocatalytic and structural studies of PAN:EC:PC:TBAI:I₂ GPEs are being presented in this chapter. This chapter also presents the DSSCs characteristics such as *J-V*, IPCE, IMPS and IMVS.

5.1 Electrochemical impedance spectroscopy (EIS) measurement

5.1.1 Ionic conductivity study

The EIS results are presented in the form of Nyquist plots for the PAN:EC:PC:TBAI:I₂ GPEs containing different amounts of TBAI (0 wt %, 10 wt %, 30 wt % and 40 wt %) at different temperatures in Figure 5.1. For 0 wt % TBAI, the Nyquist plots show a semicircle, but the Nyquist plots of GPEs with TBAI salt show only a spike. The bulk resistance, R_b was obtained from the Nyquist plots. The values of R_b was used to calculate ionic conductivity (σ) of the GPEs. Table 5.1 shows the values of R_b and σ for the GPEs. Evidently, R_b goes down with the rise of TBAI percentage and is lowest at 23 Ω for 30 wt % TBAI containing GPE. Consequently, σ rises with the rising of salt concentrations and reached the highest value of $3.46 \times 10^{-3} \text{ S cm}^{-1}$ at 30 wt % TBAI and then declined with further addition of TBAI.

5.1.2 Activation energy for ionic conduction

The $\ln\sigma$ versus $1000/T$ curves which follow the Arrhenius relation (Equation 3.5) for the GPEs containing different percentages of TBAI are shown in Figure 5.2. The activation energies for transportation of ions are presented in Table 5.1. The E_a value is decreased with TBAI percentage and is lowest, 12.59 kJ/mol for 30 wt % TBAI containing GPE. Above 30 wt % TBAI the E_a value increased.

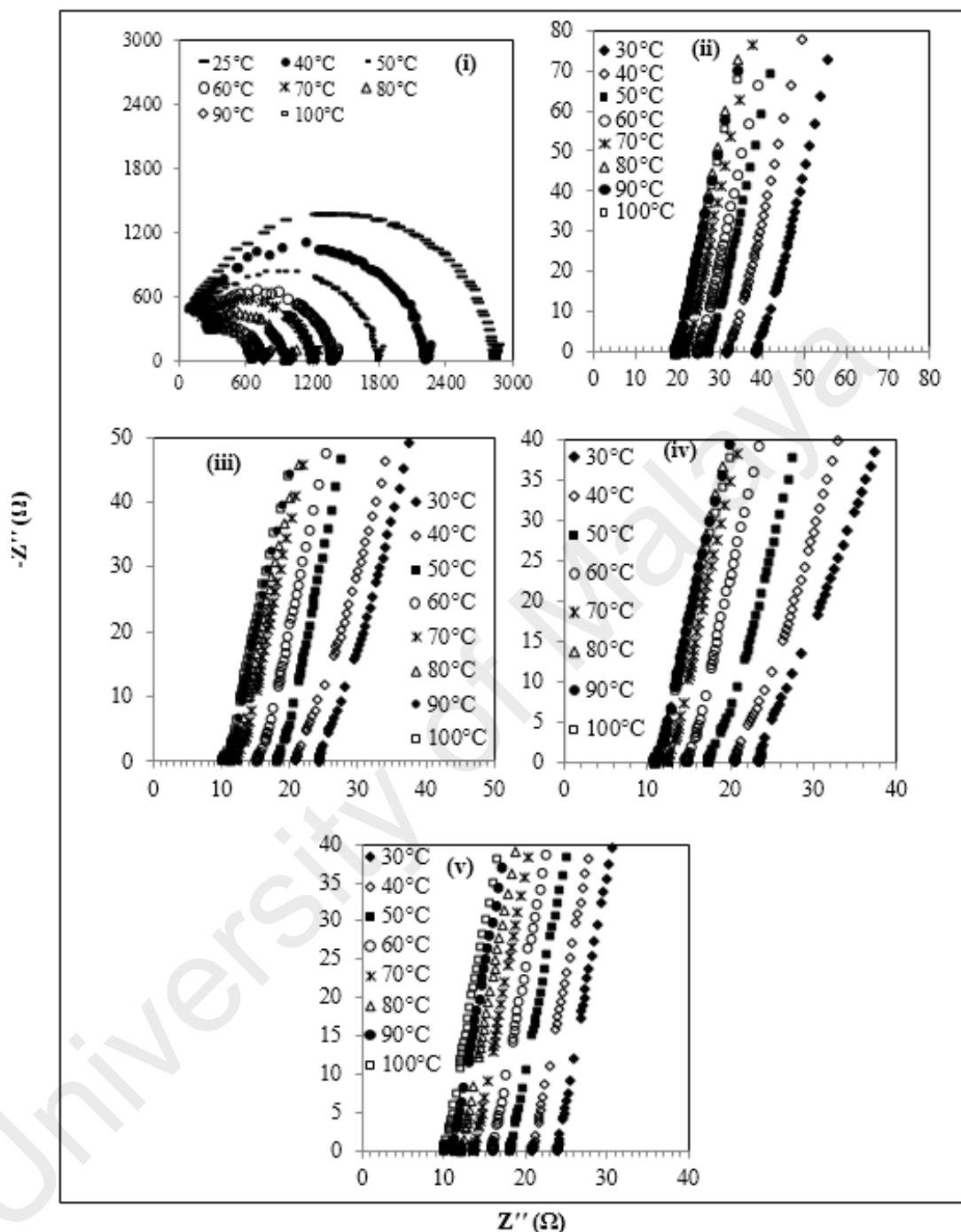


Figure 5.1: Nyquist plots for PAN:EC:PC:TBAI:I₂ GPEs, (i) 0 wt % TBAI, (ii) 10 wt % TBAI, (iii) 20 wt % TBAI, (iv) 30 wt % TBAI and (v) 40 wt % TBAI.

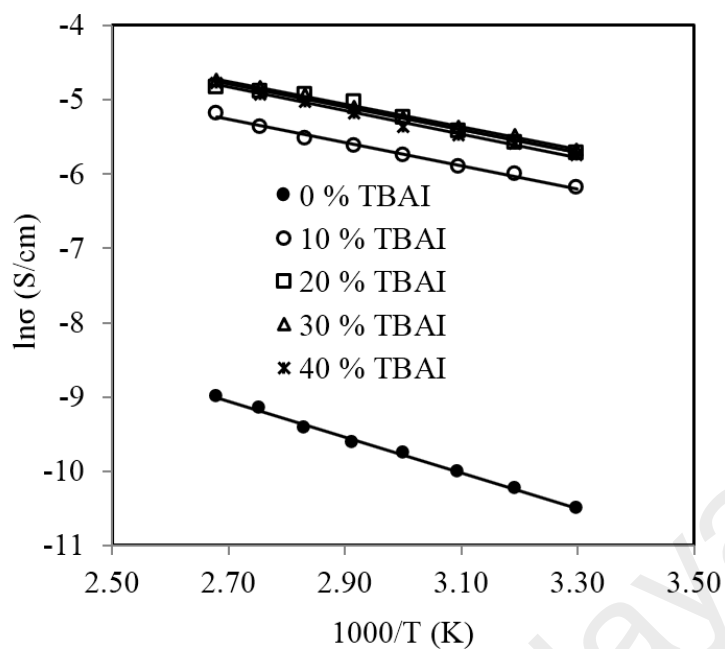


Figure 5.2: $\ln\sigma$ versus $1000/T$ graphs for different TBAI containing GPEs.

Table 5.1: Bulk impedance, R_b (ohm), ionic conductivity, $\sigma \times 10^{-3}$ (S/cm) and Activation energy, E_a (kJ/mol) for ion conduction for the TBAI containing GPEs.

wt % TBAI	R_b (ohm)	Conductivity, $\sigma \times 10^{-3}$ (S/cm)	Activation energy	
			E_a (kJ/mol)	E_a (eV)
0	2900	0.03	19.94	0.207
10	39.00	2.04	12.93	0.134
20	24.00	3.32	12.75	0.132
30	23.00	3.46	12.59	0.130
40	25.00	3.18	13.08	0.136

5.2 Linear sweep voltammetry (LSV) measurement

5.2.1 Limiting current and I_3^- Diffusion coefficient study

The linear sweep voltammograms for the GPEs containing different compositions of TBAI are shown in Figure 5.3. The anodic and cathodic limiting current density plateaus are quite similar indicating the equilibrium steady state conditions. The limiting current densities (J_{lim}) have been utilized to calculate apparent diffusion coefficient of triiodide, $D_{I_3}^*$ using Equation 3.7.

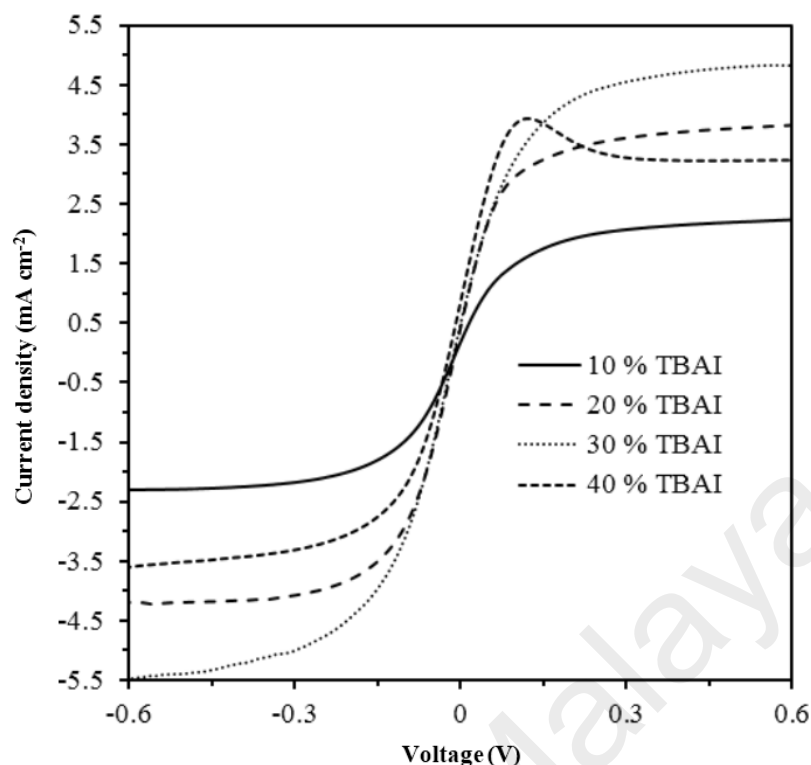


Figure 5.3: Linear sweep voltammograms (LSV) of GPEs at varying concentration of TBAI with Pt ultramicroelectrode. Scan rate: 10 mV/s.

The J_{lim} and $D_{I_3}^*$ values for TBAI containing gel polymer electrolyte systems are presented in Tables 5.2. The J_{lim} value is found highest at 5.00 mA cm^{-2} for 30 wt % TBAI GPE. The values of $D_{I_3}^*$ increase with the increase of I_2 content and reach the highest $6.59 \times 10^{-7} \text{ cm}^2 \text{ s}^{-1}$ for 0.09 g I_2 containing electrolyte with 30 wt % TBAI content. After higher composition of I_2 , the value of $D_{I_3}^*$ decreased.

5.2.2 Tafel polarization curve and Exchange current density, J_0

From the LSV measurements, the exchange current density, J_0 has also been estimated using Tafel polarization technique. To find the Tafel polarization curves, the LSV curves obtained from symmetrical cells have been converted to logarithmic current-voltage (Log J - V) (Figure 5.4) (Bard et al., 1980). From the extrapolation of the anodic or cathodic curves in its Tafel zone crossing at 0 V, the exchange current density, J_0 has been obtained and tabulated in Table 5.2. The J_0 values were observed to increase with the increase of

TBAI concentration. The GPE with 30 wt % TBAI showed the highest J_0 of 0.63 mA cm⁻².

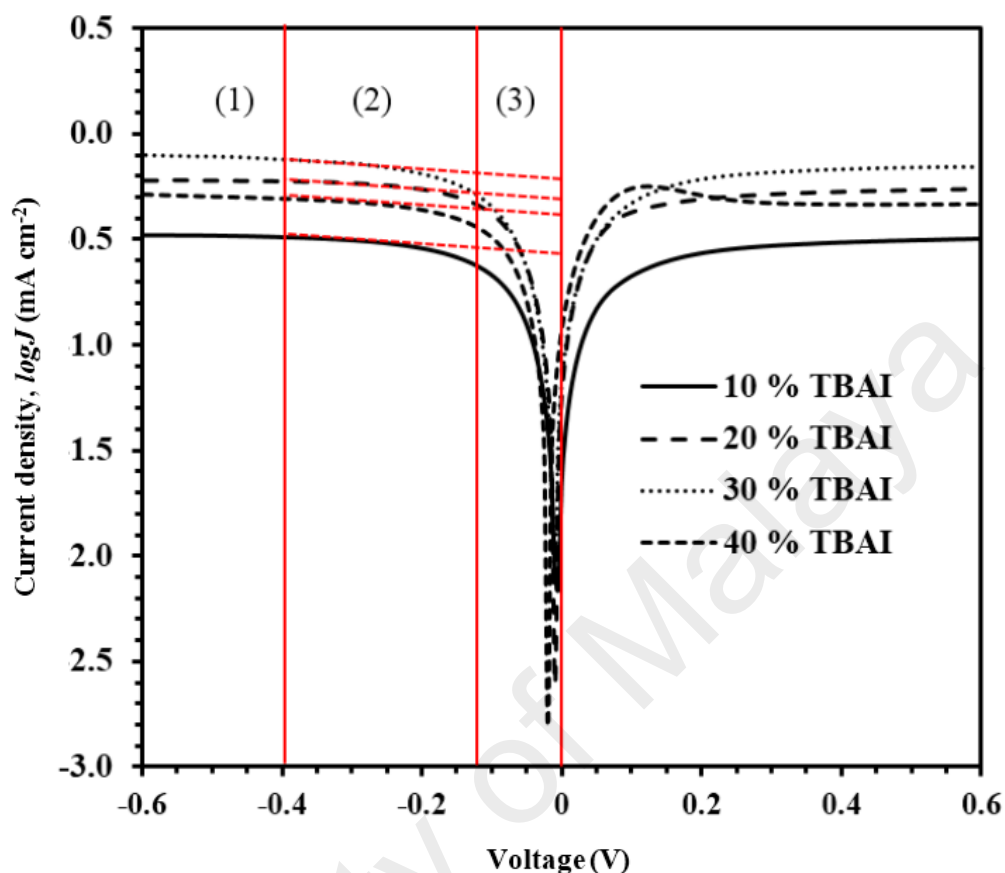


Figure 5.4: Tafel polarization curves for the electrolytes with different TBAI containing GPEs.

Table 5.2: Limiting current or steady state current (J_{lim}), diffusion coefficients of I_3^- ion ($D_{I_3^-}^*$), exchange current density (J_0) of GPEs containing different composition of iodine.

TBAI (wt %)	10	20	30	40
I_2 (g)	0.034	0.052	0.069	0.086
J_{lim} (mA cm ⁻²)	2.13	3.88	5.00	3.25
$D_{I_3^-}^*$ ($\times 10^{-7}$ cm ² s ⁻¹)	4.31	5.77	6.59	3.82
$J_{0, Tafel}$ (mA cm ⁻²)	0.28	0.45	0.63	0.40

5.3 X-ray diffraction (XRD) studies

X-ray diffraction (XRD) studies were carried out for the structural characterization of GPEs with different TBAI compositions. The XRD peaks of pure PAN and PAN:EC:PC GPE have been shown in chapter 4. Here XRD results for the GPEs with different TBAI

contents have been shown. Figure 5.5 exhibits the X-ray diffraction patterns of PAN:EC:PC:xTBAI:I₂ GPEs where x stands for 10 wt %, 20 wt %, 30 wt % and 40 wt %. It is observed that TBAI salt can reform XRD pattern of PAN such as: (1) a systematic shifting and enlargement of the main peak ($2\theta \approx 17^\circ$) in PAN toward higher angle ($2\theta \approx 20^\circ$) at 10 wt %, 20 wt % and 30 wt % TBAI containing GPEs, (2) generation of new peak at $2\theta \approx 10^\circ$ from the salt concentration of 20 wt. % and (4) a gradual decrease in the intensity of PAN peak (20°) with an addition of TBAI which eventually disappears at 40 wt % salt concentration. An up-shifting of XRD peak is due to the increase in d-spacing of the polymer matrix which is the evidence of the polymer-salt interaction and emerges from the possible complexation of cation (TBA⁺ ion) with lone pair electron containing site (-CN) in the host polymer matrix. Further enhancement of the polymer-salt interaction (complexation) is also evident by a gradual reduction in intensity of 20° peak on addition of TBAI salt followed by diminishing in the GPEs with 40 wt % TBAI. One can easily understand that there may be an optimum concentration limit of salt dissolution into the PAN matrix. Furthermore, the addition of TBAI containing long butyl chain (-CH₂-CH₂-CH₂-CH₂-) prevents polymer chain reorganization causing significant disorder in the polymer chains which promotes the interaction between them. TBA⁺ ions may break the regular arrangement of H-bonding network of PAN polymer backbone and aggregate through non-polar hydrophobic chain initiated micellization, which severely disturbs the order of crystalline phase of polymer and hinders the molecular chains from packing closely together in a regular array causing development of amorphousness in the GPEs.

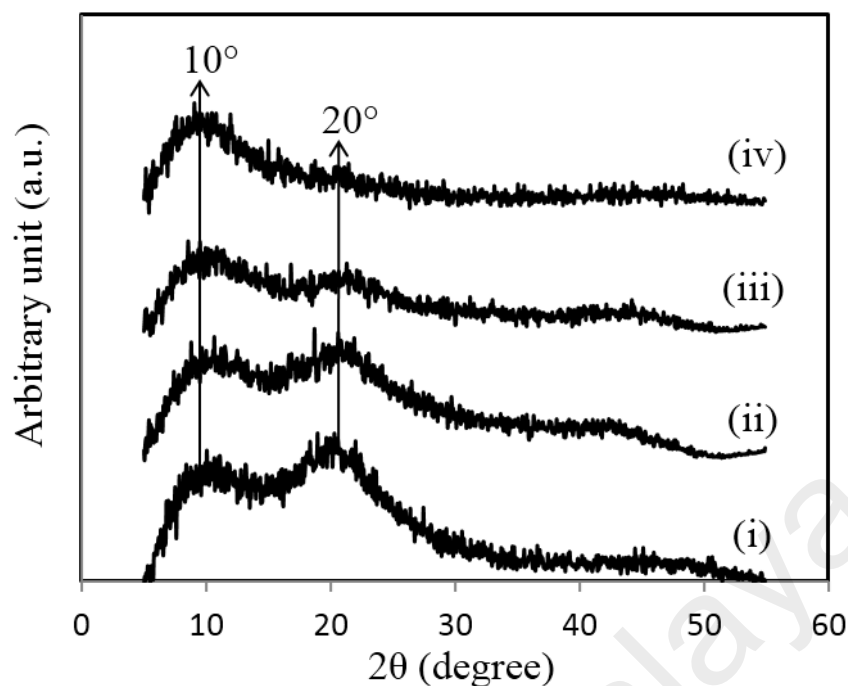


Figure 5.5: XRD pattern of PAN:EC:PC:xTBAI:I₂ GPEs, x = (i) 10 wt %, (ii) 20 wt %, (iii) 30 wt % and (iv) 40 wt %.

5.4 DSSC performance analysis

5.4.1 Photovoltaic (J-V) characteristics

PAN:EC:PC GPEs based DSSCs were fabricated and characterized. The photovoltaic characteristics (J - V) of these cells have been presented in Figure 5.6. Table 5.3 displays the open-circuit voltage (V_{oc}), short-circuit current (J_{sc}), fill factor (FF) and the efficiency (η) which were estimated from photovoltaic data. Following the similar variation of conductivity versus TBAI concentration, J_{sc} and efficiency (η) of DSSC increases with increasing TBAI concentration as with the GPEs, reached the maximum J_{sc} (12.66 mAcm⁻²) and η (3.32 %) for the 30 % TBAI GPE and then decreased with further addition of salt. The fill factors do not change remarkably except DSSC with 40 % TBAI in the GPE.

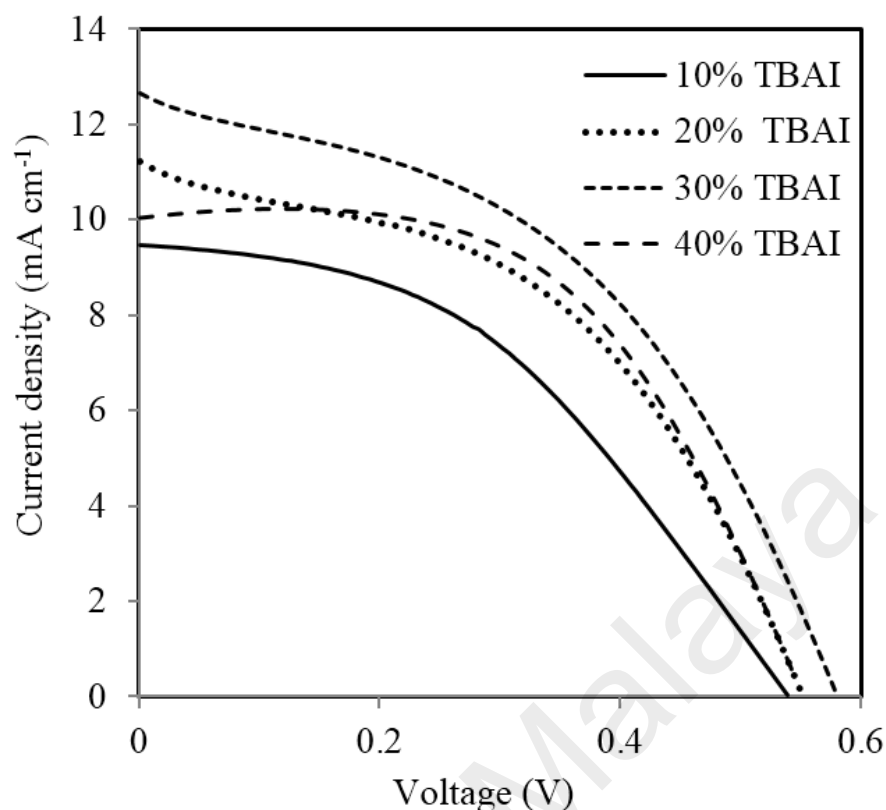


Figure 5.6: J–V curves of DSSCs for PAN:EC:PC:TBAI:I₂ GPEs systems.

Table 5.3: Photovoltaic performance of PAN:EC:PC:TBAI:I₂ with different weight contents of TBAI-added polymer electrolytes.

TBAI	J_{sc} (mA cm ⁻²)	V_{oc} (mV)	FF	η %
10 wt %	9.47	548.9	0.42	2.22
20 wt %	11.22	553.8	0.47	2.88
30 wt %	12.66	548.9	0.45	3.32
40 wt %	10.03	579.0	0.56	3.04

5.4.2 Incident-photon-to-current efficiency (IPCE)

The incident-photon-to-current efficiency (IPCE) was performed to provide the supplementary evidence for light-harvesting efficiency of the DSSCs. Figure 5.7 shows the IPCE spectra at the wavelength from 400 to 800 nm for different GPEs in the DSSCs. It is observed that the IPCE curves of the four cells show similar pattern with maximum efficiencies between 520 and 550 nm. This implies that the absorption peak is associated with the N719 dye. The values of IPCE of the DSSCs follow the order: 30 wt % TBAI > 40 wt % TBAI > 20 wt % TBAI > 10 wt % TBAI in the visible light wavelength. This

order was also observed for the J_{SC} values of the cells. The 30 wt % TBAI containing DSSC showed the highest IPCE value of 54.02 % among these four DSSCs.

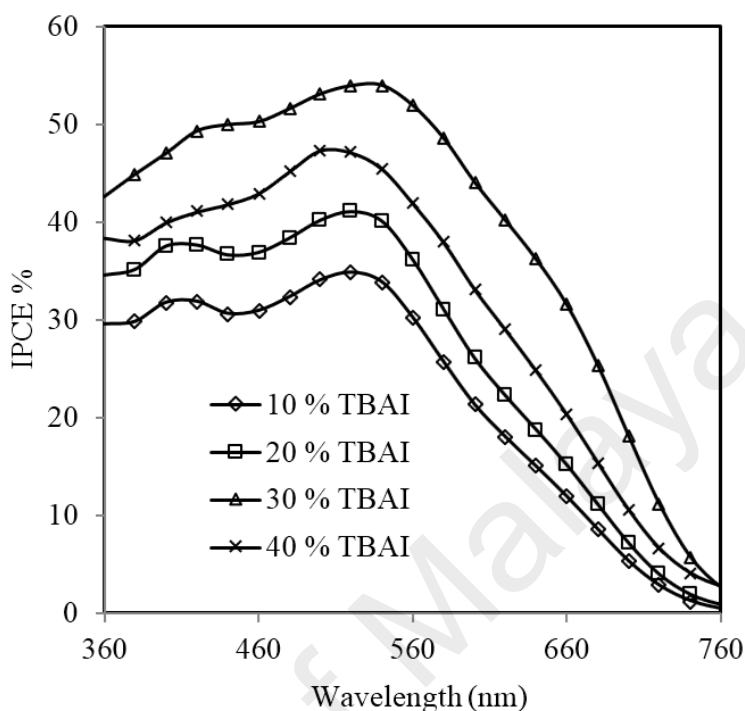


Figure 5.7: IPCE % vs. wavelength for the DSSCs with different TBAI containing GPEs.

5.4.3 IMPS and IMVS study of DSSCs

Figure 5.8 displays the IMPS curves as Nyquist-type plots at different base intensities (0.03, 0.06 and 0.09 mW). It can be observed that, the radius of the semicircle slightly decreased as the intensity increased. Each of the curves posed a maximum at intermediate frequencies, f_{IMPS} which is the characteristic parameter for the transportation of electron through the TiO_2 pores to the back layer (O'Regan & Lenzmann, 2004). This value gives the electron transfer time (τ_{tr}) in the DSSC.

The IMVS experimental curves have been depicted in Figure 5.9 as Nyquist-type plots at the base intensities as for IMPS. The radius of the semicircle decreases with increasing intensity. The frequencies f_{IMVS} were obtained from the maxima of the Nyquist-type semicircles. The f_{IMVS} is associated with electron recombination time (τ_{rec}). The τ_{tr} and τ_{rec} were calculated from corresponding characteristic frequencies using the

Equation 3.12 and Equation 3.13 of Chapter 3, respectively. All the values have been tabulated in Table 5.4.

Table 5.4: Summary of parameters obtained from IMPS and IMVS experiments for different DSSCs fabricated with GPEs containing various percentages of TBAI.

wt % TBAI	f_{IMPS} (Hz)	τ_{tr} (ms)	f_{IMVS} (Hz)	τ_{rec} (ms)	η_{cc}	D (mm ² /s)	L_D (mm)
10	3.1623	50.35	2.8371	56.13	0.10	0.04	0.05
20	3.9811	40.00	1.9953	79.81	0.50	0.05	0.06
30	4.4965	35.41	1.7901	88.95	0.60	0.06	0.07
40	3.5717	44.58	2.5119	63.39	0.30	0.05	0.05

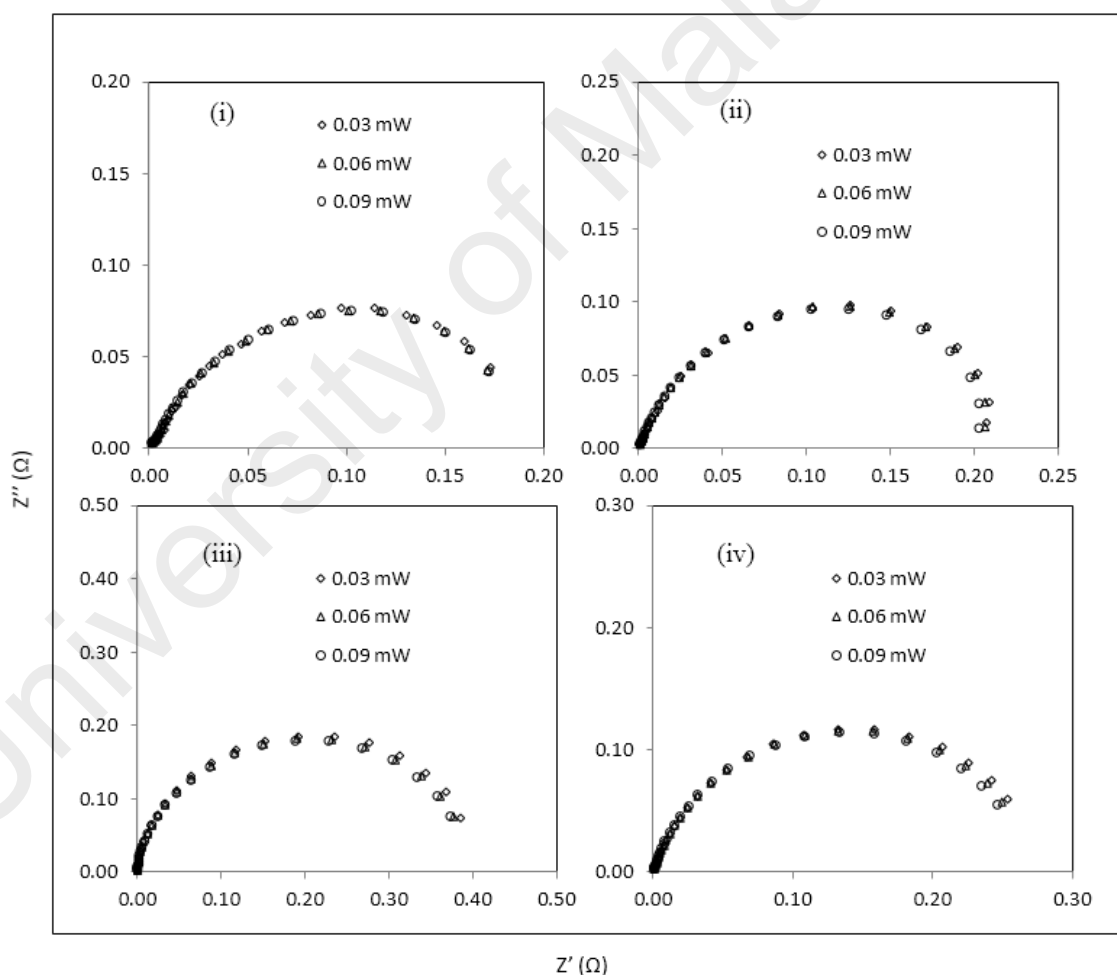


Figure 5.8: IMPS Nyquist type plots at different intensities for the DSSCs assembled with GPEs containing (i) 10 wt %, (ii) 20 wt %, (iii) 30 wt % and (iv) 40 wt % TBAI.

The DSSC with 30 wt % TBAI GPE showed lowest τ_{tr} value (35.41 ms) and highest τ_{rec} value (88.95 ms). The charge collection efficiencies for 10 wt %, 20 wt %, 30 wt %

and 40 wt % TBAI GPEs based DSSCs are 10.28 %, 49.88 %, 60.19 % and 29.67 %, respectively. The best value of η_{cc} is 60.19 % observed for the DSSC with 30 wt % TBAI. Additionally, the value of electron diffusion coefficient, D for the same DSSC is observed highest ($0.06 \text{ mm}^2\text{s}^{-1}$). The same cell (30 wt % TBAI GPE based) also exhibited maximum effective diffusion length, L_D which is 0.07 mm. The value of L_D is a higher than working electrode thickness (0.07 mm).

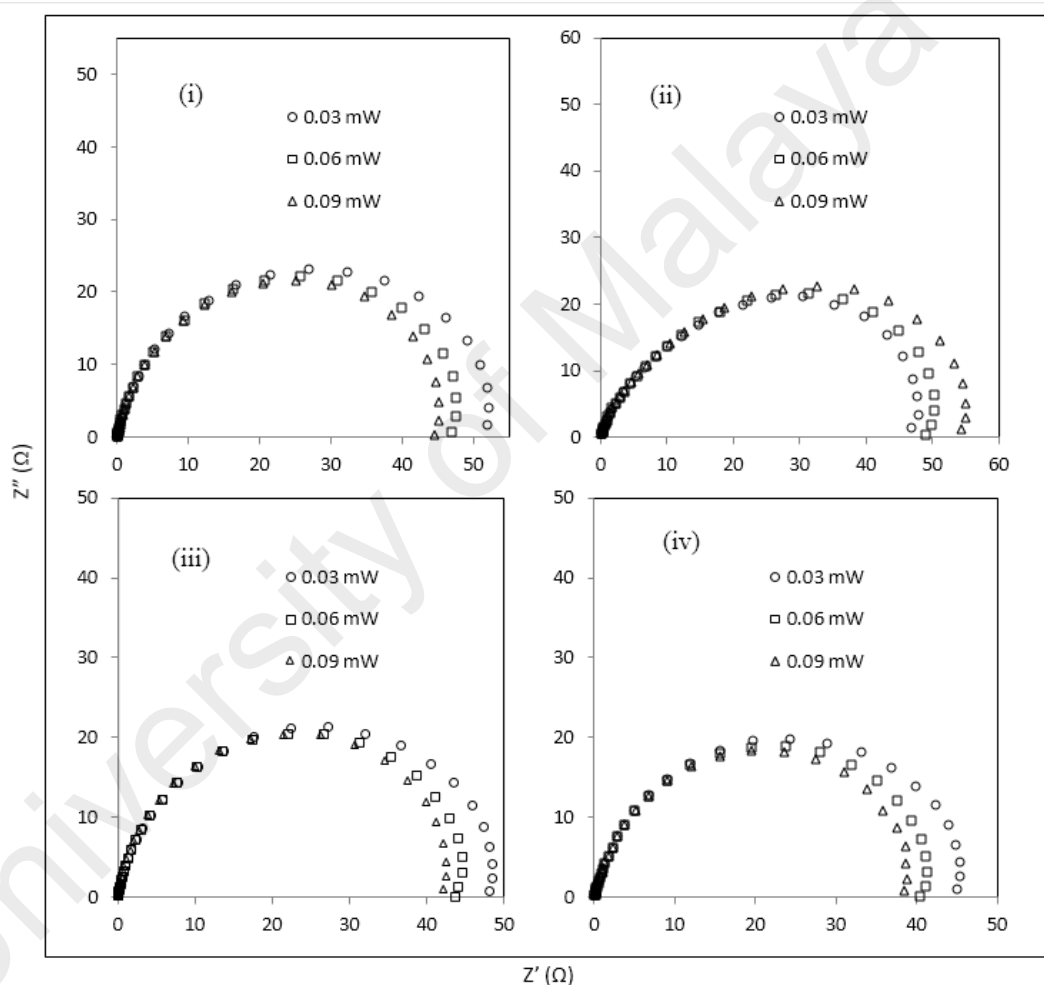


Figure 5.9: IMVS Nyquist type plots at different intensities for the DSSCs assembled with GPEs containing (i) 10 wt %, (ii) 20 wt %, (iii) 30 wt % and 40 wt % TBAI.

5.5 Summary of the chapter

- The value of R_b for 30 wt % TBAI containing GPE is found smallest 23Ω and corresponding σ value is $3.46 \times 10^{-3} \text{ S cm}^{-1}$ which is highest among other

composition of TBAI. The activation energy for ion conduction through the GPE for 30 % TBAI was the lowest, 12.59 kJ/mol.

- The $D_{I_3}^*$ is observed to increase with increasing I_2 content followed by highest value $6.59 \times 10^{-7} \text{ cm}^2 \text{ s}^{-1}$ for 0.069 g I_2 containing electrolyte and 30 wt % TBAI.
- The exchange current density J_0 increased with increasing TBAI percentage. The J_0 is highest (0.63 mA cm^{-2}) at 30 wt % TBAI containing GPEs.
- The short circuit current density, J_{SC} and the cell efficiency, η rised with increasing of TBAI percentage. The maximum J_{SC} (12.66 mA cm^{-2}) and η (3.32 %) were found at 30 wt % TBAI GPE.
- The 30 wt % TBAI containing GPE showed the highest IPCE value of 54.02 %.
- Among the all four DSSCs, 30 wt % TBAI containing GPE showed lowest electron transport time (τ_{tr}) value (35.41 ms) and highest recombination time (τ_{rec}) value (88.95 ms) at a given intensity which is necessary for better performance of a DSSC.
- The DSSC with 30 wt % TBAI GPE had the best charge collection efficiency η_{cc} of 0.60.
- The cell also shows the highest electron diffusion coefficient (D) $0.059 \text{ mm}^2 \text{ s}^{-1}$ and the corresponding electron effective diffusion length, L_D is 0.072 mm which is also highest.

CHAPTER 6: RESULTS ON THE PAN:EC:PC:TPAI:PMII:I₂ GPE SYSTEM

The gel polymer electrolytes (GPEs) of PAN:EC:PC:TPAI:PMII:I₂ have been studied based on electrochemical, electrocatalytic and structural characteristics and are discussed in this chapter. This chapter also deals with *J-V*, IPEC, IMPS and IMVS characteristics of the DSSCs fabricated with these GPEs.

6.1 Electrochemical impedance spectroscopy (EIS) measurement

6.1.1 Ionic conductivity study

The EIS results in the form of Nyquist plots for PAN:EC:PC:TPAI:PMII:I₂ GPEs containing different percentage of PMII (4 wt %, 6 wt %, 8 wt %, 10 wt % and 12 wt %) at different temperatures are depicted in Figure 6.1. The GPEs with 30 wt % TPAI salt and different percentage of PMII ionic liquid have only a spike in their Nyquist plots. From the Nyquist plots, the bulk resistance, R_b was estimated and used to calculate ionic conductivity (σ) of the GPEs. The values of R_b and σ for the GPEs are presented in Table 6.1. It has been observed that R_b decreases with the rise of PMII percentage and shows the lowest value of 13.5 Ω at 10 wt % PMII containing GPE. Accordingly, σ increases with the increase of salt concentrations and reaches to the highest value of 5.90×10^{-3} S.cm⁻¹ at 10 wt % PMII and then again declines with further addition of PMII.

6.1.2 Activation energy for ionic conduction

The variation of conductivity with temperature in the form of $\ln\sigma$ versus $1000/T$ plots is presented in Figure 6.2 for the GPEs containing different percentages of PMII. All the plots have been fitted with the Arrhenius type equation (Equation 3.5) from which activation energy (E_a) has been calculated. The activation energy for transportation of ions is decreased with PMII percentage and is lowest (6.14 kJ/mol) for 10 wt % PMII containing GPE which is agreeable with the conductivity behavior.

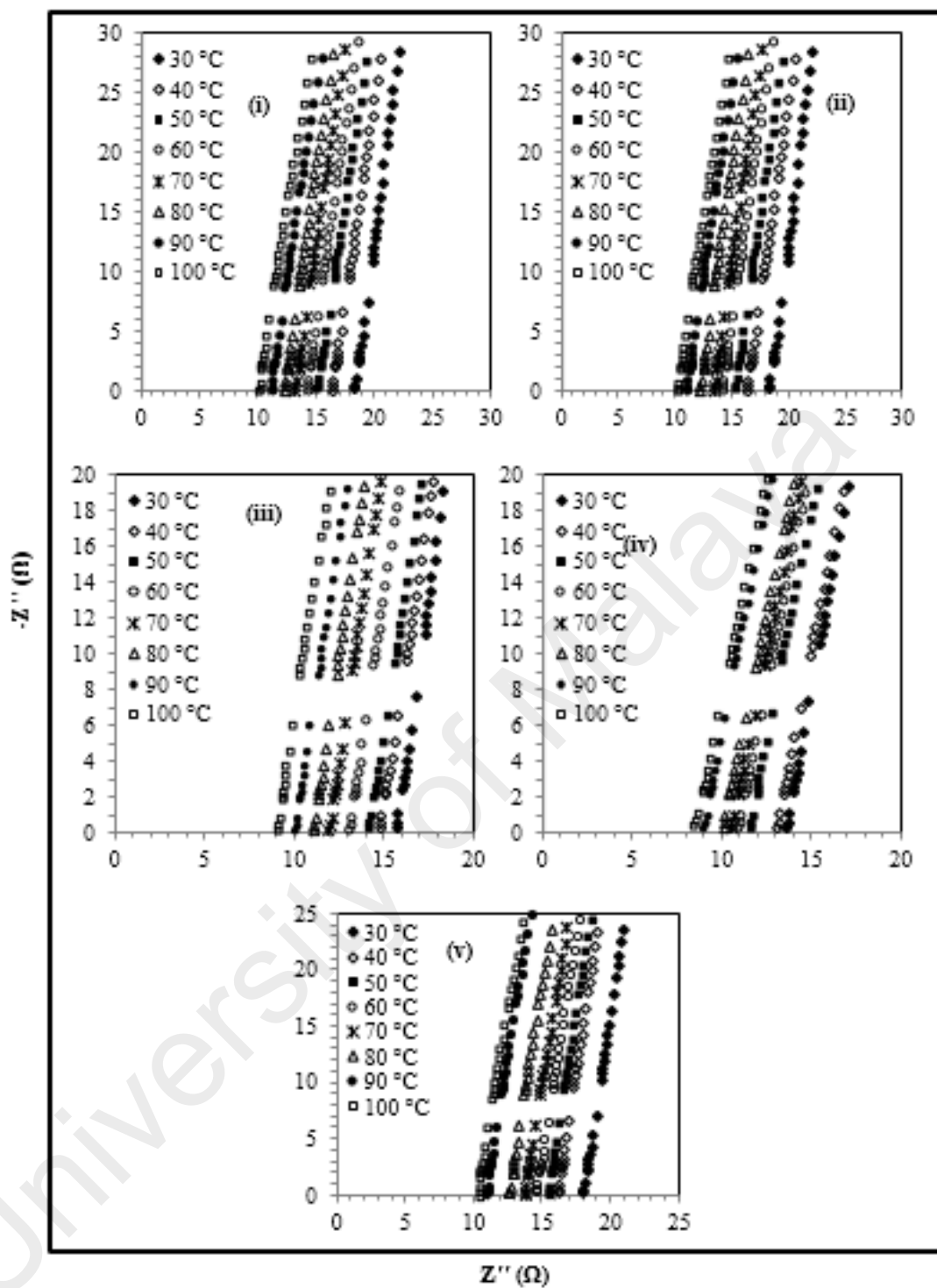


Figure 6.1: Nyquist plots for PAN:EC:PC:TPAI:PMII:I₂ GPEs: (i) 4 wt % PMII, (ii) 6 wt % PMII, (iii) 8 wt % PMII, (iv) 10 wt % PMII and (v) 12 wt % PMII.

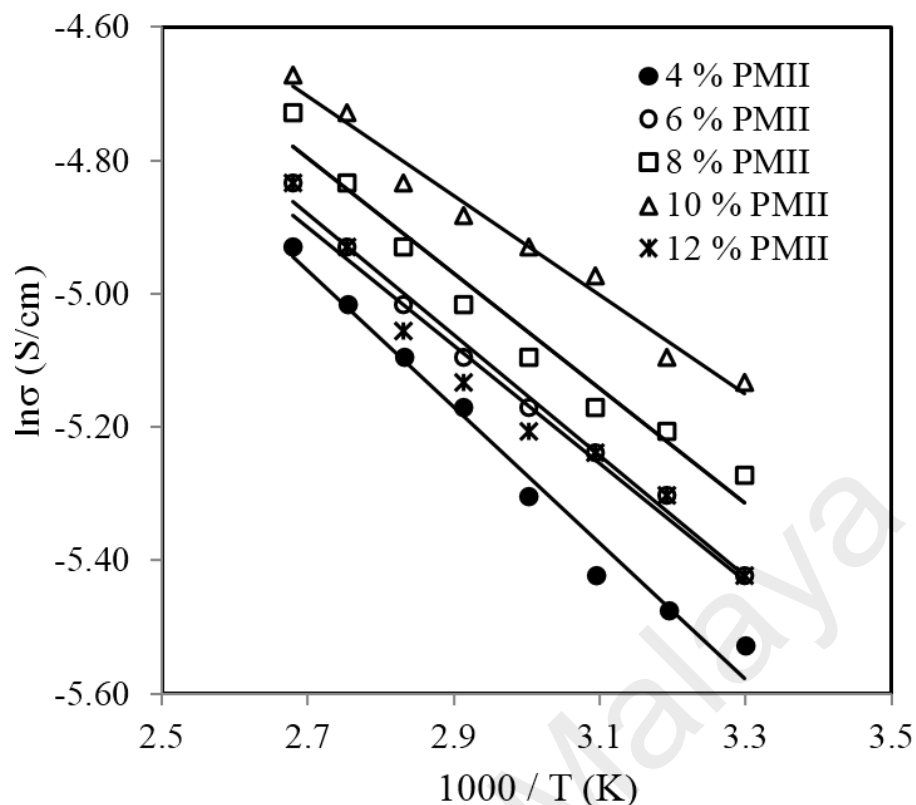


Figure 6.2: $\ln\sigma$ versus $1000/T$ graphs for different PMII containing GPEs.

Table 6.1: Bulk impedance, R_b (ohm), ionic conductivity, $\sigma \times 10^{-3}$ (S/cm) and Activation energy, E_a (kJ/mol) for ion conduction for the PMII containing GPEs.

wt % PMII	R_b (ohm)	Conductivity, $\sigma \times 10^{-3}$ (S/cm)	Activation energy	
			E_a (kJ/mol)	E_a (eV)
4	20.00	3.98	10.09	0.105
6	18.00	4.42	9.55	0.099
8	15.50	5.13	7.78	0.081
10	13.50	5.90	6.14	0.064
12	18.00	4.42	11.66	0.121

6.2 Linear sweep voltammetry (LSV) measurement

6.2.1 Limiting current and I_3^- Diffusion coefficient study

In Figure 6.3, the characteristic linear sweep voltammetry plots for the GPEs containing different compositions of PMII are depicted. The current densities reach saturations for both polarities at above 0.3 V. The anodic and cathodic limiting current plateaus are quite similar which indicate that the equilibrium steady state conditions attain. As the J_{lim} is associated with the triiodide ions as iodide concentration is greater

than the concentration of I_2 (Papageorgiou et al., 1996), that has been used to estimate the apparent diffusion coefficient of triiodide, $D_{I_3}^*$ using Eq. (3.7).

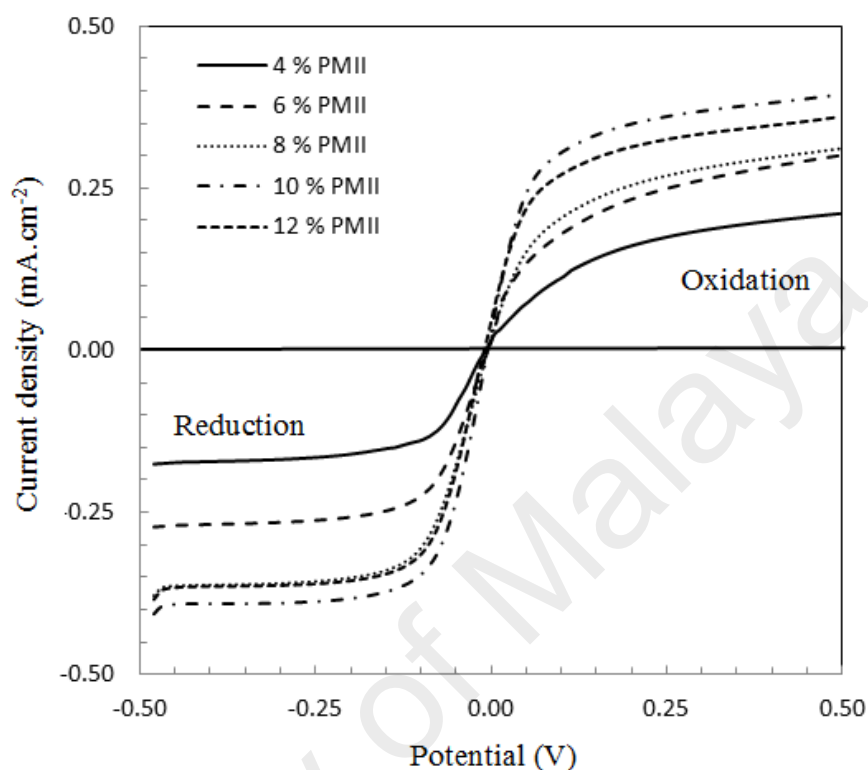


Figure 6.3: Linear sweep voltammograms (LSV) of GPEs at varying concentration of PMII with Pt ultramicroelectrode. Scan rate: 10 mV/s.

All the values of J_{lim} and $D_{I_3}^*$ for PMII containing GPEs are presented in Table 6.2. The values of J_{lim} increase amount of PMII increases until a maximum value (0.70 mA cm^{-2}) at 10 wt % PMII GPE and then the values declined if more PMII was added. The value of $D_{I_3}^*$ increased with the increase of IL amount and was highest at $1.36 \times 10^{-7} \text{ cm}^2 \text{ s}^{-1}$ for 10 wt % PMII containing electrolyte. The values of $D_{I_3}^*$ decreased if more IL was added.

6.2.2 Tafel polarization curve and Exchange current density, J_0

The exchange current density, J_0 for the PMII GPEs has been estimated by using Tafel polarization curves (Figure 6.4).

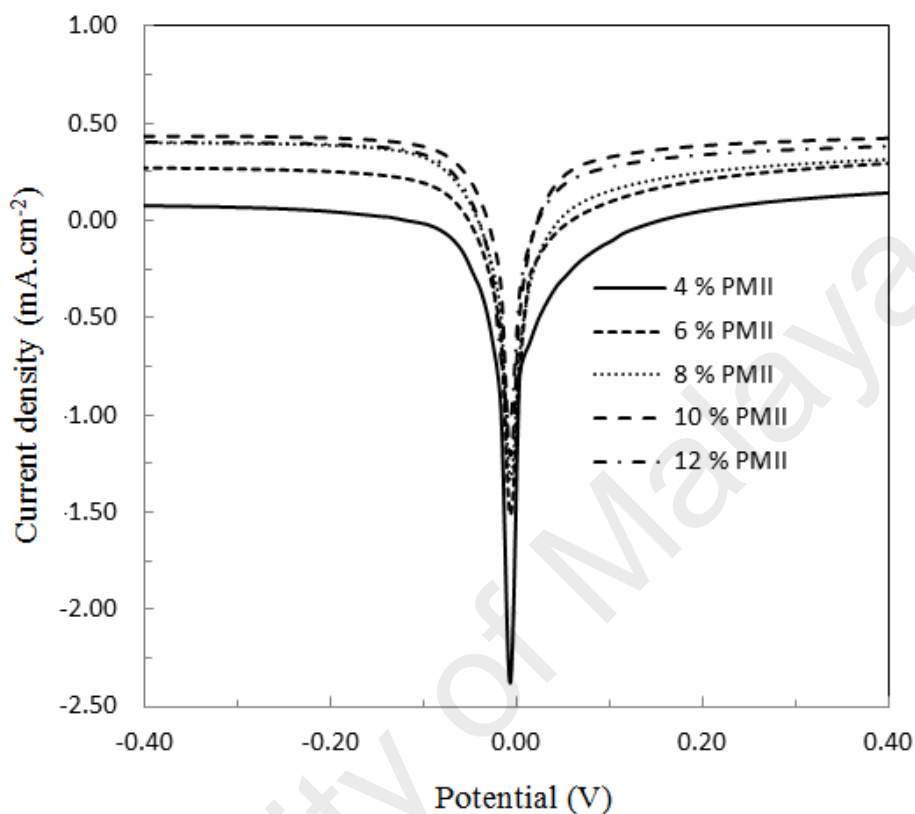


Figure 6.4: Tafel polarization curves for the electrolytes with different PMII containing GPEs.

By extrapolating the anodic or cathodic curves in its Tafel zone and the cross point at 0 V, the exchange current density values have been obtained and are summarized in Table 6.2. The J_0 estimated from LSV are closer to those obtained from EIS measurement and show similar variational trend. The values are rising with the rise of PMII concentration. At 10 wt % PMII containing GPEs, the J_0 value is highest (2.29 mA.cm⁻²).

Table 6.2: Limiting current or steady state current (J_{lim}), diffusion coefficients of I_3^- ion ($D_{I_3^-}^*$), exchange current density (J_0) of GPEs containing different composition of iodine.

PMII	4 wt %	6 wt %	8 wt %	10 wt %	12 wt %
I_2 (g)	0.069	0.069	0.069	0.069	0.069
J_{lim} (mA cm ⁻²)	0.30	0.46	0.60	0.70	0.65
$D_{I_3^-}^*$ ($\times 10^{-7}$ cm ² s ⁻¹)	0.48	0.77	1.03	1.24	1.18
$J_{0, Tafel}$ (mA cm ⁻²)	1.05	1.58	1.78	2.29	2.13

6.3 X-ray diffraction (XRD) studies

For the GPEs with different PMII compositions, X-ray diffraction (XRD) studies were carried out to characterize their structural features. Detail discussion on XRD peaks of pure PAN, PAN:EC:PC, PAN:EC:PC:TPAI:I₂, and PAN:EC:PC:TBAI:I₂ GPE have been made in Chapter 4 and Chapter 5. Here XRD results for the GPEs systems of different PMII contents will be discussed. Figure 6.5 displays the XRD patterns of PAN:EC:PC:TPAI:xPMII:I₂ GPEs where x stands for 4 wt %, 6 wt %, 8 wt %, 10 wt % and 12 wt %. It is observed that PMII salt can reform XRD pattern of PAN:EC:PC:TPAI:I₂ GPEs. The peak at $2\theta = 20^\circ$ has been shifted to $2\theta = 21^\circ$ at 6 wt % and 8 wt % PMII containing GPEs and after that the peak is disappeared. The shifting of XRD peak towards higher degree is the indication of the increase in d-spacing of the polymer matrix which is the evidence of the polymer-salt interaction and emerges from the possible complexation of cation (PMI⁺ ion) with lone pair electron containing site (-CN) in the host polymer matrix. One can simply understand that there may be an optimum concentration limit of IL composition into the PAN matrix.

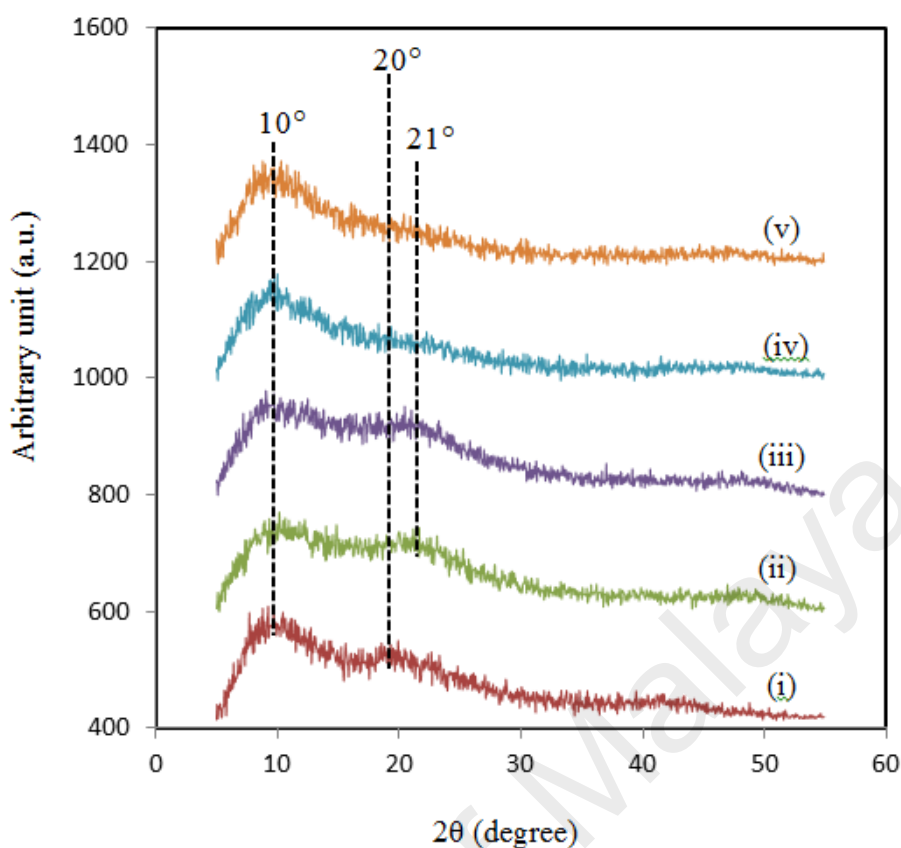


Figure 6.5: XRD pattern of PAN:EC:PC:30 wt % TPAI:PMII-I₂: (i) 0 wt % PMII, (ii) 6 wt % PMII, (iii) 8 wt % PMII, (iv) 10 wt % PMII and (v) 12 wt % PMII.

6.4 DSSC performance analysis

6.4.1 Photovoltaic (*J-V*) characteristics

The photovoltaic (*J-V*) characteristics of DSSCs developed with PAN:EC:PC:(30 wt %)TPAI:xPMII (x = 4 wt %, wt %, 8 wt %, 10 wt % and 12 wt %) GPEs have been presented in Figure 6.6. Table 6.3 shows the open-circuit voltage (V_{oc}), short-circuit current (J_{sc}), fill factor (FF) and the efficiency (η) estimated from *J-V* curves.

Table 6.3: Photovoltaic performance of PAN:EC:PC:TPAI:I₂ with different weight contents of PMII-added polymer electrolytes.

PMII	J_{sc} (mA cm ⁻²)	V_{oc} (mV)	FF	η %
4 wt %	20.14	528.9	0.4756	5.07
6 wt %	20.59	533.8	0.5037	5.54
8 wt %	21.13	553.8	0.4871	5.70
10 wt %	21.23	573.8	0.5012	6.10
12 wt %	19.27	548.9	0.5226	5.53

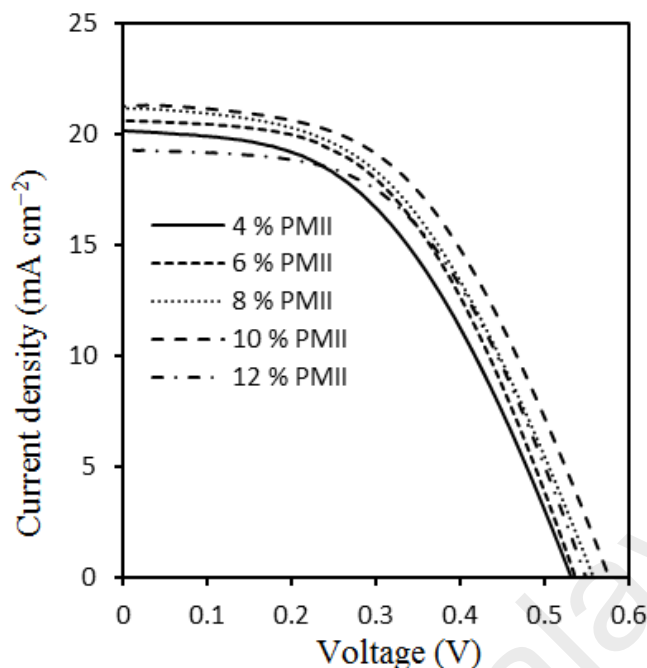


Figure 6.6: J–V curves of DSSCs for PAN:EC:PC:TPAI-I₂ GPEs systems.

The J_{SC} as well as efficiency (η) of DSSC increases with the addition of PMII in the GPEs and reaches the maximum J_{SC} (21.23 mA cm^{-2}) and η (6.10 %) (Figure 6.6 and Table 6.3) for the 10 wt % PMII and then declines with further addition of IL. The V_{OC} is also observed highest value as 573.8 mV for 10 wt % PMII containing. The fill factor (FF) is observed highest 0.5226.

6.4.2 Incident-photo-to-current efficiency (IPCE)

The incident photo to current efficiency (IPCE) spectra been collected as for supporting evidence on the light-harvesting efficiency of the DSSCs. Figure 6.7 represents the IPCE spectra as a function of wavelength from 400 to 800 nm for different DSSCs with GPEs containing various concentration of PMII. It is observed that the IPCE curves of the five cells display similar shape of spectrum with maximum efficiencies at 520 - 550 nm which corresponds to the absorption peak of the N719 dye. The DSSC fabricated by GPE with 10 wt % PMII shows the highest IPCE value of 69.0 % among five DSSCs.

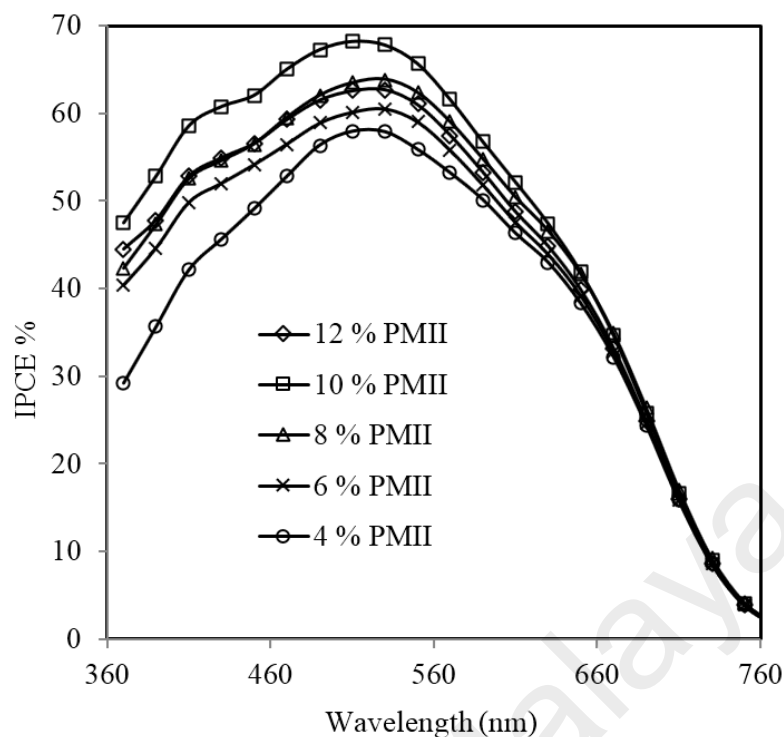


Figure 6.7: IPCE % vs. wavelength for the DSSCs with different TPAI containing GPEs.

6.4.3 IMPS and IMVS study of DSSCs

Intensity modulated photovoltaic spectroscopy (IMPS) graphs in the form of Nyquist-type plots at different base intensities (0.03, 0.06 and 0.09 mW) have been presented in Figure 6.8. It is to be noted that, as the intensity increases the radius of the semicircle slightly decreases. The radius of the semicircle for the IMPS plots are not changed significantly with the intensity of the light. All curves show maxima at intermediate frequencies, f_{IMPS} which is the characteristic frequency for the electron transport through the pores of the anode to the back layer.

IMVS experimental results have been presented as Nyquist-type plots at different base intensities (0.03, 0.06 and 0.09 mW) in the Figure 6.9. It is observed that, the radius of the semicircle decreases as the intensity increases. All the diagrams exhibit a maximum at intermediate frequencies, f_{IMVS} which is used to calculate the recombination time τ_{rec} . The values of f_{IMVS} and τ_{rec} have been tabulated in Table 6.4.

Among the all DSSCs based on the GPEs 10 wt % PMII containing GPE shows lowest τ_{tr} value (10.0470 ms) and highest τ_{rec} value (102.8056 ms) at a given intensity which is necessary for better performance of a DSSC. The charge collection efficiencies for 4 wt %, 6 wt %, 8 wt %, 10 wt % and 12 wt % PMII GPEs are 0.1028, 0.3690, 0.5563, 0.9023 and 0.5503, respectively. The best charge collection efficiency η_{cc} (0.9023) is observed for the 10 wt % PMII GPE based DSSC. Furthermore, the electron diffusion coefficient, D for this DSSC is also highest ($0.21 \text{ mm}^2\text{s}^{-1}$). The corresponding effective diffusion length, L_D is greatest (0.15 mm) for 10 wt % PMII GPE) for the same GPE compared to other GPEs based DSSEs.

Table 6.4: Summary of parameters obtained from IMPS and IMVS experiments for different DSSCs fabricated with GPEs containing various percentages of PMII.

PMII (wt %)	f_{IMPS} (Hz)	τ_{tr} (ms)	f_{IMVS} (Hz)	τ_{rec} (ms)	η_{cc}	D (mm^2/s)	L_D (mm)
4	3.9811	40.00	3.5717	44.58	0.10	0.05	0.05
6	4.4965	35.41	2.8371	56.13	0.37	0.06	0.06
8	5.6608	28.13	2.5119	63.39	0.56	0.07	0.07
10	15.8490	10.05	1.5489	102.81	0.90	0.21	0.15
12	12.5890	12.65	5.6608	28.13	0.55	0.16	0.07

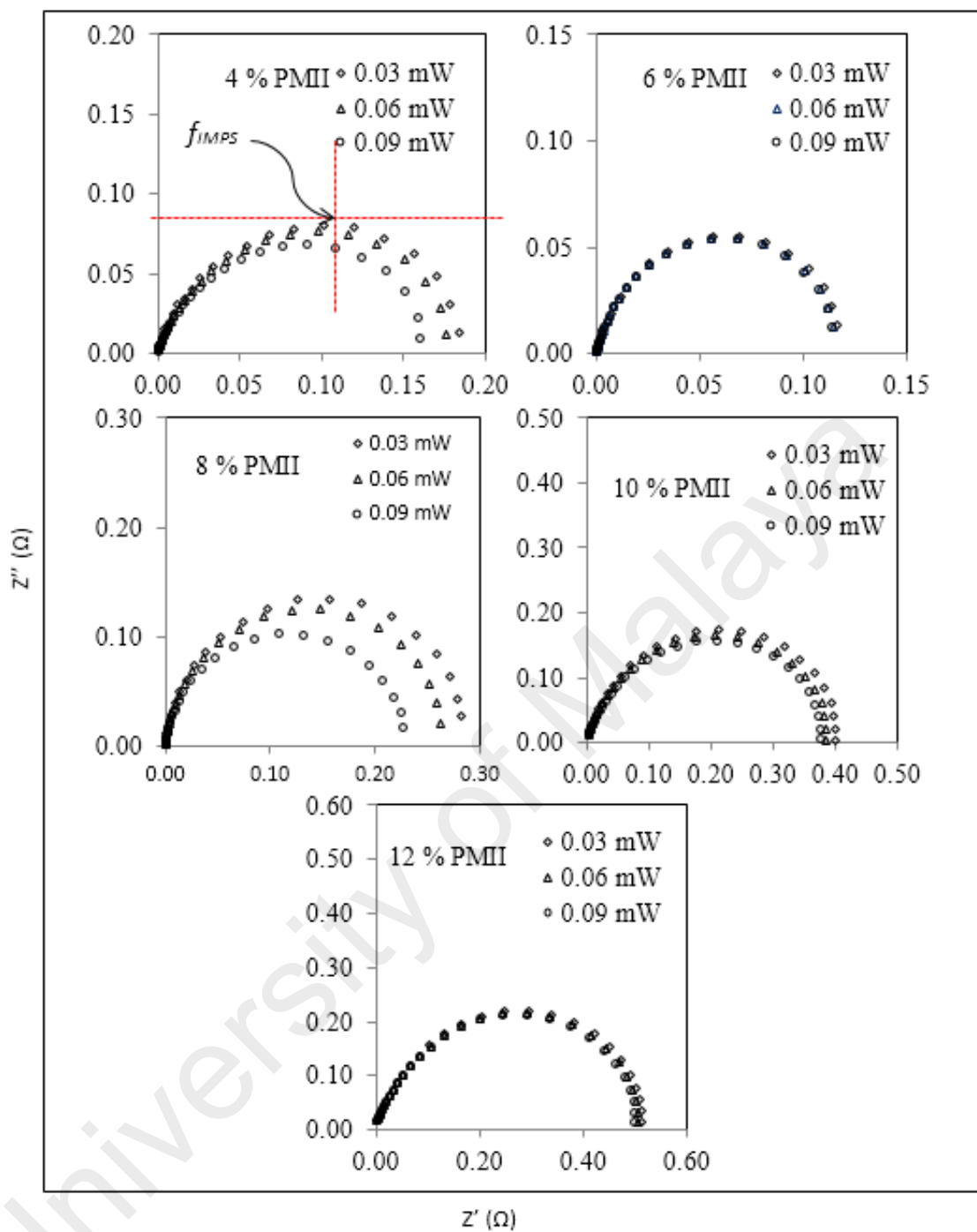


Figure 6.8: IMPS Nyquist type plots at different intensities for the DSSCs assembled with PAN:EC:PC:30 wt % TPAI:PMII:I₂ GPEs.

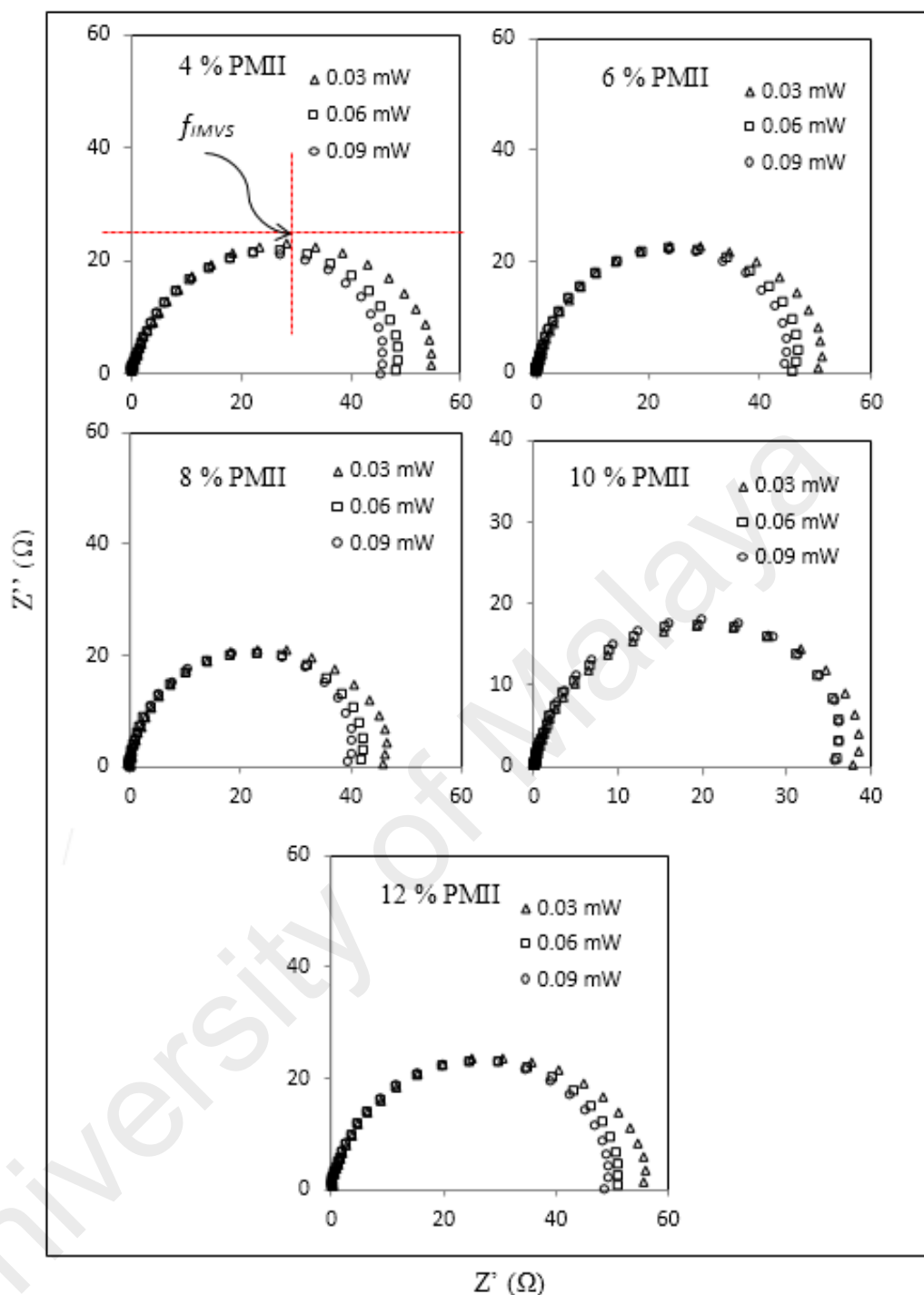


Figure 6.9: IMVS Nyquist type plots at different intensities for the DSSCs assembled with PAN:EC:PC:30wt % TPAI:PMII:I₂ GPEs.

6.5 Summary of the chapter

- The GPE with 10 wt % PMII had the lowest R_b of 13.50 Ω and highest σ of 5.90×10^{-3} S cm^{-1} . The activation energy for ion conduction had shown the lowest value as 6.14 kJ/mol.

- The triiodide diffusion coefficient, $D_{I_3}^*$ was observed highest of $1.24 \times 10^{-7} \text{ cm}^2 \text{ s}^{-1}$ for 0.069 g I_2 containing electrolyte and 10 wt % PMII.
- The value of J_0 was the highest (2.29 mA cm^{-2}) at 10 wt % PMII containing GPEs.
- The DSSC parameters of 10 wt % PMII based GPE such as: short circuit current density, J_{SC} , open circuit voltage, V_{OC} and the cell efficiency, η were found their greatest values as 21.23 mA cm^{-2} , 573.8 mV and 6.10 %, respectively.
- The 10 wt % TBAI containing GPE based DSSC showed the highest IPCE value of 69.0 %.
- The DSSCs based on 10 wt % PMII containing GPE produced lowest electron transport time (τ_{tr}) (10.05 ms) and highest recombination time (τ_{rec}) value (102.81 ms) at a given intensity which was necessary for better performance of a DSSC.
- The charge collection efficiency for DSSC with 10 wt % PMII GPE had the best η_{cc} of 0.90.
- Also, the same cell had the highest electron diffusion coefficient (D) $0.21 \text{ mm}^2 \text{ s}^{-1}$ and electron effective diffusion length, L_D of 0.15 mm which were also highest.

CHAPTER 7: RESULTS ON THE PAN:EC:PC:TPAI:BMII:I₂ GPE SYSTEM

The gel polymer electrolytes (GPEs) of PAN:EC:PC:TPAI:BMII:I₂ have been studied based on electrochemical, electrocatalytic and structural characteristics and are discussed in this chapter. This chapter also deals with *J-V*, IPEC, IMPS and IMVS characteristics of the DSSCs fabricated with these GPEs.

7.1 Electrochemical impedance spectroscopy (EIS) measurement

7.1.1 Ionic conductivity study

The EIS results in the form of Nyquist plots for PAN:EC:PC:TPAI:BMII:I₂ GPEs containing different percentage of BMII (4 wt %, 6 wt %, 8 wt %, 10 wt % and 12 wt %) at different temperatures are depicted in Figure 7.1. The GPEs with 30 wt % TPAI salt and different percentage of BMII ionic liquid have only a spike in their Nyquist plots. From the Nyquist plots, the bulk resistance, R_b was estimated and used to calculate ionic conductivity (σ) of the GPEs. The values of R_b and σ for the GPEs are presented in Table 7.1. It has been observed that R_b decreases with the rise of BMII percentage and shows the lowest value of 18.0 Ω at 10 wt % BMII containing GPE. Accordingly, σ increase with the increase of salt concentrations and reaches to the highest value of 4.42×10^{-3} S cm^{-1} at 8 wt % BMII and then again declines with further addition of BMII.

7.1.2 Activation energy for ionic conduction

The variation of conductivity with temperature in the form of $\ln\sigma$ versus $1000/T$ plots is presented in Figure 7.2 for the GPEs containing different percentages of BMII. The activation energy for ion conduction (E_a) has been determined from the fitting of the Arrhenius type equation (Equation 3.5). The activation energy for transportation of ions decreased with BMII percentage and is lowest, 6.20 kJ/mol for 8 wt % BMII containing GPE.

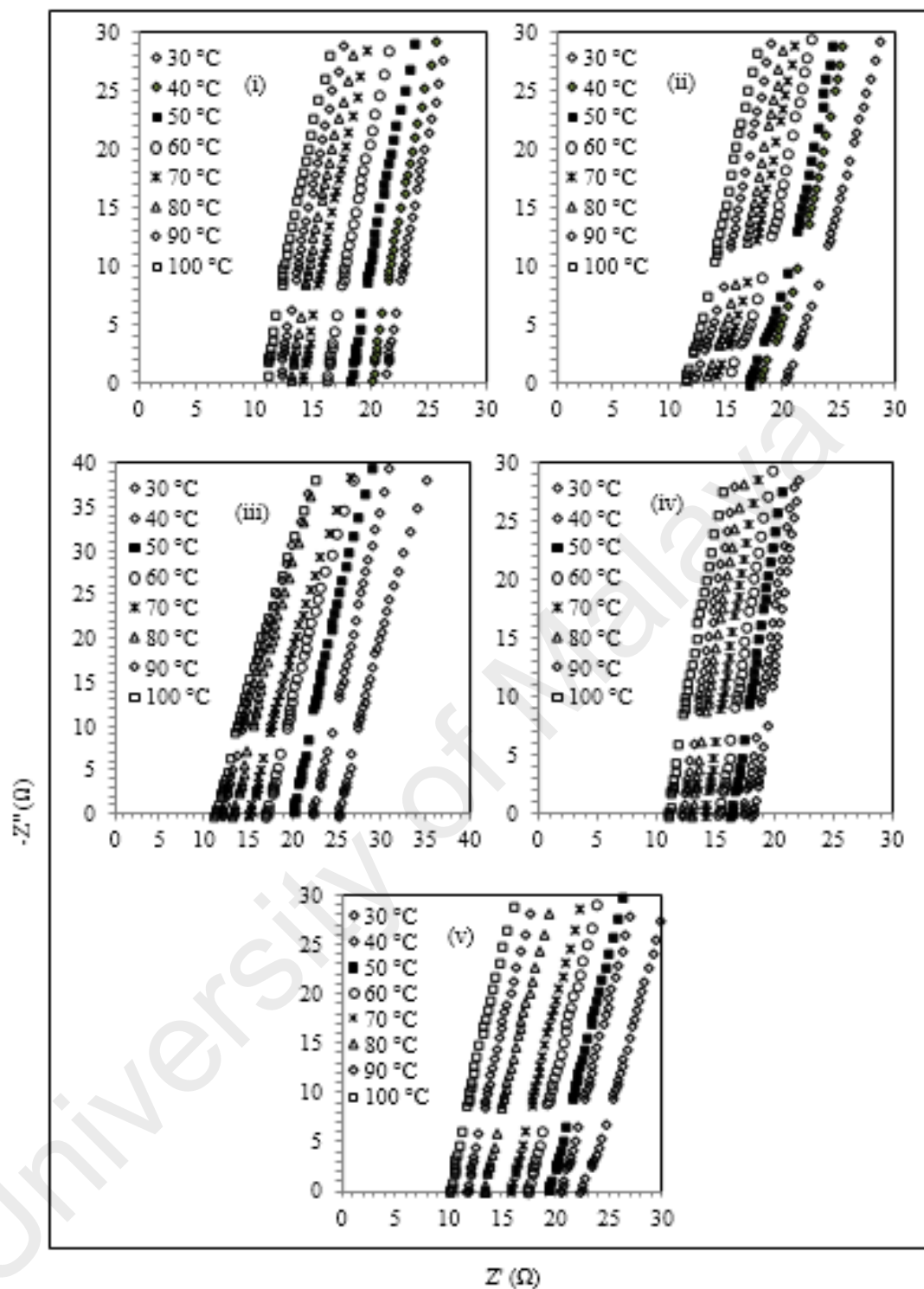


Figure 7.1 Nyquist plots for PAN:EC:PC:TPAI:BMII:I₂ GPEs: (i) 4 wt % BMII, (ii) 6 wt % BMII, (iii) 8 wt % BMII, (iv) 10 wt % BMII and (v) 12 wt % BMII.

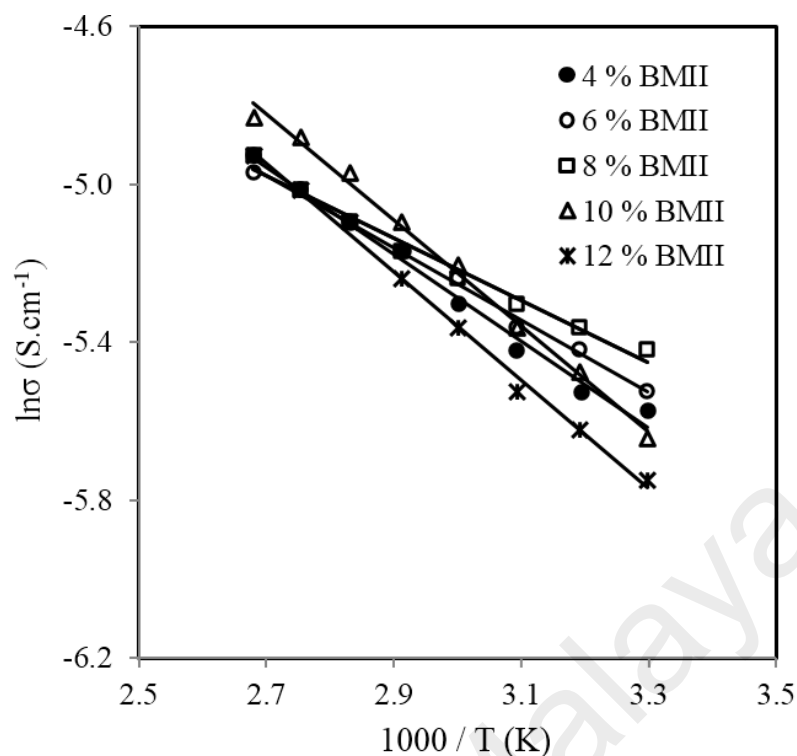


Figure 7.2: $\ln\sigma$ versus $1000/T$ graphs for different BMII containing GPEs

Table 7.1: Bulk impedance, R_b (ohm), ionic conductivity, $\sigma \times 10^{-3}$ (S/cm) and Activation energy, E_a (eV) for ion conduction for the BMII containing GPEs.

wt % BMII	R_b (ohm)	Conductivity, $\sigma \times 10^{-3}$ (S/cm)	Activation energy	
			E_a (kJ/mol)	E_a (eV)
4	21.00	3.79	8.47	0.088
6	20.00	3.98	7.52	0.078
8	18.00	4.42	6.20	0.064
10	22.50	3.54	7.18	0.074
12	25.00	3.18	7.35	0.076

7.2 Linear sweep voltammetry (LSV) measurement

7.2.1 Limiting current and I_3^- Diffusion coefficient study

Linear sweep voltammetry (LSV) is a powerful technique for the characterization of electrocatalytic activity of electrocatalysts (Wu et al., 2012). Figure 7.3 represents the characteristic linear sweep voltammetry plots for the PAN:EC:PC:TPAI:BMII:I₂ GPEs. In this case, the current densities attain saturations for both polarities at above 0.3 V. Following the previous procedure, limiting current densities (J_{lim}) as well as the apparent

diffusion coefficient of triiodide ions, $D_{I_3^*}^*$ have been calculated and tabulated in Table

7.2.

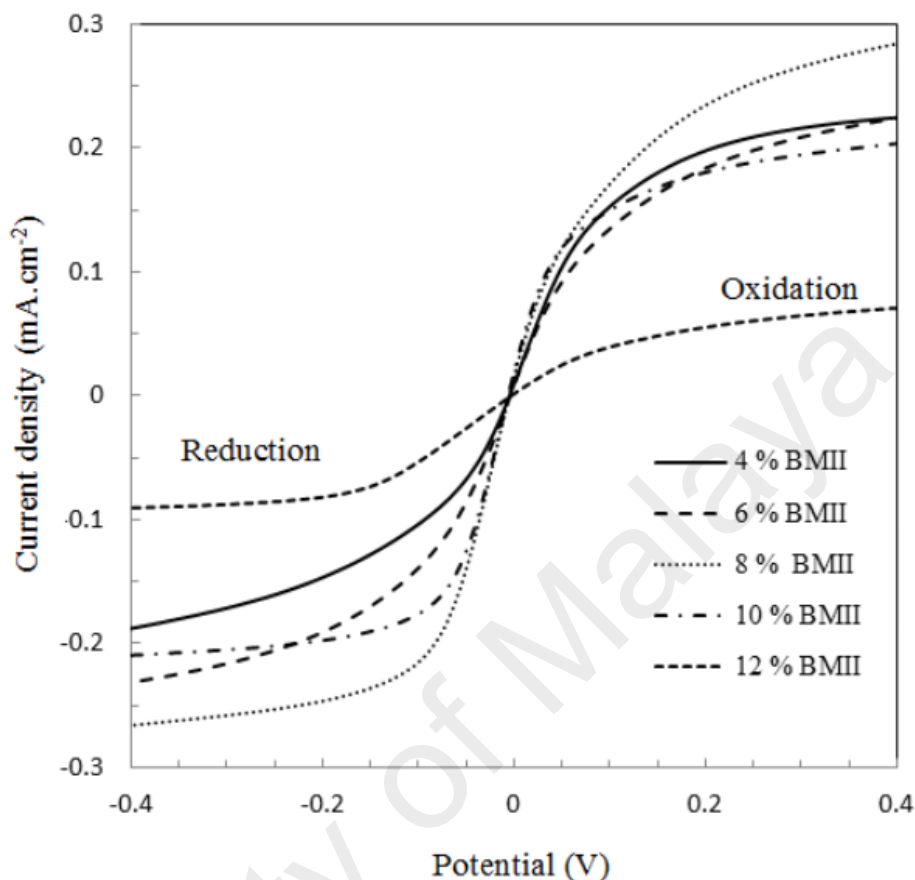


Figure 7.3: Linear sweep voltammograms (LSV) of GPEs at varying concentration of BMII with Pt ultramicroelectrode. Scan rate: 10 mV/s.

The limiting current density, J_{lim} rises with the rise of BMII content until a maximum value (0.43 mA cm^{-2}) in GPEs at 8 wt % BMII and then the values declined if more BMII was added. The value of $D_{I_3^*}^*$ increased with the increase of IL amount and was highest at $0.82 \times 10^{-7} \text{ cm}^2 \text{ s}^{-1}$ for 8 wt % BMII containing electrolyte. The values of $D_{I_3^*}^*$ decreased if more IL was added.

7.2.2 Tafel polarization curve and Exchange current density, J_0

The exchange current density, J_0 has been determined by using Tafel polarization technique. To constructed the Tafel polarization curves, linear sweep voltammetry (LSV) plot obtained from symmetrical cells have been converted to logarithmic current-voltage ($\text{Log } J-V$) (Figure 7.4) (Bard et al., 1980). By extrapolating the anodic or cathodic curves

in its Tafel zone and the cross point at 0 V, the exchange current density (J_0) values have been obtained and are summarized in Table 7.2. The values are rising with the addition of BMII in the GPE. At 8 wt % BMII containing GPEs, the J_0 value is highest (0.82 mA.cm⁻²).

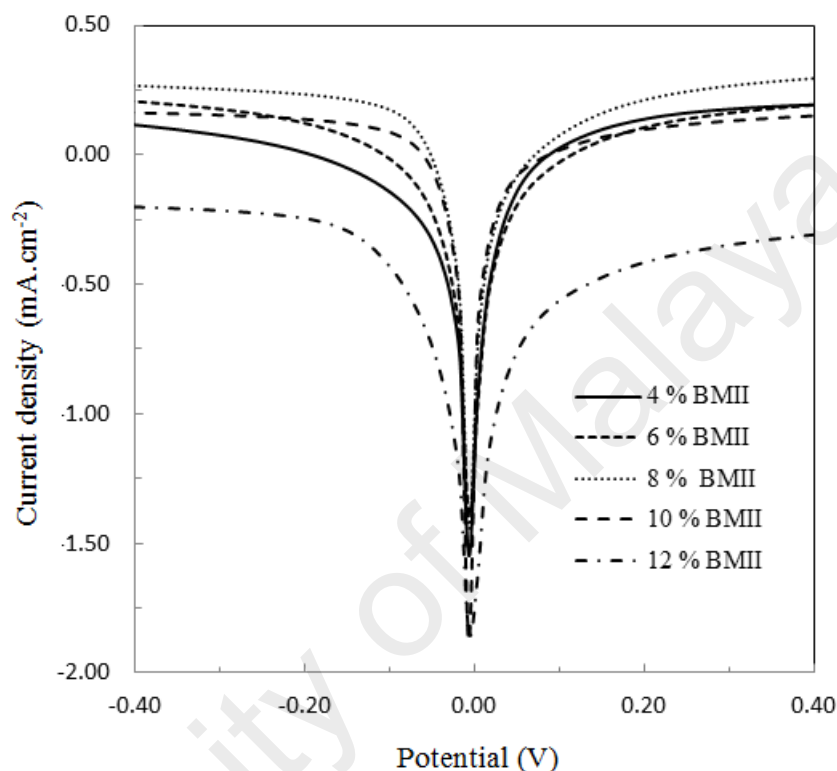


Figure 7.4: Tafel polarization curves for the electrolytes with different BMII containing GPEs.

Table 7.2: Limiting current or steady state current (J_{lim}), diffusion coefficients of I_3^- ion ($D_{I_3}^*$), exchange current density (J_0) of GPEs containing different composition of iodine.

BMII (wt %)	4	6	8	10	12
I_2 (g)	0.069	0.069	0.069	0.069	0.069
J_{lim} (mA cm ⁻²)	0.30	0.35	0.43	0.36	0.13
$D_{I_3}^*$ ($\times 10^{-7}$ cm ² s ⁻¹)	0.48	0.58	0.73	0.64	0.23
$J_{0, Tafel}$ (mA cm ⁻²)	1.01	1.19	1.50	1.26	0.41

7.3 X-ray diffraction (XRD) studies

For the GPEs with different BMII compositions, X-ray diffraction (XRD) studies were carried out to characterize their structural features. Chapter 4 and Chapter 5 have dealt

the discussion on XRD data for different GPEs systems. Here XRD data for the GPEs systems of different BMII contents will be discussed. The XRD results for the GPEs systems PAN:EC:PC:(30 wt %)TPAI:xBMII:I₂ GPEs, where x stands for 4 wt %, 6 wt %, 8 wt %, 10 wt % and 12 wt % have been depicted in Figure 7.5. It can be noticed that BMII salt can modify XRD pattern of this GPEs. The peak at $2\theta = 20^\circ$ has been shifted to $2\theta = 21^\circ$ at 6 wt % and 8 wt % BMII containing GPEs and after that the peak is disappeared. The peak at 8 % BMII GPE is little bit broader than those for 0 wt % and 6 wt % BMII GPEs. The pick broadening for $2\theta = 20^\circ$ peak is also observed at 8 wt % BMII GPE. The shifting XRD peak to words higher degree and their broadening may be due to the increase in d-spacing of the polymer matrix which is the evidence of the polymer-salt interaction and emerges from the possible complexation of cation (BMI⁺ ion) with lone pair electron containing site (-CN) in the host polymer matrix. One can simply understand that there may be an optimum concentration limit of IL composition into the PAN matrix.

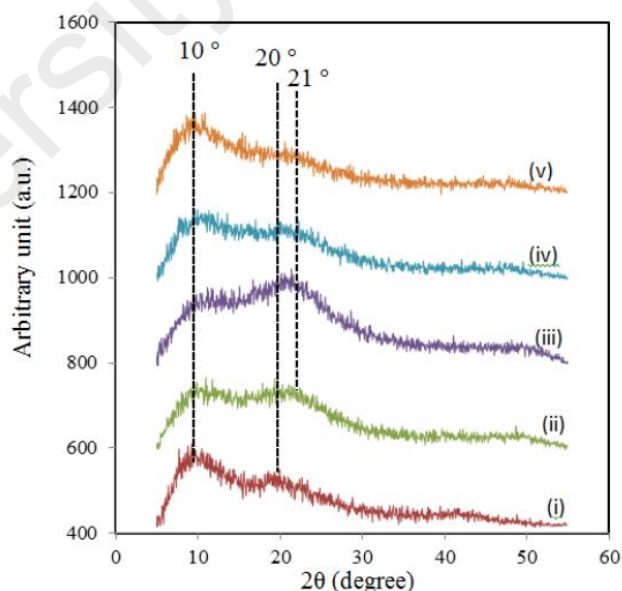


Figure 7.5: XRD pattern of PAN:EC:PC:30 wt % TPAI:I₂ GPEs with different amount of BMII (i) 0 wt %, (ii) 4 wt %, (iii) 6 wt %, (iv) 8 wt %, (v) 10 wt % and (vi) 12 wt %.

7.4 DSSC performance analysis

7.4.1 Photovoltaic (J - V) characteristics

The photovoltaic (J - V) characteristics of DSSCs developed with PAN:EC:PC:(30 wt %) TPAI: x BMII: I_2 ($x = 4$ wt %, 6 wt %, 8 wt %, 10 wt % and 12 wt %) GPEs have been presented in Figure 7.6. Table 3 shows the open-circuit voltage (V_{oc}), short-circuit current (J_{sc}), fill factor (FF) and the efficiency (η) estimated from J - V curves.

The J_{sc} and efficiency (η) of DSSC increases with the addition of BMII in the GPEs and reaches the maximum J_{sc} (17.62 mA cm⁻²) and η (5.50 %) (Figure 7.6 and Table 7.3) for the 8 wt % BMII and then declines with further addition of IL. The V_{oc} is also observed highest value as 563.9 mV for 8 wt % BMII containing GPE based DSSC.

Table 7.3: Photovoltaic performance of PAN:EC:PC:TPAI:BMII: I_2 with different weight contents of TPAI-added polymer electrolytes.

BMII	J_{sc} (mA cm ⁻²)	V_{oc} (mV)	FF	η %
4 wt %	17.01	553.8	0.5218	4.91
6 wt %	17.21	562.9	0.5232	5.07
8 wt %	17.62	563.9	0.5533	5.50
10 wt %	17.43	533.7	0.5057	4.70
12 wt %	16.37	538.8	0.4997	4.41

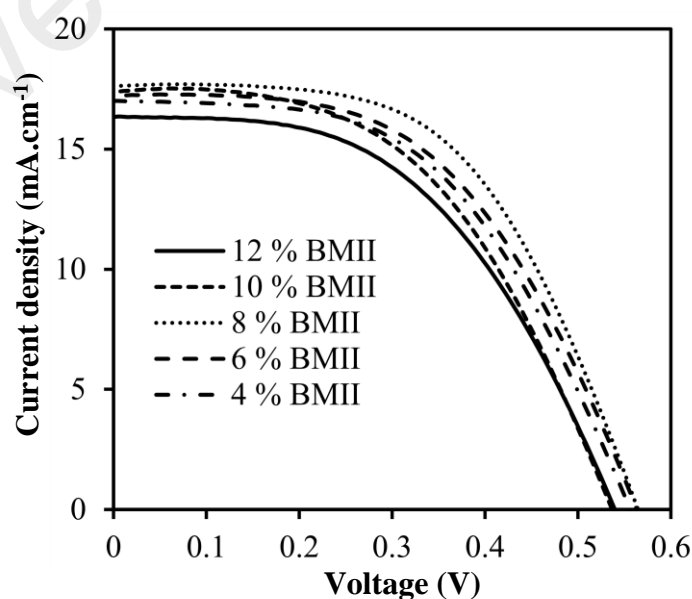


Figure 7.6: J - V curves of DSSCs for PAN:EC:PC:TPAI:BMII: I_2 GPEs systems.

7.4.2 Incident-photon-to-current efficiency (IPCE)

The incident photon to current efficiency (IPCE) spectra been collected as for supporting evidence on the light-harvesting efficiency of the DSSCs. Figure 7.7 represents the IPCE spectra as a function of wavelength from 400 to 800 nm for different DSSCs with GPEs containing various concentration of BMII.

It is observed that the IPCE curves of the five cells display similar shape of spectrum with maximum efficiencies at 520 - 550 nm which corresponds to the absorption peak of the N719 dye (O'Regan & Lenzmann, 2004). The highest IPCE value (62.5 %) among the different DSSCs at the range of visible light wavelength is observed for 8 wt % BMII GPE.

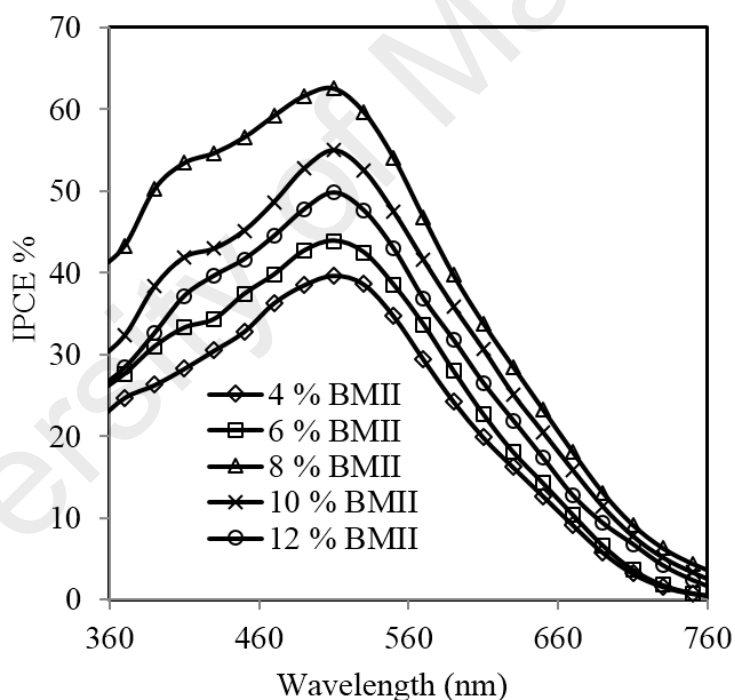


Figure 7.7: IPCE % vs. wavelength for the DSSCs with different TPAI containing GPEs.

It is observed that the IPCE curves of the five cells display similar shape of spectrum with maximum efficiencies at 520 - 550 nm which corresponds to the absorption peak of the N719 dye. The highest IPCE value (62.5 %) among the different DSSCs at the range of visible light wavelength is observed for 8 wt % BMII GPE.

7.4.3 IMPS and IMVS study of DSSCs

Intensity modulated photovoltaic spectroscopy (IMPS) graphs in the form of Nyquist-type plots at different base intensities (0.03, 0.06 and 0.09 mW) have been presented in Figure 7.8. It is to be noted that, as the intensity increases the radius of the semicircle slightly decreases. The radius of the semicircle for the IMPS plots are not changed significantly with the intensity of the light. All curves show maxima at intermediate frequencies, f_{IMPS} which is the characteristic frequency for the electron transport through the pores of the anode to the back layer.

IMVS experimental results have been presented as Nyquist-type plots at different base intensities (0.03, 0.06 and 0.09 mW) in the Figure 7.9. It is observed that, the radius of the semicircle decreases as the intensity increases. All the diagrams exhibit a maximum at intermediate frequencies, f_{IMVS} which is used to calculate the recombination time τ_{rec} . The values of f_{IMVS} and τ_{rec} have been tabulated in Table 7.4.

Among the all DSSCs based on the GPEs the one with 8 wt % BMII in the GPE showed the smallest τ_{tr} value (12.65 ms) and highest τ_{rec} value (44.58 ms) at a given intensity which is necessary for better performance of a DSSC. The charge collection efficiencies for 4 wt %, 6 wt %, 8 wt %, 10 wt % and 12 wt % BMII GPEs were 0.11, 0.29, 0.72, 0.65 and 0.37 respectively. The best charge collection efficiency η_{cc} (0.72) was observed for the 8 wt % BMII GPE based DSSC. Furthermore, the electron diffusion coefficient, D for this DSSC was also highest ($0.16 \text{ mm}^2\text{s}^{-1}$). The corresponding effective diffusion length, L_D was greatest (0.09 mm for 8 wt % BMII GPE) for the same GPE compared to other GPE which was higher than electrode thickness (0.07 mm).

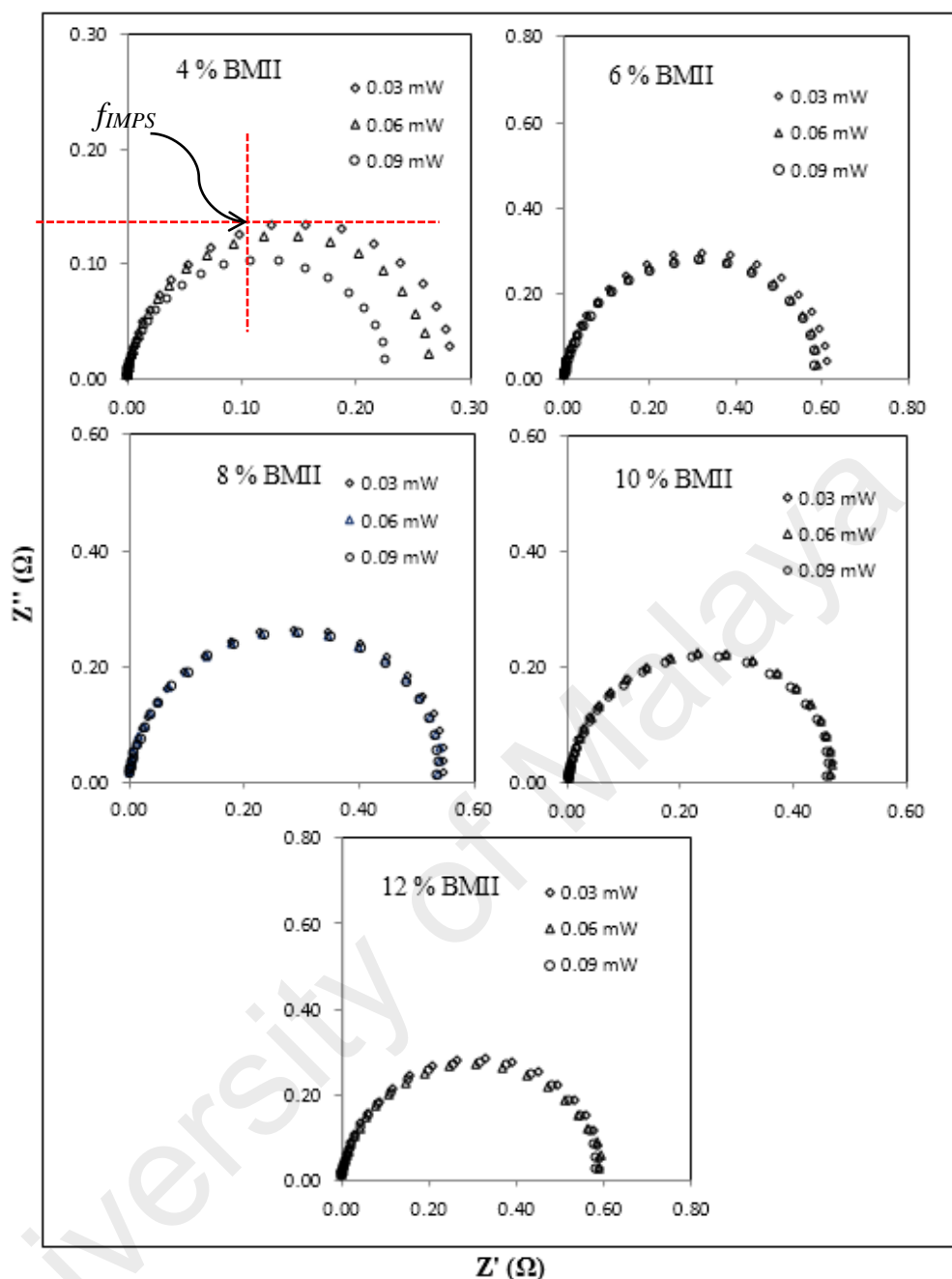


Figure 7.8: IMPS Nyquist type plots at different intensities for the DSSCs assembled with GPEs containing different percentages of BMII.

Table 7.4: Summary of parameters obtained from IMPS and IMVS experiments for different DSSCs fabricated with GPEs containing various percentages of BMII.

BMII	f_{IMPS} (Hz)	τ_{tr} (ms)	f_{IMVS} (Hz)	τ_{rec} (ms)	η_{cc}	D (mm ² /s)	L_D (mm)
4 wt %	5.6608	28.13	5.0119	31.77	0.11	0.07	0.05
6 wt %	6.3096	25.24	4.4965	35.41	0.29	0.08	0.05
8 wt %	12.589	12.65	3.5717	44.58	0.72	0.16	0.09
10 wt %	11.295	14.10	3.9811	40.00	0.65	0.15	0.08
12 wt %	7.9433	20.05	5.0119	31.77	0.37	0.10	0.06

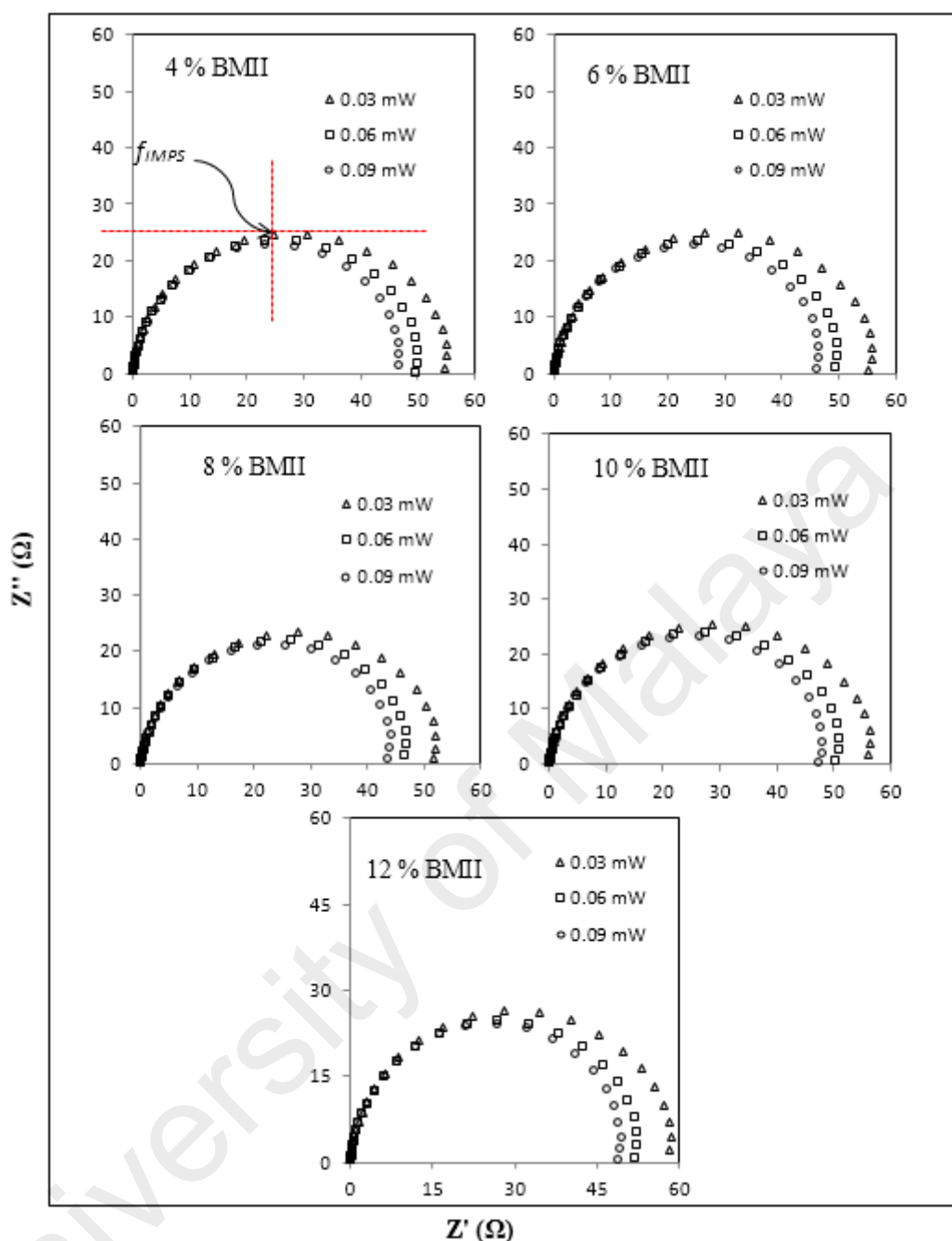


Figure 7.9: IMVS Nyquist type plots at different intensities for the DSSCs assembled with GPEs containing different percentage of BMII.

7.5 Summary of the chapter

- The 8 wt % BMII containing GPE showed the lowest R_b of 18.00 Ω and highest conductivity (σ) of $4.42 \times 10^{-3} \text{ S cm}^{-1}$. This electrolyte also showed the smallest activation energy (6.20 kJ/mol) for ionic conduction.
- The triiodide diffusion coefficient, $D_{I_3}^*$ was observed highest value of $0.64 \times 10^{-7} \text{ cm}^2 \text{ s}^{-1}$ for 0.069 g I_2 containing electrolyte and 8 wt % BMII.

- The value of J_0 was highest (1.26 mA cm^{-2}) at 8 wt % BMII containing GPE.
- The DSSC parameters of 8 % BMII based GPE such as: short circuit current density, J_{sc} , open circuit voltage, V_{oc} and the cell efficiency, η were found their greatest values as 17.62 mA cm^{-2} , 563.9 mV and 5.50% , respectively.
- The 8 wt % BMII containing GPE based DSSC showed the highest IPCE value of 62.5% .
- The DSSCs based on 8 wt % BMII containing GPE produced lowest electron transport time (τ_{tr}) (14.10 ms) and highest recombination time (τ_{rec}) value (40.00 ms) at a given intensity which was necessary for better performance of a DSSC.
- The charge collection efficiency for DSSC based on 10 wt % BMII GPE had the best η_{cc} of 0.65 .
- The cell showed the highest electron diffusion coefficient (D) $0.16 \text{ mm}^2\text{s}^{-1}$ and electron effective diffusion length, L_D of 0.09 mm which are also highest.

CHAPTER 8: DISCUSSION

The four series of GPEs: (1) PAN:EC:PC:TPAI:I₂, (ii) PAN:EC:PC:TBAI:I₂, (iii) PAN:EC:PC:TPAI:PMII:I₂ and (iv) PAN:EC:PC:TPAI:BMII:I₂ were prepared and characterized by EIS, LSV and XRD techniques. All the GPEs were used to fabricate the DSSCs. The DSSCs were characterized by *J-V*, IPCE, IMPS and IMVS techniques. As shown in Table 8.1, the ionic conductivity of the GPEs containing TPAI and TBAI are highest at 30 wt % salt concentrations and the values are $3.62 \times 10^{-3} \text{ S.cm}^{-1}$ and $3.46 \times 10^{-3} \text{ S.cm}^{-1}$, respectively.

Table 8.1: Conductivity (σ) and activation energy (E_a) of GPEs with different percentage of TPAI and TBAI, respectively.

Parameters	30 wt % TPAI	30 wt % TBAI	10 wt % PMII	8 wt % BMII
$\sigma \times 10^{-3} \text{ (S/cm)}$	3.62	3.46	5.90	4.42
$E_a \text{ (kJ/mol)}$	10.09	12.59	6.14	6.20

It is observed that, GPEs with TPAI exhibit higher ionic conductivities compared to that with TBAI. From the structural view point of quaternary ammonium iodide salts the σ varies as $\text{CH}_3\text{-CH}_2\text{-CH}_2\text{-} > \text{CH}_3\text{-CH}_2\text{-CH}_2\text{-CH}_2\text{-}$. An attempt has been taken to further increase the ionic conductivity of 30 wt % TPAI containing GPE by adding RTILs. For better choice of RTIL and to find out their best composition two series of GPEs containing PMII and BMII, respectively have been examined. The PMII and BMII show the highest conductivities $5.90 \times 10^{-3} \text{ S.cm}^{-1}$ and $4.42 \times 10^{-3} \text{ S.cm}^{-1}$ at 10 wt % and 8 wt % IL compositions, respectively and the conductivity of GPE with PMII is higher than that with BMII. As is the case of GPE-salt conductivity behavior of quaternary ammonium iodide salts, the GPEs with lesser carbons in the IL structure exhibit higher conductivity i.e., $\sigma (\text{CH}_3\text{-CH}_2\text{-CH}_2\text{-}) > \sigma (\text{CH}_3\text{-CH}_2\text{-CH}_2\text{-CH}_2\text{-})$. In other words, σ decreases with increase of alkyl chain length attached to ILs.

Increase of alkyl chain length may increase the steric hindrance and hence viscosity resulting in the decrease of ionic mobility in the gel matrix. Furthermore, addition of

RTIL may increase the liquidity and decrease the viscosity which resulted in ionic conductivity enhancement. On the other hand, in the case of PMII and BMII ILs, the conductivity decreased with increased chain length. It is well known that the ionic conductivity strongly depended on the viscosity of ILs (Papović et al., 2016). According to the Walden rule (Walden, 1921) molar conductivity $A_m \propto 1/\eta^\alpha$ where A_m is molar conductivity, η is the viscosity of IL and α is a constant. The longer chain slows the movement of the particle resulting in increased IL viscosity.

From the Arrhenius relation ($\ln \sigma = -(E_a/kT) + \ln C$) the activation energy for ion conduction, E_a was calculated. Results imply that the lower the activation energy, the higher is the ionic conductivity. If the activation energy for ion conduction is lower, the ion can easily overcome the energy barrier to move. This increased ionic mobility and ionic conductivity also increased. The E_a value is higher in TBAI and BMII containing GPEs. This implied that the bulkier groups or longer chain containing elements need higher energy to overcome the energy barrier than lighter groups or shorter chain compounds.

From the linear sweep voltammograms (LSVs) of GPEs carried out at Pt-ultramicroelectrodes cells, the limiting current density (J_{lim}), triiodide ion diffusion coefficient ($D_{I_3}^*$) and exchange current density (J_0) have been calculated. The electrochemical reaction at the Pt/electrolyte interface due to the application of potential is: $I_3^- + 2e^- \rightleftharpoons 3I^-$. The limiting current was considered for triiodide ions as iodide concentration was taken greater than the concentration of I_2 in the mixture (Papageorgiou et al., 1996). Therefore, limiting current densities (J_{lim}) was used to determine the apparent diffusion coefficient of triiodide, $D_{I_3}^*$ according to the following relation, $D_{I_3}^* = (J_{lim} \times d)/(2nFC_0)$. Here, n equals 2 and is the electron number required for the reduction of triiodide to iodide, C_0 is the initial concentration of the triiodide ions, d the thickness of the cell which is 53 μm and F the Faraday constant. For both polarities, the

current density was saturated at $> \sim 300$ mV. The plateaus of the anodic and cathodic limiting current are almost alike which indicated that oxidation-reduction reaction on the Pt surface is in equilibrium or in steady state (Kontos et al., 2006).

The maximum values of these parameters for the four systems are tabulated in Table 8.2. The values of J_{lim} , $D_{I_3^-}^*$ and J_0 for TPAI containing GPEs at 30 wt % salt TPAI are higher than that of GPEs with the same concentration of TBAI. After addition of PMII or BMII in 30 wt % TPAI GPE, these parameters showed decreased values and the maxima have been observed at 10 wt % and 8 wt % IL compositions. However, the GPEs with TPAI and PMII still exhibited higher values than that of GPEs with TBAI and BMII.

Table 8.2: Maximum values of limiting current density (J_{lim}), triiodide ion diffusion coefficient ($D_{I_3^-}^*$) and exchange current density (J_0).

Composition	30 wt % TPAI	30 wt % TBAI	10 wt % PMII	8 wt % BMII
J_{lim} (mA cm ⁻²)	12.76	5.00	0.70	0.43
$D_{I_3^-}^*$ ($\times 10^{-7}$ cm ² s ⁻¹)	16.83	6.59	1.24	0.73
$J_0, Tafel$ (mA cm ⁻²)	11.22	0.63	2.29	1.50

As like ionic conductivity, the triiodide diffusion also increased with the addition of salt. There are two ways for the I^- and I_3^- ion to migrate through the GPEs. One way of ion migration can happen through the interconnected pores and the other way the ion migrates through the amorphous region in the gel matrix (Zhang et al., 2016). The salt is dissociated to form ions and creates free volume space and pores in between the polymer chains providing ion transporting channels. Addition of more salt and iodine provides more I_3^- . They are passing through the channels in the polymer matrix resulted in increased I_3^- ion diffusion. The I_3^- diffusion coefficient decreased when the ion content crosses the optimum limit, i.e., 30 % of the salt concentration. This can be attributed to salt aggregation that led to increased crystallinity squeezing the ion transporting channels or free volumes in GPEs that finally led to lowering of ion diffusion. Additionally,

polymer chain could not be able to accommodate or disperse excess salt in the GPEs effectively, which increased the viscosity of electrolyte. This phenomenon lowered ion migration and resulted in decreased diffusion coefficient (Zhang et al., 2016).

As shown in Table 8.2, after addition of PMII or BMII in 30 wt % TPAI GPE, J_{lim} , $D_{I_3^-}^*$ and J_0 decreased. In the case of doping IL in the GPEs, the I_2 content was fixed (0.069 g). As the IL was added keeping the amount of I_2 as well as I_3^- constant, the molar concentration of the I_3^- ion was decreased which may be one of the causes for lowering of LSV parameter (J_{lim} , $D_{I_3^-}^*$ and J_0) after addition of IL.

The J - V characteristic parameters: (open-circuit voltage (V_{oc}), short-circuit current (J_{sc}), fill factor (FF) and the efficiency (η) of the dye-sensitized solar cells (DSSCs) fabricated with the GPEs are presented in Table 8.3.

Table 8.3: Maximum values of short circuit current (J_{sc}), open circuit voltage (V_{oc}) and fill factor (FF) for DSSCs fabricated with different salt and or ILs containing GPEs.

Salts/ILs	J_{sc} (mA cm ⁻²)	V_{oc} (mV)	FF	η %
30 wt % TPAI	19.74	553.8	0.4400	4.76
30 wt % TBAI	12.66	548.9	0.4500	3.32
10 wt % PMII	21.23	573.8	0.5012	6.10
8 wt % BMII	17.62	563.9	0.5533	5.50

Following the similar trend of conductivity versus salt concentration, J_{sc} as well as efficiency (η) of DSSCs increased with the addition of salt in the GPEs attaining the maximum at their 30 wt % salt containing GPEs. The value of V_{oc} for the DSSC with 30 wt % TPAI containing GPE was the highest. One may interpret that after a certain concentration of I_3^- , the distance between anion and cation might not be enough to overcome completely the electrostatic force of attraction among the ions i.e. the lowering of the dissociation of the salt which resulted in the lower diffusion rate of I_3^- ions and polyiodides (I_5^- , I_7^- and I_9^-) may be formed. Similarly, more salt provided more ions in

the electrolyte which may cause ion aggregation and/or restriction of ion diffusion due to the reduction of free space.

Again, the rising of power conversion efficiency of the DSSCs based on PAN:EC:PC:TPAI:I₂ and PAN:EC:PC:TBAI:I₂ GPEs with addition of more salt may be due to the increase of conduction band level of TiO₂ positively which diminishes the energy gap between LUMO level of the dye and the TiO₂ conduction band. Also, this can increase the driving force for the electron to be injected into the TiO₂ conduction band (Lee et al., 2009; Theerthagiri et al., 2015).

It is necessary for the optimum functioning of the cells to screen the charges injected to the TiO₂ nano-particles by the electrolyte through facilitation of electron percolation in the anode towards FTO (Bandara et al., 2012; Grätzel, 2005). The cation screens the electron from the electrolyte. The ion diffusion in the electrolyte and interfacial electron transferring are coupled with the motion of the electron in the conduction band of the TiO₂ film. Therefore, the electron movement in the conduction band of TiO₂ layer is accompanied by charge-compensating cation diffusion in the anode surface that is in contact with the electrolyte layer. The cations screen the electrons' Coulomb charges circumventing the uncompensated local space charge formation (Bandara et al., 2012; Grätzel, 2005). The space charge is occurred due to the repulsion of emitted electrons by the electron cloud of the electrons in its neighborhood. From electrophoresis measurements it was observed that the bulkier cation such as TBA⁺ cannot be adsorbed on the dye coated TiO₂ film efficiently (Pelet et al., 2000). The efficiency of the cells showed highest values at the 30 wt % of salts. After that the efficiency values decreased.

Addition of ILs in to the 30 wt % TPAI containing GPE can enhance the ionic conductivity and hence DSSC performance. With the addition of PMII and BMII, the power conversion efficiency of DSSC increased to 6.10 % and 5.50 %, respectively and

can be associated with increased V_{oc} and J_{sc} of the respective systems. The improvement of J_{sc} may be accounted for the rise of the ionic conductivity of iodide ions coming from the IL. Also, it might be due to the plasticizing effect of IL which could decrease the viscosity of the GPEs leading to enhanced ionic mobility of the iodide ion through GPEs (Lin et al., 2014). The fill factors of the DSSCs with IL-GPEs showed a slight increase in values.

The efficiencies of DSSCs fabricated with PMII is higher than that with BMII. This variation is also followed by other electrolyte properties such as ionic conductivity, parameters obtained from LSV and DSSC characteristic parameters (J_{sc} and V_{oc}). The variation of carbon chain length between PMII and BMII is the cause of the differences in their properties. The viscosity is the fundamental property of ILs which governs their behavior in the electrolyte systems. The viscosity of BMII and PMII are 1024 cP and 1110 cP, respectively (Bidikoudi et al., 2014). According to the previous report (Bidikoudi et al., 2013), increase in chain length, increase resistance that led to increased viscosity. The more viscous media hindered ion mobility resulting to slower diffusion. Comparatively low viscosity can lift the mass transfer through the Grotthuss mechanism of charge transferring process (Hao & Lin, 2013) affecting the ionic conductivity and triiodide diffusion coefficient. Hence the efficiency of the DSSC of PMII is higher than that of BMII. Furthermore, the smaller ion can enhance the dye to TiO_2 electron injection yield, electron diffusion through the TiO_2 layer and regeneration of dye (Bandara et al., 2012).

The cells fabricated with the highest ionic conducting GPEs showed the best performance, respectively. The highest values of J_{sc} , V_{oc} and η for different GPEs based DSSCs follow the trend as TPAI+PMII > TPAI+BMII > TPAI > TBAI. Similar trend is also observed for the ionic conductivity behavior of the GPE. After addition of IL into the GPEs, FF is also increased. The differences of FF values of GPEs containing TPAI

and TBAI or PMII and BMII is very small. This implied the effect of alkyl chain length attached to the salts or ILs on FF is negligible.

The incident-photo-to-current efficiency (IPCE) spectra complemented the light-harvesting efficiency of the DSSCs. The IPCE values are found to follow the order TPAI+PMII (69.00 %) > TPAI+BMII (62.5 %) > TPAI (58.50 %) > TBAI (54.00 %). It is observed that the IPCE curves of the cells displayed similar shape of spectrum with maximum efficiencies at 520 - 550 nm which corresponded to the absorption peak of the N719 dye (Yang Bai et al., 2012).

Table 8.4 displays the electron transport time, τ_{tr} through the pores of the anode to the back layer and the electron recombination time, τ_{rec} which indicated the degradation of DSSCs efficiency. The τ_{tr} is lowest (10.05 ms) and the τ_{rec} is highest (102.81 ms) for TPAI+PMII GPEs based DSSCs among all the four DSSC systems which confirmed its superiority in electron transferring ability through TiO₂ surface to FTO substrate that could lead to the best cell efficiency. This finding is conceivable with the photovoltaic (J - V) characteristics of the DSSC and ionic conductivity result of the GPE. The τ_{tr} is much higher than τ_{rec} which means that the transfer of photo-excited electrons to the CB of TiO₂ was fast enough preventing the electrons from undergoing recombination. A good solar cell must have such electrodynamic character. The charge collection efficiency (η_{cc}), electron diffusion (D) and effective diffusion length (L_D) for the TPAI+PMII GPE showed the highest values of 0.9023, 0.2075 mm²/s and 0.1461 mm, respectively. This data further supports the best efficient cell with this electrolyte. The effective diffusion length, L_D is higher than anode film thickness (0.07 mm). For good performance of a DSSC, the electron diffusion length should be higher than working electrode thickness. If electrode thickness is greater than electron diffusion length, electron recombination becomes easier, hence cell efficiency diminishes (Laurence Peter, 2009; Rezvani et al.,

2016). All the results have been found to show well conceivable with other DSSC and electrochemical characterizations. Also, it indicates that the DSSC fabricated with TPAI+PMII GPE is superior to other DSSCs in the present investigation.

Table 8.4: The electron transfer time (τ_{tr}), electron recombination time (τ_{rec}), charge collection efficiency (η_{cc}), electron diffusion coefficient (D) and diffusion length (L_D) for DSSCs fabricated with different salts and or ILs containing GPEs.

Salts/ILs	τ_{tr} (mS)	τ_{rec} (mS)	η_{cc}	D (mm ² /s)	L_D (mm)
30 wt % TPAI	20.05	159.24	0.87	0.10	0.13
30 wt % TBAI	35.41	88.95	0.60	0.06	0.07
10 wt % PMII	10.05	102.81	0.90	0.21	0.15
8 wt % BMII	12.65	44.58	0.72	0.16	0.09

With decreasing the chain length from butyl to propyl, the efficiency of DSSC increased by ~ 44 % for quaternary ammonium iodide salts (TBAI and TPAI) and by ~ 11 % for ImILs (BMII and PMII). Similarly, J_{sc} has increased by ~ 66 % and ~ 21 % for salts and ILs, respectively in this experiment. On the other hand, V_{oc} has increased only slightly (~ 1-2 %). Furthermore, the conductivity has been observed to increase by ~ 5 % from TBAI to TPAI containing GPEs and by ~ 35 % from BMII to PMII.

Comparison of the IMPS and IMVS results revealed that the electron transfer time, τ_{tr} decreased by 77 % and electron recombination time, τ_{rec} increased by 44 % from TBAI to TPAI salt which indicated the efficient electron transfer ability and reduced electron recombination tendency for their corresponding DSSCs. The τ_{tr} and τ_{rec} showed 26 % decrement and 57 % increment, respectively from BMII to PMII ionic liquid based DSSCs which further supports the superiority of the DSSC of PMII based GPE over BMII based GPE. Furthermore, the current collector efficiency, electron diffusion and diffusion length increased by 31%, 43 % and 44 % when the salt was changed from TBAI to TPAI and by 21 %, 21 % and 41 % from BMII to PMII ILs. The electrocatalytic activity in terms of limiting current density and exchange current density enhanced by 46 % and 78

%, respectively for changing salts (TBAI to TPAI) and 63 % and 53 % for changing ILs (BMII to PMII). Similarly, the triiodide diffusion was raised by 46 % and 66 % for salt and IL, respectively.

The DSSC fabricated with (1-hexyl-3-methylidazolium iodide) HMImI incorporated quasi-solid-state liquid was reported with energy conversion efficiency of 5.0 %. The short-circuit currents (J_{SC}) of these electrolytes based DSSCs were observed about 70 % higher than those obtained from DSSCs using an organic liquid electrolyte (Kubo et al., 2003; Kubo et al., 2002). These results illustrate that the lower diffusion of I_3^- to the counter electrode through the electrolyte limits the J_{SC} values and that a larger amount of I_3^- would be required to sustain efficiency. In addition, the higher diffusion is caused by the higher cation number in the IL based GPEs. The electron diffusion length is increased by the addition of IL and with the shorter alkyl chain addition in the salt or IL.

CHAPTER 9: CONCLUSIONS AND SUGGESTIONS FOR FUTURE WORK

9.1 Conclusions

To achieve the objectives related to the preparation and characterization of GPEs, firstly two gel polymer electrolytes were prepared based on PAN:EC:PC:TPAI:I₂ and PAN:EC:PC:TBAI:I₂ complexes and characterized by EIS, XRD and LSV techniques. The host polymer was PAN and the doping salts were TPAI and TBAI. The GPE with TPAI showed higher conductivity ($3.62 \times 10^{-3} \text{ S.cm}^{-1}$) than that of TBAI ($3.46 \times 10^{-3} \text{ S.cm}^{-1}$). For further improvement of electrolyte performance which was another objective of this thesis, TPAI based GPE was chosen to be added with PMII and BMII ionic liquids. The conductivity of PMII ($5.90 \times 10^{-3} \text{ S.cm}^{-1}$) > BMII ($3.54 \times 10^{-3} \text{ S.cm}^{-1}$). On the basis of ionic conductivity, the GPE PAN (7 wt %):EC (28 wt %):PC (28 wt %):TPAI (27 wt %):PMII (10 wt %):I₂ was found as best system among other systems in this study. Conductivity, σ and temperature, T were observed to obey the Arrhenius relationship. The activation energy for ion conduction, E_a decreased accordingly as: TBAI (12.59 kJ/mol) > TPAI (10.09 kJ/mol) > TPAI+BMII (6.20 kJ/mol) > TPAI+PMII (6.14 kJ/mol). The lowest value of E_a for PMII containing GPE indicated that the energy barrier for the ion conduction was minimal and hence maximum conductivity. The values of J_{lim} , $D_{I_3}^*$ and J_0 were higher for TPAI containing GPE when compared to TBAI containing GPE at 30 wt % salt compositions and for all other salt compositions. After doping the ILs, polyiodides (I₅⁻ and I₇⁻) may be formed which may reduce the J_{lim} , $D_{I_3}^*$ and J_0 .

One vital objective was to examine the suitability of the GPEs for DSSC application. To achieve this objective, author fabricated and tested the DSSCs based on these GPEs. The parameters estimated from J - V characteristics, J_{sc} , V_{oc} and η showed that these parameters were higher for DSSCs with electrolytes containing TPAI + 10 wt % PMII followed by TPAI + 8 wt % BMII and then by DSSCs with electrolytes containing TPAI

and TBAI. With reduction in alkyl chain length from butyl to propyl the efficiency, η of DSSC was observed to increase by $\sim 44\%$ in the quaternary ammonium salts and $\sim 11\%$ for ImILs. Similarly, J_{sc} increased by $\sim 66\%$ and $\sim 21\%$ for salts and ILs, respectively. On the other hand, V_{oc} has increased very slightly ($\sim 1-2\%$). Also, the IPCE values for the DSSCs were found to follow the order TPAI+PMII (69.00 %) > TPAI+BMII (62.5 %) > TPAI (58.50 %) > TBAI (54.00 %).

IMPS and IMVS data showed that the electron transfer time, τ_{tr} decreased by 77 % and electron recombination time, τ_{rec} increased by 44 % from TBAI to TPAI salt. The τ_{tr} and τ_{rec} showed 26 % decrement and 57 % increment, respectively from BMII to PMII ionic liquid based DSSCs. Furthermore, the current collector (η_{cc}), electron diffusion (D) and diffusion length (L_D) increased by 31 %, 43 % and 44 % from TBAI to TPAI and by 21 %, 21 % and 41 % from BMII to PMII in their respective DSSCs. The objective related to the study of electron transport properties of the DSSCs fabricated with these GPEs has been fulfilled by the IMPS and IMVS study.

We also observed that the propyl group ($\text{CH}_3\text{-CH}_2\text{-CH}_2\text{-}$) side chain containing quaternary ammonium iodide salts and ILs show better DSSC performance compared to butyl group ($\text{CH}_3\text{-CH}_2\text{-CH}_2\text{-CH}_2\text{-}$) side chain containing salts and ILs. One of the objectives was to study the influence of the alkyl group chain length in the imidazolium ionic liquids on the performance of DSSCs which has been achieved.

9.2 Suggestions for future work

The present study has developed some thoughts for future dimension of research. For the continuation of this research in future, some suggestions can be made based on the findings/insights of the present work.

- Transference number, ion pairs and mobility of these electrolyte systems will enrich the literature.

- Additives e.g. 4-tert-butylpyridine (TBP) can be doped in this GPE system for further enhancement of DSSC efficiency.
- Modeling and simulation of the J - V characteristics of these GPEs based DSSCs can contribute to the knowledge of DSSC study.
- Other side chain groups such as: methyl, ethyl, pentyl, hexyl can be introduced in the GPEs and tested for DSSCs to get a more comprehensive understanding of the alkyl chain length effect in DSSC performance.
- The effect of side chain length on electron trapping-detrapping of the DSSCs can be studied.

University of Malaya

REFERENCES

- Adachi, M., Murata, Y., Takao, J., Jiu, J., Sakamoto, M., & Wang, F. (2004). Highly efficient dye-sensitized solar cells with a titania thin-film electrode composed of a network structure of single-crystal-like TiO₂ nanowires made by the “oriented attachment” mechanism. *Journal of the American Chemical Society*, *126*(45), 14943-14949.
- Alkire, R. C., Bartlett, P. N., & Lipkowsky, J. (2015). *Electrochemical Engineering Across Scales: From Molecules to Processes*: John Wiley & Sons.
- Arof, A. K., Jun, H. K., Sim, L. N., Kufian, M. Z., & Sahraoui, B. (2013). Gel polymer electrolyte based on LiBOB and PAN for the application in dye-sensitized solar cells. *Optical Materials*, *36*(1), 135-139.
- Asbury, J. B., Ellingson, R. J., Ghosh, H. N., Ferrere, S., Nozik, A. J., & Lian, T. (1999). Femtosecond IR Study of Excited-State Relaxation and Electron-Injection Dynamics of Ru(dcbpy)₂(NCS)₂ in Solution and on Nanocrystalline TiO₂ and Al₂O₃ Thin Films. *The Journal of Physical Chemistry B*, *103*(16), 3110-3119.
- Bai, Y., Cao, Y., Zhang, J., Wang, M., Li, R., Wang, P., Grätzel, M. (2008). High-performance dye-sensitized solar cells based on solvent-free electrolytes produced from eutectic melts. *Nature Materials*, *7*(8), 626-630.
- Bai, Y., Yu, H., Li, Z., Amal, R., Lu, G. Q., & Wang, L. (2012). In Situ Growth of a ZnO Nanowire Network within a TiO₂ Nanoparticle Film for Enhanced Dye-Sensitized Solar Cell Performance. *Advanced Materials*, *24*(43), 5850-5856.
- Bailes, M., Cameron, P. J., Lobato, K., & Peter, L. M. (2005). Determination of the density and energetic distribution of electron traps in dye-sensitized nanocrystalline solar cells. *The Journal of Physical Chemistry B*, *109*(32), 15429-15435.
- Bandara, T., Aziz, M. F., Fernando, H., Careem, M. A., Arof, A. K., & Mellander, B. E. (2015). Efficiency enhancement in dye-sensitized solar cells with a novel PAN-based gel polymer electrolyte with ternary iodides. *Journal of Solid State Electrochemistry*, *19*(8), 2353-2359.
- Bandara, T., Jayasundara, W., Dissanayake, M., Furlani, M., Albinsson, I., & Mellander, B. E. (2012) Effect of cation size on the performance of dye-sensitized nanocrystalline TiO₂ solar cells based on quasi-solid state PAN electrolytes containing quaternary ammonium iodides. *Electrochimica Acta*, *109*, 609-616.
- Bandara, T., Svensson, T., Dissanayake, M., Furlani, M., Jayasundara, W., & Mellander, B. E. (2012). Tetrahexylammonium iodide containing solid and gel polymer electrolytes for dye-sensitized solar cells. *Energy Procedia*, *14*, 1607-1612.
- Bandara, T. M., Fernando, H. D., Furlani, M., Albinsson, I., Dissanayake, M. A., Ratnasekera, J. L., & Mellander, B. E. (2016). Effect of the alkaline cation size on the conductivity in gel polymer electrolytes and their influence on photo

electrochemical solar cells. *Physical Chemistry Chemical Physics*, 18(16), 10873-10881.

Bandara, T. M. W. J., Dissanayake, M. A. K. L., Jayasundara, W. J. M. J. S. R., Albinsson, I., & Mellander, B. E. (2012). Efficiency enhancement in dye-sensitized solar cells using gel polymer electrolytes based on a tetrahexylammonium iodide and MgI₂ binary iodide system. *Physical Chemistry Chemical Physics*, 14(24), 8620-8627.

Bandara, T. M. W. J., Jayasundara, W. J. M. J. S. R., Dissanayake, M. A. K. L., Furlani, M., Albinsson, I., & Mellander, B. E. (2013). Effect of cation size on the performance of dye-sensitized nanocrystalline TiO₂ solar cells based on quasi-solid state PAN electrolytes containing quaternary ammonium iodides. *Electrochimica Acta*, 109(Supplement C), 609-616.

Bandara, T. W. J., Ekanayake, P., Dissanayake, M. L., Albinsson, I., & Mellander, B.-E. (2010). A polymer electrolyte containing ionic liquid for possible applications in photoelectrochemical solar cells. *Journal of Solid State Electrochemistry*, 14(7), 1221-1226.

Bard, A. J., Faulkner, L. R., Leddy, J., & Zoski, C. G. (1980). *Electrochemical Methods: Fundamentals and Applications* (Vol. 2): Wiley New York.

Bashir, Z. (1992). Thermoreversible gelation and plasticization of polyacrylonitrile. *Polymer*, 33(20), 4304-4313.

Bashir, Z. (1993). The effect of solvent on the X-ray scattering from polyacrylonitrile. *Journal of Materials Science Letters*, 12(19), 1526-1528.

Baskaran, R., Selvasekarapandian, S., Kuwata, N., Kawamura, J., & Hattori, T. (2006). Conductivity and thermal studies of blend polymer electrolytes based on PVAc-PMMA. *Solid State Ionics*, 177(26), 2679-2682.

Bella, F., Sacco, A., Pugliese, D., Laurenti, M., & Bianco, S. Additives and salts for dye-sensitized solar cells electrolytes: what is the best choice? *Journal of Power Sources*, 264, 333-343.

Bella, F., Sacco, A., Pugliese, D., Laurenti, M., & Bianco, S. (2014). Additives and salts for dye-sensitized solar cells electrolytes: what is the best choice? *Journal of Power Sources*, 264, 333-343.

Benedetti, J. E., de Paoli, M. A., & Nogueira, A. F. (2008). Enhancement of photocurrent generation and open circuit voltage in dye-sensitized solar cells using Li⁺ trapping species in the gel electrolyte. *Chemical Communications* (9), 1121-1123.

Benkö, G., Skårman, B., Wallenberg, R., Hagfeldt, A., Sundström, V., & Yartsev, A. P. (2003). Particle size and crystallinity dependent electron injection in fluorescein 27-sensitized TiO₂ films. *The Journal of Physical Chemistry B*, 107(6), 1370-1375.

Bidikoudi, M., Stergiopoulos, T., Likodimos, V., Romanos, G. E., Francisco, M., Iliev, B., Falaras, P. (2013). Ionic liquid redox electrolytes based on binary mixtures of

- 1-alkyl-methylimidazolium tricyanomethanide with 1-methyl-3-propylimidazolium iodide and implication in dye-sensitized solar cells. *Journal of Materials Chemistry A*, 1(35), 10474-10486.
- Bidikoudi, M., Zubeir, L. F., & Falaras, P. (2014). Low viscosity highly conductive ionic liquid blends for redox active electrolytes in efficient dye-sensitized solar cells. *Journal of Materials Chemistry A*, 2(37), 15326-15336.
- Bisquert, J., Cahen, D., Hodes, G., Rühle, S., & Zaban, A. (2004). Physical chemical principles of photovoltaic conversion with nanoparticulate, mesoporous dye-sensitized solar cells. *The Journal of Physical Chemistry B*, 108(24), 8106-8118.
- Bisquert, J., & Vikhrenko, V. S. (2004). Interpretation of the time constants measured by kinetic techniques in nanostructured semiconductor electrodes and dye-sensitized solar cells. *The Journal of Physical Chemistry B*, 108(7), 2313-2322.
- Bohn, C., Schaeffgen, J., & Statton, W. (1961). Laterally ordered polymers: Polyacrylonitrile and poly (vinyl trifluoroacetate). *Journal of Polymer Science*, 55(162), 531-549.
- Boschloo, G. K., & Goossens, A. (1996). Electron trapping in porphyrin-sensitized porous nanocrystalline TiO₂ electrodes. *The Journal of Physical Chemistry*, 100(50), 19489-19494.
- Burke, A., Ito, S., Snaith, H., Bach, U., Kwiatkowski, J., & Gratzel, M. (2008). The function of a TiO₂ compact layer in dye-sensitized solar cells incorporating "Planar" organic dyes. *Nano Letters*, 8(4), 977-981.
- Burschka, J., Pellet, N., Moon, S.-J., Humphry-Baker, R., Gao, P., Nazeeruddin, M. K., & Grätzel, M. (2013). Sequential deposition as a route to high-performance perovskite-sensitized solar cells. *Nature*, 499(7458), 316-319.
- Buzzeo, M. C., Evans, R. G., & Compton, R. G. (2004). Non-haloaluminate room-temperature ionic liquids in electrochemistry-A review. *ChemPhysChem*, 5(8), 1106-1120.
- Cameron, P. J., & Peter, L. M. (2005). How does back-reaction at the conducting glass substrate influence the dynamic photovoltage response of nanocrystalline dye-sensitized solar cells? *The Journal of Physical Chemistry B*, 109(15), 7392-7398.
- Cameron, P. J., Peter, L. M., & Hore, S. (2005). How important is the back reaction of electrons via the substrate in dye-sensitized nanocrystalline solar cells? *The Journal of Physical Chemistry B*, 109(2), 930-936.
- Chen, H.-W., Liang, C.-P., Huang, H.-S., Chen, J.-G., Vittal, R., Lin, C.-Y., Ho, K.-C. (2011). Electrophoretic deposition of mesoporous TiO₂ nanoparticles consisting of primary anatase nanocrystallites on a plastic substrate for flexible dye-sensitized solar cells. *Chemical Communications*, 47(29), 8346-8348.
- Cho, T.-Y., Yoon, S.-G., Sekhon, S., & Han, C.-H. (2011). Effect of Ionic Liquids with Different Cations in I⁻/I₃⁻ Redox Electrolyte on the Performance of Dye-sensitized Solar Cells. *Bulletin of the Korean Chemical Society*, 32(6), 2058-2062.

- Colvin, B., & Storr, P. (1974). The crystal structure of polyacrylonitrile. *European Polymer Journal*, 10(4), 337-340.
- Costa, L. T., Lavall, R. L., Borges, R. S., Rieumont, J., Silva, G. G., & Ribeiro, M. C. C. (2007). Polymer electrolytes based on poly (ethylene glycol) dimethyl ether and the ionic liquid 1-butyl-3-methylimidazolium hexafluorophosphate: Preparation, physico-chemical characterization, and theoretical study. *Electrochimica Acta*, 53(4), 1568-1574.
- de Freitas, J. N., de Souza Gonçalves, A., De Paoli, M.-A., Durrant, J. R., & Nogueira, A. F. (2008). The role of gel electrolyte composition in the kinetics and performance of dye-sensitized solar cells. *Electrochimica Acta*, 53(24), 7166-7172.
- de Freitas, J. N., Nogueira, A. F., & De Paoli, M.-A. (2009). New insights into dye-sensitized solar cells with polymer electrolytes. *Journal of Materials Chemistry*, 19(30), 5279-5294.
- Dhungel, S. K., & Park, J. G. (2010). Optimization of paste formulation for TiO₂ nanoparticles with wide range of size distribution for its application in dye-sensitized solar cells. *Renewable Energy*, 35(12), 2776-2780.
- Dissanayake, M., Bandara, L., Bokalawala, R. S. P., Jayathilaka, P., Ileperuma, O. A., & Somasundaram, S. (2002). A novel gel polymer electrolyte based on polyacrylonitrile (PAN) and its application in a solar cell. *Materials Research Bulletin*, 37(5), 867-874.
- Duffy, N. W., Peter, L. M., Rajapakse, R. M. G., & Wijayantha, K. G. U. (2000). A novel charge extraction method for the study of electron transport and interfacial transfer in dye sensitised nanocrystalline solar cells. *Electrochemistry Communications*, 2(9), 658-662.
- Fabregat-Santiago, F., Bisquert, J., Palomares, E., Haque, S. A., & Durrant, J. R. (2006). Impedance spectroscopy study of dye-sensitized solar cells with undoped spiro-OMeTAD as hole conductor. *Journal of Applied Physics*, 100(3), 034510.
- Fisher, A., Peter, L., Ponomarev, E., Walker, A., & Wijayantha, K. (2000). Intensity dependence of the back reaction and transport of electrons in dye-sensitized nanocrystalline TiO₂ solar cells. *The Journal of Physical Chemistry B*, 104(5), 949-958.
- Fukui, A., Komiya, R., Yamanaka, R., Islam, A., & Han, L. (2006). Effect of a redox electrolyte in mixed solvents on the photovoltaic performance of a dye-sensitized solar cell. *Solar Energy Materials and Solar Cells*, 90(5), 649-658.
- Ghadiri, E., Taghavinia, N., Zakeeruddin, S. M., Grätzel, M., & Moser, J.-E. (2010). Enhanced electron collection efficiency in dye-sensitized solar cells based on nanostructured TiO₂ hollow fibers. *Nano Letters*, 10(5), 1632-1638.
- Grätzel, M. (2005). Solar energy conversion by dye-sensitized photovoltaic cells. *Inorganic Chemistry*, 44(20), 6841-6851.

- Green, A. N. M., Palomares, E., Haque, S. A., Kroon, J. M., & Durrant, J. R. (2005). Charge transport versus recombination in dye-sensitized solar cells employing nanocrystalline TiO₂ and SnO₂ films. *The Journal of Physical Chemistry B*, 109(25), 12525-12533.
- Günes, S., & Sariciftci, N. S. (2008). Hybrid solar cells. *Inorganica Chimica Acta*, 361(3), 581-588.
- Hagfeldt, A., Boschloo, G., Sun, L., Kloo, L., & Pettersson, H. (2010). Dye-sensitized solar cells. *Chemical Reviews*, 110(11), 6595-6663.
- Hagfeldt, A., & Gratzel, M. (2000). Molecular photovoltaics. *Accounts of Chemical Research*, 33(5), 269-277.
- Hagiwara, R., & Ito, Y. (2000). Room temperature ionic liquids of alkylimidazolium cations and fluoroanions. *Journal of Fluorine Chemistry*, 105(2), 221-227.
- Hamideh Mortazavi, S., Pilehvar, S., Ghoranneviss, M., Hosseinejad, M. T., Zargham, S., Mirarefi, A. A., & Mirarefi, A. Y. (2013). Plasma oxidation and stabilization of electrospun polyacrylonitrile nanofiber for carbon nanofiber formation. *Applied Physics A*, 113(3), 703-712.
- Hao, F., & Lin, H. (2013). Recent molecular engineering of room temperature ionic liquid electrolytes for mesoscopic dye-sensitized solar cells. *RSC Advances*, 3(45), 23521-23532.
- Haque, S. A., Palomares, E., Cho, B. M., Green, A. N. M., Hirata, N., Klug, D. R., & Durrant, J. R. (2005). Charge separation versus recombination in dye-sensitized nanocrystalline solar cells: the minimization of kinetic redundancy. *Journal of the American Chemical Society*, 127(10), 3456-3462.
- Haque, S. A., Tachibana, Y., Willis, R. L., Moser, J. E., Grätzel, M., Klug, D. R., & Durrant, J. R. (2000). Parameters influencing charge recombination kinetics in dye-sensitized nanocrystalline titanium dioxide films. *The Journal of Physical Chemistry B*, 104(3), 538-547.
- Hara, K., Horiguchi, T., Kinoshita, T., Sayama, K., Sugihara, H., & Arakawa, H. (2000). Highly efficient photon-to-electron conversion with mercurochrome-sensitized nanoporous oxide semiconductor solar cells. *Solar Energy Materials and Solar Cells*, 64(2), 115-134.
- Herbert, I. R., Tipping, A., & Bashir, Z. (1993). NMR and x-ray studies on the morphology of thermoreversible polyacrylonitrile gels. *Journal of Polymer Science Part B: Polymer Physics*, 31(11), 1459-1470.
- Hidalgo, M., Colón, G., & Navío, J. (2002). Modification of the physicochemical properties of commercial TiO₂ samples by soft mechanical activation. *Journal of Photochemistry and Photobiology A: Chemistry*, 148(1), 341-348.
- Hore, S., & Kern, R. (2005). Implication of device functioning due to back reaction of electrons via the conducting glass substrate in dye-sensitized solar cells. *Applied Physics Letters*, 87(26), 263504.

- Hsu, H.-L., Tien, C.-F., Yang, Y.-T., & Leu, J. (2013). Dye-sensitized solar cells based on agarose gel electrolytes using allylimidazolium iodides and environmentally benign solvents. *Electrochimica Acta*, *91*, 208-213.
- Hu, P., Chai, J., Duan, Y., Liu, Z., Cui, G., & Chen, L. (2016). Progress in nitrile-based polymer electrolyte for high performance lithium batteries. *Journal of Materials Chemistry A*, *4*, 10070-10083.
- Ileperuma, Dissanayake, M., Somasunderam, & Bandara, L. (2004). Photoelectrochemical solar cells with polyacrylonitrile-based and polyethylene oxide-based polymer electrolytes. *Solar Energy Materials and Solar Cells*, *84*(1), 117-124.
- Ileperuma, O. A., Kumara, G. R. A., & Murakami, K. (2007). Quasi-solid polymer electrolytes based on polyacrylonitrile and plasticizers for indoline dye-sensitized solar cells of efficiency 5.3%. *Chemistry Letters*, *37*(1), 36-37.
- Ileperuma, O. A., Kumara, G. R. A., Yang, H.-S., & Murakami, K. (2011). Quasi-solid electrolyte based on polyacrylonitrile for dye-sensitized solar cells. *Journal of Photochemistry and Photobiology A: Chemistry*, *217*(2), 308-312.
- Ito, S., Liska, P., Comte, P., Charvet, R. I., Péchy, P., Bach, U., Nazeeruddin, M. K. (2005). Control of dark current in photoelectrochemical (TiO₂/I⁻/I₃⁻) and dye-sensitized solar cells. *Chemical Communications* (34), 4351-4353.
- Jayathilaka, P. A. R. D., Dissanayake, M. A. K. L., Albinsson, I., & Mellander, B. E. (2002). Effect of nano-porous Al₂O₃ on thermal, dielectric and transport properties of the (PEO)₉LiTFSI polymer electrolyte system. *Electrochimica Acta*, *47*(20), 3257-3268.
- Khanmirzaei, M. H., Ramesh, S., & Ramesh, K. (2015). Hydroxypropyl Cellulose Based Non-Volatile Gel Polymer Electrolytes for Dye-Sensitized Solar Cell Applications using 1-methyl-3-propylimidazolium iodide ionic liquid. *Scientific Reports*, *5*.
- Kim, J. H., Chi, Y. S., & Kang, T. J. (2013). Optimization of quasi-solid-state dye-sensitized photovoltaic fibers using porous polymer electrolyte membranes. *Journal of Power Sources*, *229*, 84-94.
- Kontos, A., Fardis, M., Prodromidis, M., Stergiopoulos, T., Chatzivasiloglou, E., Papavassiliou, G., & Falaras, P. (2006). Morphology, ionic diffusion and applicability of novel polymer gel electrolytes with LiI/I₂. *Physical Chemistry Chemical Physics*, *8*(6), 767-776.
- Kubo, W., Kambe, S., Nakade, S., Kitamura, T., Hanabusa, K., Wada, Y., & Yanagida, S. (2003). Photocurrent-determining processes in quasi-solid-state dye-sensitized solar cells using ionic gel electrolytes. *The Journal of Physical Chemistry B*, *107*(18), 4374-4381.
- Kubo, W., Kitamura, T., Hanabusa, K., Wada, Y., & Yanagida, S. (2002). Quasi-solid-state dye-sensitized solar cells using room temperature molten salts and a low molecular weight gelator. *Chemical Communications* (4), 374-375.

- Kumara, G., Konno, A., Shiratsuchi, K., Tsukahara, J., & Tennakone, K. (2002). Dye-sensitized solid-state solar cells: use of crystal growth inhibitors for deposition of the hole collector. *Chemistry of Materials*, 14(3), 954-955.
- Lan, Z., Wu, J., Lin, J., & Huang, M. (2010). Quasi-solid-state dye-sensitized solar cell based on a polymer gel electrolyte with in situ synthesized ionic conductors. *Comptes Rendus Chimie*, 13(11), 1401-1405.
- Lan, Z., Wu, J., Lin, J., Huang, M., Li, P., & Li, Q. (2008). Influence of ionic additives NaI/I₂ on the properties of polymer gel electrolyte and performance of quasi-solid-state dye-sensitized solar cells. *Electrochimica Acta*, 53(5), 2296-2301.
- Lee, K.-M., Suryanarayanan, V., & Ho, K.-C. (2009). High efficiency quasi-solid-state dye-sensitized solar cell based on polyvinylidene fluoride-co-hexafluoro propylene containing propylene carbonate and acetonitrile as plasticizers. *Journal of Photochemistry and Photobiology A: Chemistry*, 207(2), 224-230.
- Li, B., Wang, L., Kang, B., Wang, P., & Qiu, Y. (2006). Review of recent progress in solid-state dye-sensitized solar cells. *Solar Energy Materials and Solar Cells*, 90(5), 549-573.
- Li, P. J., Wu, J. H., Huang, M. L., Lan, Z., Li, Q., & Kang, S. (2007). The application of P (MMA-co-MAA)/PEG polyblend gel electrolyte in quasi-solid state dye-sensitized solar cell at higher temperature. *Electrochimica Acta*, 53(2), 903-908.
- Li, Q., Chen, X., Tang, Q., Cai, H., Qin, Y., He, B., Liu, Z. (2014). Enhanced photovoltaic performances of quasi-solid-state dye-sensitized solar cells using a novel conducting gel electrolyte. *Journal of Power Sources*, 248, 923-930.
- Liew, C.-W., Ramesh, S., & Arof, A. K. Characterization of ionic liquid added poly (vinyl alcohol)-based proton conducting polymer electrolytes and electrochemical studies on the supercapacitors. *International Journal of Hydrogen Energy*, 40(1), 852-862.
- Lin, B., Shang, H., Chu, F., Ren, Y., Yuan, N., Jia, B., Ding, J. (2014). Ionic liquid-tethered graphene oxide/ionic liquid electrolytes for highly efficient dye-sensitized solar cells. *Electrochimica Acta*, 134, 209-214.
- Liu, Y., Hagfeldt, A., Xiao, X.-R., & Lindquist, S.-E. (1998). Investigation of influence of redox species on the interfacial energetics of a dye-sensitized nanoporous TiO₂ solar cell. *Solar Energy Materials and Solar Cells*, 55(3), 267-281.
- Longo, C., & De Paoli, M.-A. (2003). Dye-sensitized solar cells: a successful combination of materials. *Journal of the Brazilian Chemical Society*, 14(6), 898-901.
- Lu, H., Ma, Y., Gu, B., Tian, W., & Li, L. (2015). Identifying the optimum thickness of electron transport layers for highly efficient perovskite planar solar cells. *Journal of Materials Chemistry A*, 3(32), 16445-16452.

- Lu, W., Henry, K., Turchi, C., & Pellegrino, J. (2008). Incorporating ionic liquid electrolytes into polymer gels for solid-state ultracapacitors. *Journal of the Electrochemical Society*, 155(5), A361-A367.
- Marinado, T. (2009). *Photoelectrochemical studies of dye-sensitized solar cells using organic dyes*. KTH.
- Mathew, S., Yella, A., Gao, P., Humphry-Baker, R., Curchod, B. F., Ashari-Astani, N., Grätzel, M. (2014). Dye-sensitized solar cells with 13% efficiency achieved through the molecular engineering of porphyrin sensitizers. *Nature Chemistry*, 6(3), 242-247.
- Mistler, R. E., & Twiname, E. R. (2000). *Tape casting: theory and practice*: American ceramic society.
- Mover, B. A., & McDowell, W. J. (1981). Factors influencing phase disengagement rates in solvent extraction systems employing tertiary amine extractants. *Separation Science and Technology*, 16(9), 1261-1289.
- Nakade, S., Kanzaki, T., Kubo, W., Kitamura, T., Wada, Y., & Yanagida, S. (2005). Role of Electrolytes on Charge Recombination in Dye-Sensitized TiO₂ Solar Cell (1): The Case of Solar Cells Using the I⁻/I₃⁻ Redox Couple. *The Journal of Physical Chemistry B*, 109(8), 3480-3487.
- Nakade, S., Kanzaki, T., Wada, Y., & Yanagida, S. (2005). Stepped light-induced transient measurements of photocurrent and voltage in dye-sensitized solar cells: application for highly viscous electrolyte systems. *Langmuir*, 21(23), 10803-10807.
- Nath, A. K., & Kumar, A. Scaling of AC conductivity, electrochemical and thermal properties of ionic liquid based polymer nanocomposite electrolytes. *Electrochimica Acta*, 129, 177-186.
- Nazeeruddin, M. K., Kay, A., Rodicio, I., Humphry-Baker, R., Mueller, E., Liska, P., & Grätzel, M. (1993). Conversion of light to electricity by cis-X₂bis (2, 2'-bipyridyl-4, 4'-dicarboxylate) ruthenium (II) charge-transfer sensitizers (X= Cl⁻, Br⁻, I⁻, CN⁻, and SCN⁻) on nanocrystalline titanium dioxide electrodes. *Journal of the American Chemical Society*, 115(14), 6382-6390.
- Nazeeruddin, M. K., Pechy, P., & Grätzel, M. (1997). Efficient panchromatic sensitization of nanocrystalline TiO₂ films by a black dye based on a trithiocyanato-ruthenium complex. *Chemical Communications* (18), 1705-1706.
- Nazeeruddin, M. K., Zakeeruddin, S. M., Humphry-Baker, R., Jirousek, M., Liska, P., Vlachopoulos, N., & Grätzel, M. (1999). Acid-base equilibria of (2, 2'-bipyridyl-4, 4'-dicarboxylic acid) ruthenium (II) complexes and the effect of protonation on charge-transfer sensitization of nanocrystalline titania. *Inorganic Chemistry*, 38(26), 6298-6305.
- Nelson, J., Haque, S. A., Klug, D. R., & Durrant, J. R. (2001). Trap-limited recombination in dye-sensitized nanocrystalline metal oxide electrodes. *Physical Review B*, 63(20), 205321.

- Nguyen, T. O., Peter, L. M., & Wang, H. (2009). Characterization of electron trapping in dye-sensitized solar cells by near-IR transmittance measurements. *The Journal of Physical Chemistry C*, 113(19), 8532-8536.
- Nguyen, T. T. O., Peter, L. M., & Wang, H. (2009). Characterization of electron trapping in dye-sensitized solar cells by near-IR transmittance measurements. *The Journal of Physical Chemistry C*, 113(19), 8532-8536.
- Ni, M., Leung, M. K. H., Leung, D. Y. C., & Sumathy, K. (2006). Theoretical modeling of TiO₂/TCO interfacial effect on dye-sensitized solar cell performance. *Solar Energy Materials and Solar Cells*, 90(13), 2000-2009.
- Nishida, T., Tashiro, Y., & Yamamoto, M. (2003). Physical and electrochemical properties of 1-alkyl-3-methylimidazolium tetrafluoroborate for electrolyte. *Journal of Fluorine Chemistry*, 120(2), 135-141.
- Nogueira, A., Longo, C., & De Paoli, M.-A. (2004). Polymers in dye-sensitized solar cells: overview and perspectives. *Coordination Chemistry Reviews*, 248(13), 1455-1468.
- Nogueira, A. F., & De Paoli, M.-A. (2000). A dye-sensitized TiO₂ photovoltaic cell constructed with an elastomeric electrolyte. *Solar Energy Materials and Solar Cells*, 61(2), 135-141.
- Nogueira, A. F., De Paoli, M.-A., Montanari, I., Monkhouse, R., Nelson, J., & Durrant, J. R. (2001). Electron transfer dynamics in dye-sensitized nanocrystalline solar cells using a polymer electrolyte. *The Journal of Physical Chemistry B*, 105(31), 7517-7524.
- Nogueira, A. F., Durrant, J. R., & De Paoli, M. A. (2001). Dye-sensitized nanocrystalline solar cells employing a polymer electrolyte. *Advanced Materials*, 13(11), 826-830.
- Nogueira, V. C., Longo, C., Nogueira, A. F., Soto-Oviedo, M. A., & De Paoli, M.-A. (2006). Solid-state dye-sensitized solar cell: improved performance and stability using a plasticized polymer electrolyte. *Journal of Photochemistry and Photobiology A: Chemistry*, 181(2), 226-232.
- Noh, J. H., Lee, S., Kim, J. Y., Lee, J.-K., Han, H. S., Cho, C. M., Hong, K. S. (2008). Functional multilayered transparent conducting oxide thin films for photovoltaic devices. *The Journal of Physical Chemistry C*, 113(3), 1083-1087.
- O'Regan, B., & Grätzel, M. (1991). A low-cost, high-efficiency solar cell based on dye-sensitized colloidal TiO₂ films. *Nature*, 353(6346), 737-740.
- O'Regan, B. C., & Lenzmann, F. (2004). Charge transport and recombination in a nanoscale interpenetrating network of n-type and p-type semiconductors: transient photocurrent and photovoltage studies of TiO₂/Dye/CuSCN photovoltaic cells. *The Journal of Physical Chemistry B*, 108(14), 4342-4350.
- Palomares, E., Clifford, J. N., Haque, S. A., Lutz, T., & Durrant, J. R. (2003). Control of charge recombination dynamics in dye-sensitized solar cells by the use of

conformally deposited metal oxide blocking layers. *Journal of the American Chemical Society*, 125(2), 475-482.

- Papageorgiou, N., Athanassov, Y., Armand, M., Bonho, P., Pettersson, H., Azam, A., & Grätzel, M. (1996). The performance and stability of ambient temperature molten salts for solar cell applications. *Journal of the Electrochemical Society*, 143(10), 3099-3108.
- Papović, S., Gadžurić, S., Bešter-Rogač, M., & Vraneš, M. (2016). Effect of the alkyl chain length on the electrical conductivity of six (imidazolium-based ionic liquids+ γ -butyrolactone) binary mixtures. *The Journal of Chemical Thermodynamics*, 102, 367-377.
- Patch, K. (2006). Solar cell doubles as battery. *Technology Research News*.
- Peiró, A. M., Colombo, C., Doyle, G., Nelson, J., Mills, A., & Durrant, J. R. (2006). Photochemical reduction of oxygen adsorbed to nanocrystalline TiO₂ films: A transient absorption and oxygen scavenging study of different TiO₂ preparations. *The Journal of Physical Chemistry B*, 110(46), 23255-23263.
- Pelet, S., Moser, J.-E., & Grätzel, M. (2000). Cooperative effect of adsorbed cations and iodide on the interception of back electron transfer in the dye sensitization of nanocrystalline TiO₂. *The Journal of Physical Chemistry B*, 104(8), 1791-1795.
- Peng, B., Jungmann, G., Jäger, C., Haarer, D., Schmidt, H.-W., & Thelakkat, M. (2004). Systematic investigation of the role of compact TiO₂ layer in solid state dye-sensitized TiO₂ solar cells. *Coordination Chemistry Reviews*, 248(13), 1479-1489.
- Peter, L. (2007). Characterization and modeling of dye-sensitized solar cells. *The Journal of Physical Chemistry C*, 111(18), 6601-6612.
- Peter, L. (2009). "Sticky electrons" transport and interfacial transfer of electrons in the dye-sensitized solar cell. *Accounts of Chemical Research*, 42(11), 1839-1847.
- Peter, L. M., Walker, A. B., Boschloo, G., & Hagfeldt, A. (2006). Interpretation of apparent activation energies for electron transport in dye-sensitized nanocrystalline solar cells. *The Journal of Physical Chemistry B*, 110(28), 13694-13699.
- Price, W. E., & Weingaertner, H. (1991). Ion pairing and redissociation in concentrated aqueous solutions of 2: 2 electrolytes: a transport coefficient study of aqueous zinc sulfate. *The Journal of Physical Chemistry*, 95(22), 8933-8938.
- Priya, A. S., Subramania, A., Jung, Y.-S., & Kim, K.-J. (2008). High-performance quasi-solid-state dye-sensitized solar cell based on an electrospun PVdF-HFP membrane electrolyte. *Langmuir*, 24(17), 9816-9819.
- Qiu, Y., Chen, W., & Yang, S. (2010). Double-layered photoanodes from variable-size anatase TiO₂ nanospindles: a candidate for high-efficiency dye-sensitized solar cells. *Angewandte Chemie*, 122(21), 3757-3761.

- Rajendran, S., Kannan, R., & Mahendran, O. (2001). Study on Li ion conduction behaviour of the plasticized polymer electrolytes based on poly acrylonitrile. *Materials Letters*, 48(6), 331-335.
- Ren, Y., Zhang, Z., Fang, S., Yang, M., & Cai, S. (2002). Application of PEO based gel network polymer electrolytes in dye-sensitized photoelectrochemical cells. *Solar Energy Materials and Solar Cells*, 71(2), 253-259.
- Rezvani, F., Parvazian, E., & Hosseini, S. (2016). Dye-sensitized solar cells based on composite TiO₂ nanoparticle–nanorod single and bi-layer photoelectrodes. *Bulletin of Materials Science*, 39(6), 1397-1402.
- Rhee, Y. H., Ahn, D. J., Ko, M. J., Jin, H.-Y., Jin, J.-H., & Min, N. K. Enhanced electrocatalytic activity of plasma functionalized multi-walled carbon nanotube-entrapped poly (3,4-ethylenedioxythiophene): poly (styrene sulfonate) photocathode. *Electrochimica Acta*, 146, 68-72.
- Rhee, Y. H., Ahn, D. J., Ko, M. J., Jin, H.-Y., Jin, J.-H., & Min, N. K. (2014). Enhanced electrocatalytic activity of plasma functionalized multi-walled carbon nanotube-entrapped poly (3,4-ethylenedioxythiophene): poly (styrene sulfonate) photocathode. *Electrochimica Acta*, 146, 68-72.
- Sauvage, F., Chen, D., Comte, P., Huang, F., Heiniger, L.-P., Cheng, Y.-B., Grätzel, M. (2010). Dye-Sensitized Solar Cells Employing a Single Film of Mesoporous TiO₂ Beads Achieve Power Conversion Efficiencies Over 10 %. *ACS Nano*, 4(8), 4420-4425.
- Sauvage, F., Di Fonzo, F., Li Bassi, A., Casari, C., Russo, V., Divitini, G., Graetzel, M. (2010). Hierarchical TiO₂ photoanode for dye-sensitized solar cells. *Nano Letters*, 10(7), 2562-2567.
- Sawai, D., Miyamoto, M., Kanamoto, T., & Ito, M. (2000). Lamellar thickening in nascent poly (acrylonitrile) upon annealing. *Journal of Polymer Science Part B: Polymer Physics*, 38(19), 2571-2579.
- Schlichthörl, G., Huang, S., Sprague, J., & Frank, A. (1997). Band edge movement and recombination kinetics in dye-sensitized nanocrystalline TiO₂ solar cells: a study by intensity modulated photovoltage spectroscopy. *The Journal of Physical Chemistry B*, 101(41), 8141-8155.
- Schwarzburg, K., & Willig, F. (1991). Influence of trap filling on photocurrent transients in polycrystalline TiO₂. *Applied Physics Letters*, 58(22), 2520-2522.
- Shaheen, S. E., Brabec, C. J., Sariciftci, N. S., Padinger, F., Fromherz, T., & Hummelen, J. C. (2001). 2.5% efficient organic plastic solar cells. *Applied Physics Letters*, 78(6), 841-843.
- Shankar, K., Bandara, J., Paulose, M., Wietasch, H., Varghese, O. K., Mor, G. K., Grimes, C. A. (2008). Highly efficient solar cells using TiO₂ nanotube arrays sensitized with a donor-antenna dye. *Nano Letters*, 8(6), 1654-1659.

- Shen, X., Xu, W., Xu, J., Liang, G., Yang, H., & Yao, M. (2008). Quasi-solid-state dye-sensitized solar cells based on gel electrolytes containing different alkali metal iodide salts. *Solid State Ionics*, *179*(35), 2027-2030.
- Shi, Y., Wang, Y., Zhang, M., & Dong, X. Influences of cation charge density on the photovoltaic performance of dye-sensitized solar cells: lithium, sodium, potassium, and dimethylimidazolium. *Physical Chemistry Chemical Physics*, *13*(32), 14590-14597.
- Son, K. M., Kang, M. G., Vittal, R., Lee, J., & Kim, K.-J. (2008). Effects of substituents of imidazolium cations on the performance of dye-sensitized TiO₂ solar cells. *Journal of Applied Electrochemistry*, *38*(12), 1647-1652.
- Štangar, U. L., Orel, B., Vuk, A. Š., Sagon, G., Colomban, P., Stathatos, E., & Lianos, P. (2002). In Situ Resonance Raman Microspectroscopy of a Solid-State Dye-Sensitized Photoelectrochemical Cell. *Journal of the Electrochemical Society*, *149*(11), E413-E423.
- Suryanarayanan, V., Lee, K.-M., Ho, W.-H., Chen, H.-C., & Ho, K.-C. (2007). A comparative study of gel polymer electrolytes based on PVDF-HFP and liquid electrolytes, containing imidazolium ionic liquids of different carbon chain lengths in DSSCs. *Solar Energy Materials and Solar Cells*, *91*(15), 1467-1471.
- Tachibana, Y., Moser, J. E., Grätzel, M., Klug, D. R., & Durrant, J. R. (1996). Subpicosecond interfacial charge separation in dye-sensitized nanocrystalline titanium dioxide films. *The Journal of Physical Chemistry*, *100*(51), 20056-20062.
- Tada, H., Teranishi, K., & Ito, S. (1999). Additive effect of sacrificial electron donors on Ag/TiO₂ photocatalytic reduction of bis (2-dipyridyl) disulfide to 2-mercaptopyridine in aqueous media. *Langmuir*, *15*(20), 7084-7087.
- Tan, S., Zhai, J., Xue, B., Wan, M., Meng, Q., Li, Y., Zhu, D. (2004). Property influence of polyanilines on photovoltaic behaviors of dye-sensitized solar cells. *Langmuir*, *20*(7), 2934-2937.
- Tan, L., Chen, H., Pan, D., & Pan, N. (2009). Investigation into the gelation and crystallization of polyacrylonitrile. *European Polymer Journal*, *45*(5), 1617-1624
- Theerthagiri, J., Senthil, R., Buraidah, M., Madhavan, J., & Arof, A. (2015). Effect of tetrabutylammonium iodide content on PVDF-PMMA polymer blend electrolytes for dye-sensitized solar cells. *Ionics*, *21*(10), 2889-2896.
- Tiautit, N., Puratane, C., Panpinit, S., & Saengsuwan, S. (2014). Effect of SiO₂ and TiO₂ nanoparticles on the performance of dye-sensitized solar cells using PVDF-HFP/PVA gel electrolytes. *Energy Procedia*, *56*, 378-385.
- Tsai, J. S., & Lin, C. H. (1991). The effect of the side chain of acrylate comonomers on the orientation, pore-size distribution, and properties of polyacrylonitrile precursor and resulting carbon fiber. *Journal of Applied Polymer Science*, *42*(11), 3039-3044.

- Villanueva-Cab, J., Anta, J. A., & Oskam, G. (2016). The effect of recombination under short-circuit conditions on the determination of charge transport properties in nanostructured photoelectrodes. *Physical Chemistry Chemical Physics*, 18(4), 2303-2308.
- Vittadello, M., Waxman, D. I., Sideris, P. J., Gan, Z., Vezzù, K., Negro, E., Di Noto, V. (2011). Iodide-conducting polymer electrolytes based on poly-ethylene glycol and MgI₂: Synthesis and structural characterization. *Electrochimica Acta*, 57, 112-122.
- Walden, P. (1921). Over the limit values λ_{∞} of the molecular conductivity in non-aqueous and aqueous solutions. *Journal of Inorganic and General Chemistry*, 115(1), 49-86.
- Wang, G., Zhou, X., Li, M., Zhang, J., Kang, J., Lin, Y., Xiao, X. (2004). Gel polymer electrolytes based on polyacrylonitrile and a novel quaternary ammonium salt for dye-sensitized solar cells. *Materials Research Bulletin*, 39(13), 2113-2118.
- Wang, M., Xiao, X., Zhou, X., Li, X., & Lin, Y. (2007). Investigation of PEO-imidazole ionic liquid oligomer electrolytes for dye-sensitized solar cells. *Solar Energy Materials and Solar Cells*, 91(9), 785-790.
- Wang, P., Zakeeruddin, S. M., Exnar, I., & Grätzel, M. (2002). High efficiency dye-sensitized nanocrystalline solar cells based on ionic liquid polymer gel electrolyte. *Chemical Communications*, (24), 2972-2973.
- Wang, Y. (2009). Recent research progress on polymer electrolytes for dye-sensitized solar cells. *Solar Energy Materials and Solar Cells*, 93(8), 1167-1175.
- Wei, Z. (2011). *Fabrication of Dye Sensitized Solar Cells With Enhanced Energy Conversion Efficiency* (Doctoral dissertation). Retrieved from <http://scholarbank.nus.edu.sg/handle/10635/30272>.
- Wen, T.-C., Kuo, H.-H., & Gopalan, A. (2002). The influence of lithium ions on molecular interaction and conductivity of composite electrolyte consisting of TPU and PAN. *Solid State Ionics*, 147(1), 171-180.
- Wishart, J. F. (2009). Energy applications of ionic liquids. *Energy & Environmental Science*, 2(9), 956-961.
- Wu, J., Lan, Z., Wang, D., Hao, S., Lin, J., Huang, Y., Sato, T. (2006). Gel polymer electrolyte based on poly (acrylonitrile-co-styrene) and a novel organic iodide salt for quasi-solid state dye-sensitized solar cell. *Electrochimica Acta*, 51(20), 4243-4249.
- Wu, M., Lin, X., Wang, Y., Wang, L., Guo, W., Qi, D., Ma, T. (2012) Economical Pt-free catalysts for counter electrodes of dye-sensitized solar cells. *Journal of the American Chemical Society*, 134(7), 3419-3428.
- Xi, C., Cao, Y., Cheng, Y., Wang, M., Jing, X., Zakeeruddin, S. M., Wang, P. (2008). Tetrahydrothiophenium-based ionic liquids for high efficiency dye-sensitized solar cells. *The Journal of Physical Chemistry C*, 112(29), 11063-11067.

- Yang, Y., Hu, H., Zhou, C.-H., Xu, S., Sebo, B., & Zhao, X.-Z. (2011). Novel agarose polymer electrolyte for quasi-solid state dye-sensitized solar cell. *Journal of Power Sources*, 196(4), 2410-2415.
- Ye, M., Wen, X., Wang, M., Iocozzia, J., Zhang, N., Lin, C., & Lin, Z. Recent advances in dye-sensitized solar cells: from photoanodes, sensitizers and electrolytes to counter electrodes. *Materials Today*, 18(3), 155-162.
- Yu, H., Zhang, S., Zhao, H., Will, G., & Liu, P. (2009). An efficient and low-cost TiO₂ compact layer for performance improvement of dye-sensitized solar cells. *Electrochimica Acta*, 54(4), 1319-1324.
- Zhang, Z., Zhang, L., Wang, S., Chen, W., & Lei, Y. (2001). A convenient route to polyacrylonitrile/silver nanoparticle composite by simultaneous polymerization-reduction approach. *Polymer*, 42(19), 8315-8318.
- Zhang, K., Cui, Z., Xing, G., Feng, Y., & Meng, S. (2016). Improved performance of dye-sensitized solar cells based on modified kaolin/PVDF-HFP composite gel electrolytes. *RSC Advances*, 6(102), 100079-100089.
- Zheng, Y., Huang, Q., Fang, S., Yang, L., & Gan, Y. (2013). Ether-functionalized pyrazolium ionic liquids as electrolytes for dye-sensitized solar cells. *International Journal of Electrochemical Science*, 8, 9558-9567.
- Zhu, K., Kopidakis, N., Neale, N. R., van de Lagemaat, J., & Frank, A. J. (2006). Influence of surface area on charge transport and recombination in dye-sensitized TiO₂ solar cells. *The Journal of Physical Chemistry B*, 110(50), 25174-25180.
- Zulkifili, A. N. B., Kento, T., Daiki, M., & Fujiki, A. (2015). The Basic Research on the Dye-Sensitized Solar Cells (DSSC). *Journal of Clean Energy Technologies*, 3(5), 382-387.

LIST OF PUBLICATIONS AND PAPERS PRESENTED

Publications

Chowdhury, F. I., Khandaker, M., Amin, Y., & Arof, A. (2017). Effect of gamma radiation on the transport and structural properties of polyacrylonitrile-lithium bis (oxalato) borate films. *Solid State Ionics*, 304, 27-39.

Chowdhury, F. I., Khandaker, M., Amin, Y., Kufian, M., & Woo, H. (2017). Vibrational, electrical, and structural properties of PVDF–LiBOB solid polymer electrolyte with high electrochemical potential window. *Ionics*, 23(2), 275-284.

Buraidah, M., Shah, S., Teo, L., **Chowdhury, F. I.**, Careem, M., Albinsson, I., . . . Arof, A. (2017). High efficient dye-sensitized solar cells using phthaloylchitosan based gel polymer electrolytes. *Electrochimica Acta*, 245, 846-853.

Papers presented

Chowdhury, F. I., Khandaker, M. U., & Arof, A. K., Polyvinylidene difluoride–Lithium bis(oxalato)borate solid polymer electrolyte thin film for Li⁺-ion battery application, International Symposium on Materials and Asset Integrity (ISMAI 2016), 16–18 May 2016, Putra World Trade Centre, Kuala Lumpur. (International)

Chowdhury, F. I., Khandaker, M. U., & Arof, A. K., Dye-sensitized solar cells based on PAN-EC-PC-TPAI-I2 gel polymer electrolytes, International Conference on Functional Materials & Devices 2017 (ICFMD - 2017) 15 – 18 August 2017, Malacca, Malaysia. (International).

Chowdhury, F. I., Khandaker, M. U., & Arof, A. K., Vibrational characterization of polyacrylonitrile (PAN) based gel polymer electrolytes blended with tetrabutylammonium iodide salt, National Workshop on Functional Materials 2017 (NWFM 2017), 17-18 January, 2017, University of Malaya, Malaysia. (National).